Università degli Studi di Napoli Federico II

Ph.D. School in Earth, Environmental and Resources Sciences (DiSTAR) - XXXI Cycle

Multi-component and multi-source approach to model subsidence in deltas. Application to Po Delta Area

Ph.D. Thesis

2018

Candidate:

Eleonora Vitagliano

Tutor:

Prof. Rosa Di Maio

Co-tutors:

Prof. Domenico Calcaterra

Prof. Umberto Riccardi

Table of contents

Acknowledgements

Acronyms

BP	Before Present
CGPS	Continuous Global Positioning System
CMA	Centered Moving Average
CPT	Coherent Pixel Technique
DEM	Digital Elevation Model
DInSAR	Differential InSAR
EDM	Electronic Distance Measurement Height
ESA	European Space Agency
ETRF	European Terrestrial Reference Frame
GB-InSAR	Ground-Based InSAR
GIS	Geographic Information System
GNSS	Global Navigation Satellite System
GPS	Global Positioning System
IAHS	International Association of Hydrological Science
IGS	International GNSS Service
InSAR	Interferometric Synthetic Aperture Radar
IPTA	Interferometric Point Target Analysis
ITRF	International Terrestrial Reference Frame
LIDAR	LIght Detection And Ranging
LGM	Last Glacial Maximum
LOS	Line Of Sight
MBES	Multi Beam Echo Sounder
MLE	Maximum Likelihood Estimator
PWD	Paleo-Water Depth
PPP	Precise Point Positioning
PSs	Permanent Scatterers
PSD	Power Spectral Density
PSI/PSInSAR	Persistent Scatterers Interferometry
PSL	Paleo-Sea level

RER	Emilia Romagna Region
RMT	Radioactive Marker Technique
SBAS-InSAR	Small BAseline Subset InSAR
SIMS	Subsidence Integrated Monitoring System
SMPS	Stanford Method for Persistent Scatterers
SPG	Seabed Pressure Gauge
SRTM	Shuttle Radar Topographic Mission
TLS	Terrestrial Laser Scanning
UNESCO	United Nations Educational Scientific and Cultural Organization
WA	Wavelet Analysis
WTC	Wavelet Transform Coherence
XWT	Cross Wavelet Transform

Abstract

This thesis focused on the definition of a study approach able to deal with the complexity of the land subsidence phenomenon in deltas. In the framework of the most up- to-date multi-methodological and multi-disciplinary studies concerning land subsidence and targeting to predict and prevent flooding risk, the thesis introduces a procedure based on two main innovations: the multi-component study and the multi-source analysis. The proposed approach is a "multi-component" procedure as it investigates, in the available geodetic datasets, the permanent component apart from the periodic one, and, at the same time, it is a "multi-source" approach because it attempts to identify the relevant processes causing subsidence (sources) by a modelling based on multi-source data analysis. The latter task is accomplished first through multi-disciplinary and multi-methodological comparative analyses, then through modelling of the selected processes.

With respect to past and current approaches for studying subsidence phenomena, the developed procedure allows one to:

    i. overcome the one-component investigation, improving the accuracy in the geodetic velocity estimate;

    ii. fix the "analyses to modelling" procedure, enhancing qualitative or semi-quantitative procedures that often characterize the "data to source" and the "residual to source" approaches;

    iii. quicken the source validation phase, accrediting the relevance of the source on the basis of the analysis results and before the modelling phase, differently from the "peering approach", which validates the source on the basis of the model findings.

The proposed procedure has been tested on the Po Delta (northern Italy), an area historically affected by land subsidence and recently interested by accurate continuous geodetic monitoring through GNSS stations. Daily-CGPS time series (three stations), weekly- CGPS time series (two stations) and seven sites of DInSAR-derived time series spanning over the time interval 2009 – 2017 constituted the used geodetic datasets. Several meteo/hydro parameters collected from fifty-seven stations and wide stratigraphic-geological information formed the base for the performed comparative analyses. From the application of the proposed procedure, it turns out that the periodic annual component highlighted in the continuous GPS stations is explained by two water mass-dependent processes: soil moisture mass change, which seems to control the ground level up-or-down lift in the southern part of the Delta, and the river water mass change, which influences the ground displacement in the central part of the Delta. As it concerns

the permanent component, the lower rate found over 2012 - 2016 period in the central part of the Delta with respect to the eastern part is interpreted as due to the sediment compaction process of the Holocene prograding sequences and to the increase of rich-clay deposits.

Introduction

Reliable estimation of land subsidence is crucial in deltas and coastal areas, where the effects of climate variability (e.g., frequent and intense rain storms, peaks in river discharge and sea level fluctuations), coupled with natural or anthropogenic land sinking, represent serious factors of inundation and flooding risk. Over the past 25 years the number of large floods in Europe has increased (Kundzewicz et al., 2013), likely due to intensification of rainfalls and inadequacy or man-made changing of river morphologies and geometries appropriate to contain the higher peak-flow discharges. The significant cost in terms of human and economic losses caused by vulnerability of the Italian landscape to flooding events (e.g. Po Plain, 1951: 84 victims; Firenze, 1966: 35 victims) has stressed the importance to establish cause-effect relationships underlying the observed phenomena. Undoubtedly, downward ground movements favour flooding processes, but understanding the causes of these movements is a challenging task due to the high number of variables involved in the natural and anthropic processes and to their complex interplay.

Today, the integration among terrestrial and space geodetic techniques, such as Global Navigation Satellite System (GNSS), Interferometry Synthetic Aperture Radar (InSAR) and high precision levelling, allows an accurate continuous or discrete monitoring of land subsidence over urban areas, rural lands and vegetated zones. When the expected magnitude of the target physical process is small and, thus, the relative geodetic signal is elusive, a realistic estimate of uncertainties in geodetic observations becomes fundamental. For instance, very accurate geodetic observations are needed to deal with studies aimed at separating current-day tectonic from other contributions (e.g. sediment compaction) or at properly interpreting subsidence driven by fluid withdrawals from that generated by natural drainage variations. Moreover, the tectonic and anthropogenic signals can be overlapped by Earth's surface deformations, caused by loading processes due to hydrological dynamics and natural mass re-distribution within the atmosphere-ocean systems. All these signals, which are characterised by different spatial and spectral features, can be recorded as temporal coordinate variations at permanent GNSS terrestrial stations.

In general, many site-position time series exhibit a linear trend plus seasonal oscillations of annual and semi-annual periods, frequently masked by the superposition of several correlated or uncorrelated noise sources (Bock and Melgar, 2016). Although periodic components observed in the geodetic signals affect the estimate of the subsidence rates and have to be recognized and properly modelled (e.g. Bos et al., 2010), nowadays the studies for prediction and prevention of subsidence-associated risks calculate

the linear rates on the basis of "data to source" and "residual to source" approaches (Dong et al., 2002), which not contemplate periodic components. Conversely, the studies focused on retrieving active tectonic processes remove the seasonal components from the original geodetic data on the basis of statistical models and rarely apply the "peering approach" (Dong et al., 2002), which allows to quantify influence, distribution and magnitude of individual processes and to understand the main mechanisms affecting the geodetic time series.

Differently from the mentioned approaches, herein a multi-component and multi-source procedure is proposed for individuating the physical mechanisms that better explain both the linear and the seasonal components, clearly exhibited by the geodetic time series. The proposed approach is "multi-component", because it investigates the linear component apart from the seasonal ones, and is "multi-source" in the sense it allows to define the key processes (sources) causing subsidence. This innovative approach is structured in steps based on multi-methodological and multi-disciplinary analyses, and on modelling of multiple processes.

The thesis is organized as follows: in Chap. 1 an overview is given on effects, occurrences and causes of the subsidence phenomena. Therein, crucial aspects are addressed, such as the integration among different monitoring techniques and the need of a proper vertical datum for making the different geodetic observations consistent and comparable. Then, the geodetic time series analysis is reported on, bearing in mind the importance of discriminating between permanent (or inelastic) and periodic (or elastic) ground displacements. Chap. 2. presents first a synthesis on the nowadays multi-methodological and multi-disciplinary procedures for studying land subsidence at regional scale. Then, the new approach is presented and discussed, pointing out specific aspects and limitations. Afterwards, Chap. 3 deals with the case study of the Po Delta, an area historically affected by land subsidence, where a continuous GNSS network operates and differential InSAR-derived time series are available. Finally, the conclusions synthetize the main results derived from the analytical and modelling phases applied to Po Delta and highlight the unresolved issues to carry on for future works.

Chapter 1

Land subsidence: state of the art

This Chapter describes the subsidence phenomenon according to the following frame: effects, observations and causes of subsidence. In particular, in the first part land subsidence is related to the human and environmental risk to point out the importance of its study. As the present PhD thesis is focused on delta systems, special emphasis is laid on the risk in coastal areas. The second part is devoted to the monitoring approach, fundamental for assessing subsidence, i.e. for orienting the damage prevention and mitigation. This part is not structured as a systematic review of the main monitoring tools, as it aims to highlight some crucial aspects of the integration among different monitoring techniques. A paragraph is also dedicated to clarify the reference levels of the measurements (normally corresponding to the mean sea level). In the third part the main processes governing both natural and anthropogenic subsidence are qualitatively described.

1.1   Land subsidence: effects, monitoring and causes

According to the most common definition given by Bates and Jackson (1980), subsidence is the "*sudden sinking or gradual downward settling of the Earth's surface with little or no horizontal motion*". It is a land lowering process, which tends to generate a depression in response to natural and anthropogenic causes (Carminati et al., 2006).

Although subsidence is differentiated in sudden and gradual processes, only the second meaning is dealt with in this study. Therefore, the term "subsidence" hereinafter used indicates the slow deepening of the soil, amounting to few millimeters per year, and it is not referred to the instantaneous fall down of the soil that occurs, for example, in the case of a sinkhole.

1.1.1. Subsidence effects & risks

Subsidence constitutes a risk for human health and economic activities because the downward ground movement is accompanied by both deformations of natural and anthropic surface elements and formation of depressions (Fig. 1.1).

Figure 1.1 – Examples of effects associated to subsidence: (a) house cracking in America; (b) change in surface water drainage in Holland; (c) landward incursion of seawater in Venice, Italy; (d) flooding in Italy.

The awareness of the risk associated to subsidence, especially to the man-induced subsidence, grew during the last few decades thanks to the cooperation between international organizations and associations of engineers and hydrological scientists. In particular, the United Nations Educational Scientific and Cultural Organization (UNESCO) and the International Association of Hydrological Science (IAHS) promoted worldwide many working groups and symposiums on land subsidence, with the aim to gather scientists, engineers and authorities and to discuss the occurrence of land subsidence, including remedial measures (Barends et al., 1995). The proceedings of these meetings (Tison, 1969; IAHS, 1977; Johnson et al., 1986; Johnson, 1991; Barends et al., 1995; Carbognin et al., 2000; Zhang et al., 2005; Carreón-Freyre et al., 2010; Daito and Galloway, 2015) clarified the environmental impact and the social harm in relation to the anthropogenic causes. In particular, these and other studies showed the relation between human development/population growth and ground sinking (Dang et al., 2014), and highlighted the role of the natural resources exploitation with respect to the subsidence risk (Fig. 1.2). In fact, it is demonstrated that the intense and programmatic exploitation of the underground resources

increases the occurrence of hazardous events and the presence of goods and people within the area exposed to risk (Ubertini, 2009).
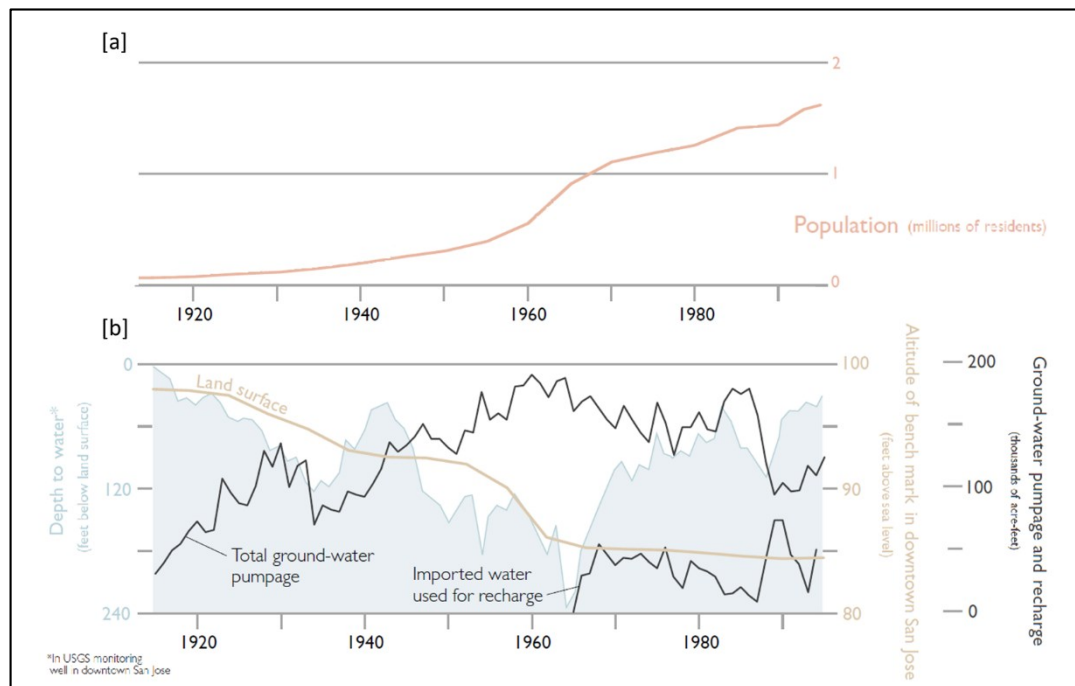

Figure 1.2 – Relation between population growth and water pumping at Santa Clara Valley (California, USA): (a) population growth; (b) pumped/recharged water and subsidence (modified after Ingebritsen and Jones, 1999).

Environmental and social harms caused by subsidence can be differentiated according to the natural contest in which the phenomenon occurs, whether in inland or in deltas and coastal areas (Galloway, 2014). The main environmental impact of the inland subsidence is given by alteration of the ground-surface gradients and, consequently, by changes in the runoff of surface water, water infiltration and in the groundwater recharging and discharging of the natural system. The alteration of the hydrological features also impacts on the ecosystems including drainage of wetland areas and formation of floods and ponds in depressed zones. The main social harms are: damage to buildings, roadways, canals, aqueducts, wells and pipelines; changes in the gradient of drainage ways (e.g. sewers, canals/aqueducts and streams) and, furthermore, formation of floods and ponds (Galloway, 2014). Otherwise, the main environmental impact of the coastal subsidence is the marine transgression, i.e. the landward incursion of seawater, which drowns the saltwater and freshwater marshes, causing the alteration of marsh ecosystem and associated biotic communities. Moreover, during the last decades, the frequency of flood events in deltas due to both man-induced soil compaction and reduced sediment deposition on floodplains (associated with the levee systems

5

construction), has increased alarmingly (Schmidt, 2015). Galloway (2014) indicates that the "*chief social harm in coastal subsidence-affected areas is coastal flooding from increased susceptibility to storms surges, but also flooding related to gradient reductions and reversals of streams and rivers coursing to the sea*". Figure 1.3 shows the storm effect in an urbanised US coastal area affected by man-induced subsidence.

Figure 1.3 – Storm impact in some urbanised USA coastal areas: Houston (a) Galveston Baytown; (b) Galveston Freeport.

Flooding risk on coasts is not only due to frequent and intense rainstorms that occur in subsiding areas, but also to subsidence associated with eustatic sea level rise (Yin et al., 2013). These two processes cause the rise of water level and potentially increase coastal or tidal flooding in the low-lying areas that were previously above high-tide level (Marfai and King, 2008). The induced anthropogenic subsidence may also alter the riverine flood hazard and the risk in flood-prone areas. Carisi et al. (2017) clarify that the presence of the levee systems favourites the growth of urban, industrial and agricultural areas on dyke-protected floodplains of the major rivers. These authors also suggest that "*many existing embankment systems were built centuries ago; they prevented the riverbed from gradually adapting to changes of topography induced by natural (and anthropogenic) land subsidence, and this may have resulted in significant modifications of the spatial distribution of flood hazard in the case of embankment failure*". Finally, several studies reveal that hydrodynamic inundation modelling is a useful modern approach for assessing and mapping flooding risk and point out that reliable results are obtained by using high resolution Digital Elevation Model (DEM) and accurate representations of the major topographic discontinuities, such as artificial irrigation lines and roads/railway. More complete simulations are needed for taking into account the potential

effects of ground-lowering gradients, which alter the safety level of river embankments and hence the flood hazard (Carisi et al., 2017).

1.1.2. General aspects of subsidence monitoring tools

The reduction of environmental and human risks may be possible by improving the understanding of subsidence processes. Subsidence monitoring is finalised to achieve this objective and therefore is the key activity for assessing ground-surface motions. Monitoring methodologies, which aim at measuring and mapping ground displacements, spatial gradients and temporal rates of regional and local subsidence (Galloway et al., 1999), are implemented for satellite, aerial, terrestrial and bathymetric surveys (Tab. 1.1).

Survey Category	Observation techniques	Acronym	References
Satellite	Global Positioning System	GPS	Bock and Melgar (2016)
Satellite	Interferometric Synthetic Aperture Radar	InSAR	Ye (2010); Tomas et al. (2014)
Aerial	LIght Detection And Ranging	LIDAR	Weitkamp (2005)
Aerial	Airborne SARs		Hensley et al. (2009)
Aerial	Photogrammetry		Glass (2013)
Terrestrial	Precise levelling		Schomaker and Berry (1981)
Terrestrial	Electronic Distance Measurement traversing	EDM	Rüeger (1990)
Terrestrial	Terrestrial Laser Scanning	TLS	Pfeifer and Lichti (2004)
Terrestrial	Ground-Based InSAR	GB-InSAR	Monserrat et al. (2014)
Terrestrial	Vertical extensometer		Riley (1986)
Terrestrial	Gravity-based		Torge (1986); Niebauer et al. (1995)
Terrestrial	Radioactive Marker Technique	RMT	Brambilla (2000)
Terrestrial	Deep Compaction Electromagnetic Monitoring		Verdecchia et al. (2011)
Terrestrial	Micro-seismic array		Maxwell et al. (2010)
Bathymetric	Sidescan sonar systems		Klaucke I. (2018)
Bathymetric	Multi Beam Echo Sounder	MBES	Lurton (2002)
Bathymetric	Seabed Pressure Gauge	SPG	Stenvold et al. (2006)

Table 1.1 – Observation techniques used for subsidence monitoring.

Tab. 1.1 contains the list of traditional and innovative techniques for subsidence monitoring and the references for finding detailed explanations on technologies, methodologies or applications. A more specific explanation of InSAR and GPS techniques will be given in Par. 2.1. in relation to the time series analysis, while the use of geodetic data derived from these tools will be detailed in Chap. 3 associated to the Po Delta case study. In particular, two aspects of the subsidence monitoring are herein addressed: the relation between monitoring tools and size of investigated processes and the importance of integration among different techniques.

As it concerns the first aspect, the monitoring instruments investigate different dynamic and kinematic components of the subsidence mechanisms (Fig. 1.4) and vary for costs, accuracy, spatial/temporal resolution, data type (punctual, linear or areal) and frequency of measures (Tomas et al., 2014). Fig. 1.4 points out that each monitoring tool provides a partial contribution to the identification of the processes driving subsidence. It also suggests that the integration of different tools enhances a more complete subsidence risk assessment and it is crucial for extracting high-precision data (Fabris et al., 2014). As it concerns the data accuracy, the degree of accuracy of high-precision levelling is lower than 1 mm per km (Bitelli et al., 2015), while Persistent Scatterers InSAR (PS-InSAR) (see also Par. 2.1.1.) can provide high density of information points with precision on the order of 1–2 mm per year. Global Navigation Satellite System (GNSS) permanent stations (see also Par. 2.1.2.) are able to provide measurements of velocity components with an accuracy of about 1 mm per year in the vertical component, after at least 3 years of continuous acquisition (Kontny and Bogusz, 2012).
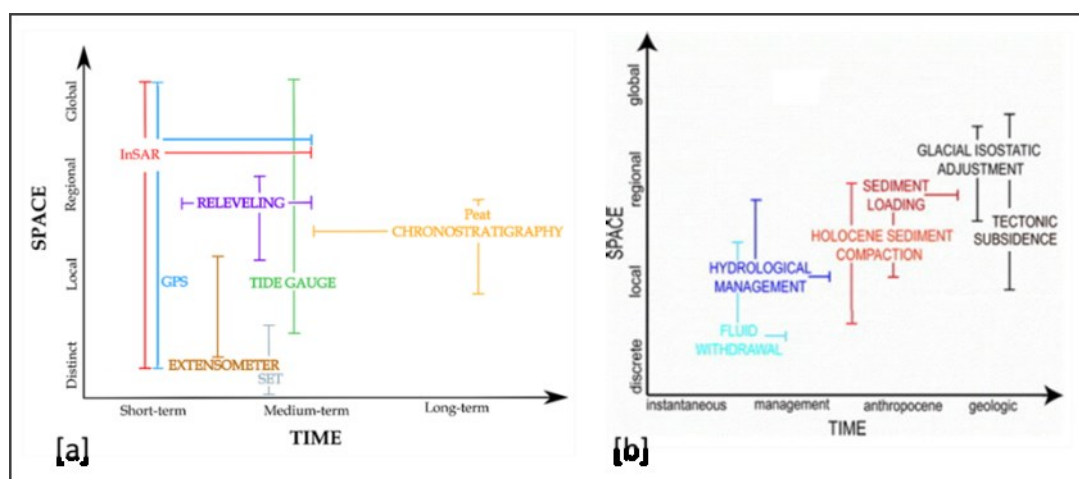
Figure 1.4 – Example of temporal and spatial scales resolution: (a) subsidence monitoring tools (modified after Kourkouli, 2015); time scale is defined as: short-term (0-1 year), medium-term (1-20 years) and long-term (20-400 years); (b) processes contributing to subsidence (modified after Yuill et al., 2009); time scale is defined as: instantaneous (0-1 year), management (1-20 years), Anthropocene (20-400 years) and geologic (more than 400 years).

With respect to the second aspect, Bitelli et al. (2015) explain that subsidence monitoring in the last few decades has followed the development of technology in the land surveying disciplines. Referring to the three main monitoring techniques (geodetic levelling, GNSS and InSAR), these authors assert that: *"Whereas geodetical infrastructures are available, the integration of the three techniques can constitute the best approach to the problem, when datum definition and transformations permit all the datasets can be aligned into a single reference frame. […] The study of subsidence, in a similar way as any other geodetic phenomenon that is described with respect to a geographically defined reference frame, requires the definition of a geometrical and velocity datum to allow the comparison between observations collected at different times (epochs). This datum can be defined according to geometrical criteria or external measurements (i.e. GNSS time series), or according to more qualitative criteria related to geological setting"*. Many scientific works today deal with this aspect and suggest both methodological and technological solutions. For instance, Fabris et al. (2014), while integrating data from high-precision levelling, differential InSAR and multi-temporal GPS surveys in the Po Delta (North Italy), provide a data checking procedure and a geoid undulations modelling in order to better compare ellipsoid and orthometric elevations, especially when historical benchmarks may have been lost and/or replaced with other points, but at different elevations. In the same area, Dacome et al. (2015) adopt a surveying technology able to collect measures from different techniques (two SAR corner reflectors, a Continuous GPS station and a levelling benchmark) keeping the same reference level, in order to improve data congruence and facilitate the integration.

1.1.3.   Subsidence monitoring and reference vertical datum

As already mentioned, the definition of vertical datum, namely the vertical component of the reference frame, is fundamental for integrating the elevation measures acquired by different tools. Furthermore, this aspect is important because the "mean sea level", normally considered as reference level for the ground elevation, is not stable over time.

Monitoring tools usually refer elevations to three surfaces that approximate the Earth's shape, defined as topography (or terrain), Geoid and Ellipsoid (Fig. 1.5a). Actually some observation techniques, mainly ground-based ones (e.g. hydrology, bore-hole stratigraphy, etc.), refer measurements to topography. The Geoid is a gravitational equipotential surface that is oriented everywhere perpendicular to the force of gravity and is used as a reference for heights above sea

level, while the Ellipsoid is a purely mathematical imaginary surface that approximates the geoid and it is used as a reference for geodetic latitude and longitude (Bock and Melgar, 2016).
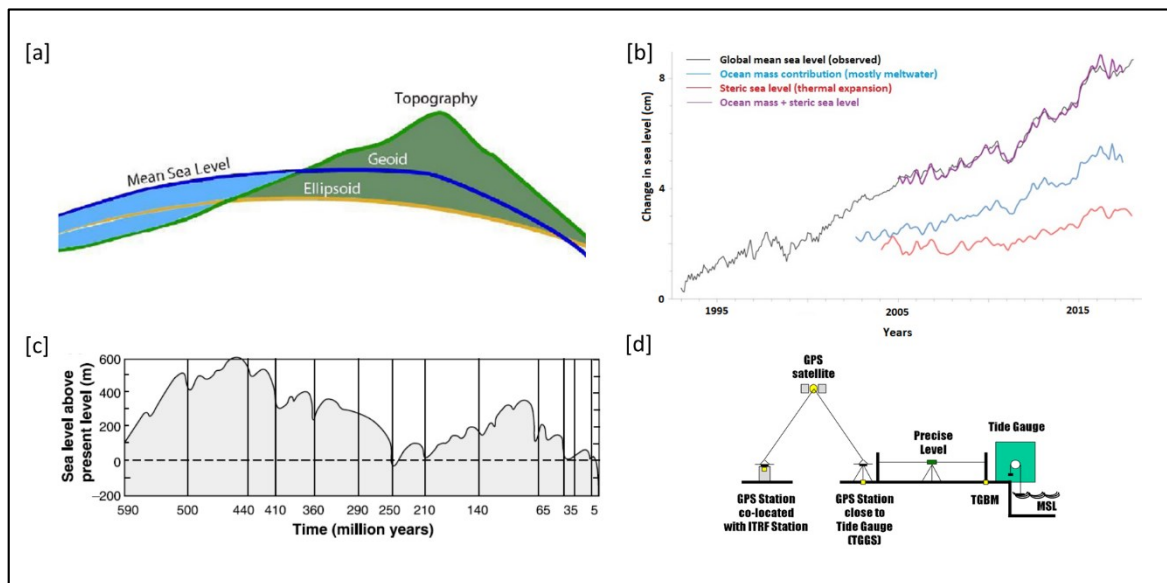

Figure 1.5 – Aspects related to reference levels: (a) reference surfaces (from Bock and Melgar, 2016); (b) sea level rise from 1993 to 2017 and main contributions (modified after NOAA 2018); (c) global sea level change through geological time (modified after Lambeck and Chappell, 2001); (d) schematic network from tidal to geodetic stations for acquiring absolute sea level data (Woodworth, teaching material).

Elevation on land, or topography, is measured with respect to the 'mean sea level' as represented by the geoid; over the oceans the topography is obtained by radar altimeters as the difference between the remotely sensed surface and the reference geoid determined by gravity measurements (Bock and Melgar, 2016). GPS observations are provided with respect to an Earth-centered global oblate ellipsoid rotating with the Earth (e.g. World Geodetic System 1984), and these measures are independent of gravity. GPS positions are expressed in terms of geodetic latitude, longitude and height above the reference ellipsoid WGS84. The height of the geoid relative to the reference ellipsoid is called "geoidal undulation". It depends on the direction and intensity of gravity at any point and ranges between -105 m and 85 m over the Earth (Bock and Melgar, 2016). The spirit levelling and the satellite gravity observations provide the detailed global gravimetric model useful to realize the geoidal surface and the connection to GPS observations through the geoidal undulation.

As it concerns the "mean sea level", global sea level data from 1901 to 2010 show a sea level rise rate ranging between 1.5 and 1.9 mm/yr (Stocker et al., 2014). These variations are classified according to changes in ocean volume/density and ocean mass (Bock and Melgar, 2016; IPCC, 2013).

Sea level changes, both globally and locally, resulting from changes in water density are called steric, and could be even related to deformation of the solid Earth for thermal expansion (thermos-steric sea level change). Global mean sea level change resulting from change in the mass of the ocean, as due for instance to the melting of land ice, is called barystatic. Both these processes are active today (Fig. 1.5b) and responsible of sea level changes of several hundred meters in the past millions of years (Fig. 1.5c). Lambeck and Chappell (2001) assume that the tectonic forces have induced changes through geological time in the ocean basin geometry, causing the main variations in the sea level. Conversely, during the Quaternary the periodic exchange of mass between ice sheets and oceans has been the dominant contribution to the sea level change.

It is worth to note that the estimate of the sea level rise may be apparent because the tide gauge stations are relative to a fixed point of the land, which is affected in many cases by subsidence or uplift. Satellite radar altimetry over the oceans provides a direct measurement of the sea surface (dynamic) topography and does not suffer from the susceptibility of sparse tide gauge measurements to vertical land motion. Otherwise, GNSS site position data from a global network of tracking stations are absolute with respect to a global terrestrial reference frame (ITRF) and can be also used to supplement and calibrate other observational systems including satellite radar altimeters, satellite gravimeters, and tide gauges (Bock and Melgar, 2016). Fig. 1.5d shows an ideal system for acquiring absolute measurements of sea level.

1.1.4. Subsidence causes

Defining the causes of the land subsidence is not an easy target because the subsidence is a complex phenomenon generally resulting from the contribution of different processes. Indeed, such processes, which are characterized by a specific origin and may act in different spatial and temporal intervals, can overlap giving rise to a single land movement effect, whose individual causes can hardly be discriminated. Moreover, these processes involve different geoscience disciplines (e.g. geology, geophysics, geothecnics, meteorology and hydrology) and thus a wide earth science knowledge is required for a proper analysis of the subsidence phenomenon. Therefore, the subsidence causes are herein not exhaustively dealt with, but only qualitatively described in accordance with the scientific knowledge achieved over the last fifty years.

With respect to the phenomenon complexity, land subsidence can occur by natural or anthropogenic drivers, which induce the onset of, or accelerate, natural processes (Galloway, 2014). The natural contribution is related mainly to geodynamic, sedimentological and climatic processes

(Carminati et al., 2006), while the anthropogenic driver is mainly due to fluid (oil and gases) withdrawal and groundwater pumping (Poland, 1984; Dang et al., 2014). Land subsidence acts at local (from few to tens of km) or regional scale (from tens to hundreds of km): the natural causes may act at both scales (Johnson, 1991), while the anthropogenic causes act mainly at local scale. Finally, the processes responsible for the ground lowering act from short to long time (from years to millions of years) and the duration of the subsidence effect is strictly related to the origin of the process and its evolution. For instance, due to geodynamic processes, many basins show higher subsidence rates during the initial phase of basin formation (syn-rift) and lower rate in the following period (post-rift) (Fig. 1.6a). This "subsidence behaviour" is due to lithospheric stretching during the syn-rift phase and to thickening for thermal cooling during the post-rift (e.g., McKenzie, 1978). Another example refers to the soil mechanics (Fig. 1.6b) and regards the settlement due to consolidation (e.g., Terzaghi and Peck, 1967). In case of urbanization on recent alluvial deposits, the over-imposed loads induce settlement due to the combination of primary consolidation processes and secondary compression. Settlements ascribable to the primary consolidation process are largely greater than those ascribable to the secondary compression and relative to the viscous behaviour of very fine-grained soils and organic soils (Stramondo et al., 2008).
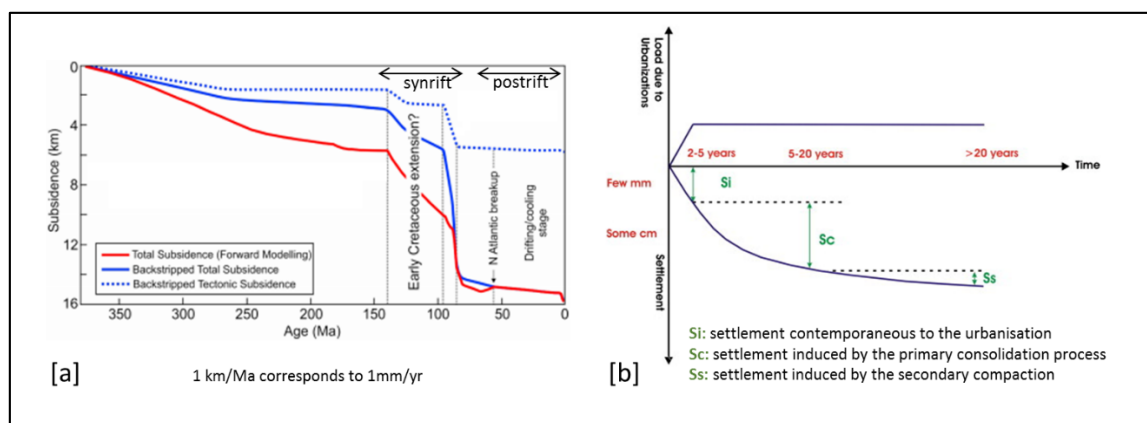

Figure 1.6 - Relevance of the time parameter in the processes causing subsidence: (a) subsidence in the Træna Basin (Norway) due to geodynamics (modified after Zastrozhnov et al., 2018); (b) subsidence in the city of Rome (Italy) due to soil mechanics (modified after Stramondo et al., 2008).

Regarding the progressive understanding of the causes, a first significant description of the processes that govern subsidence is found in Prokopovich (1972; 1979): based on data collected in the US, the author classifies subsidence in "endogenic", or caused by Earth's interior processes, and "exogenic", or caused by Earth's surface processes (Fig. 1.7). Fig. 1.7 shows that the endogenic

processes are natural and fundamentally due to plate tectonics (e.g., top magma chamber that sinks as effect of partial chamber emptying, formation of grabens), while the exogenic mechanisms are both natural and anthropogenic (e.g. hydrocompaction, piezometric decline due to aquifer depletion, oxidation of organic particles, melting of ice).
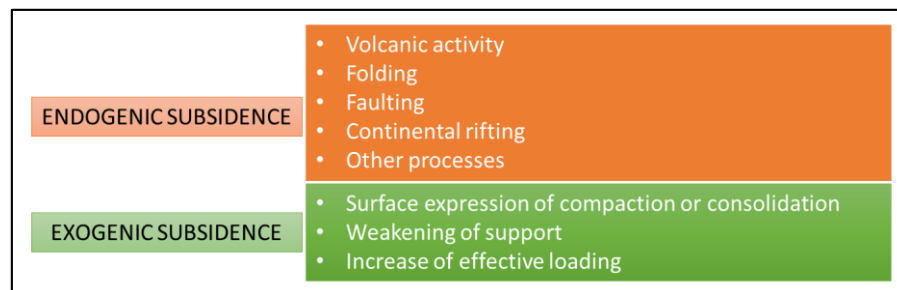

Figure 1.7 – Subsidence classification according to Prokopovich (1979).

In the same period, many case histories on subsidence collected from engineering's activity provided data useful for describing both natural and anthropogenic causes through qualitative and quantitative approaches. In particular, Allen (1984) indicates five different compaction causes: natural loading, drainage in clay and peat of low-lying areas, vibration during earthquakes, hydrocompaction due to low rainfall and fluid withdrawal. Moreover, Poland et al. (1984) differentiate the fluid extraction in three main types: withdrawal of oil, gas and associated water; withdrawal of hot water or steam for geothermal power; withdrawal of ground water. They also provide an accurate physical and mathematical description of mechanisms and properties (e.g. theory of the aquifer-system compaction, analysis of stresses causing subsidence, layers' compressibility and storage characteristics). Moreover, in relation with agricultural issues, Glopper and Ritzema (1984) propose also the loss of soil particles as a result of the oxidation of organic matter and the leaching of mineral components. Such examples refer essentially to near-surface sediment compaction processes that, in many cases, act at local or reservoir scale.

As it regards the subsidence at regional scale, likely related to processes occurring at great depths, Allen (1984) mentions the subsidence due to lateral flow of plastic material (e.g., salt), while Royden and Keen (1980) study the rifting processes. In this regard, a great impulse in quantifying crustal and rifting processes and, consequently, tectonic subsidence, derives from the basin modelling activity performed in the petroleum industry. Such a kind of modeling starts to be used for exploring the sedimentary basin formation and for quantifying burial and thermal processes, which influence the hydrocarbon generation (Hantschel and Kauerauf, 2009).

Today, many studies reveal a good understanding of some anthropogenic and natural processes: for instance, Gambolati and Teatini (2015) present a thorough review on the relation between vertical ground motion and geomechanics due to extracted/injected fluids; Oude Essink and Kooi (2012) quantify at regional scale the effect of saltwater intrusion on groundwater system and on land subsidence; other authors address their researches on the interplay between subsidence rates and fault kinematics, or in general deal with land displacements in relation with tectonic and non-tectonic processes, on the basis of GPS and InSAR data (e.g. Fuhrmann et al., 2013; Peyret et al., 2013; Karakhanian et al., 2013). Beside these improvements, great attention is given also to man-induced processes (Fig. 1.8). In particular, among the main anthropogenic drivers, Galloway (2014) indicates: the oxidation induced by drainage, the induced erosion, the induced thawing of permafrost and the sediment starvation, although he stresses that the occurrence of subsidence in particular regions in the world depends on the distribution of the geological features (e.g. sediment types, rock dynamics) and on the anthropogenic subsidence that overlays the existing natural processes.
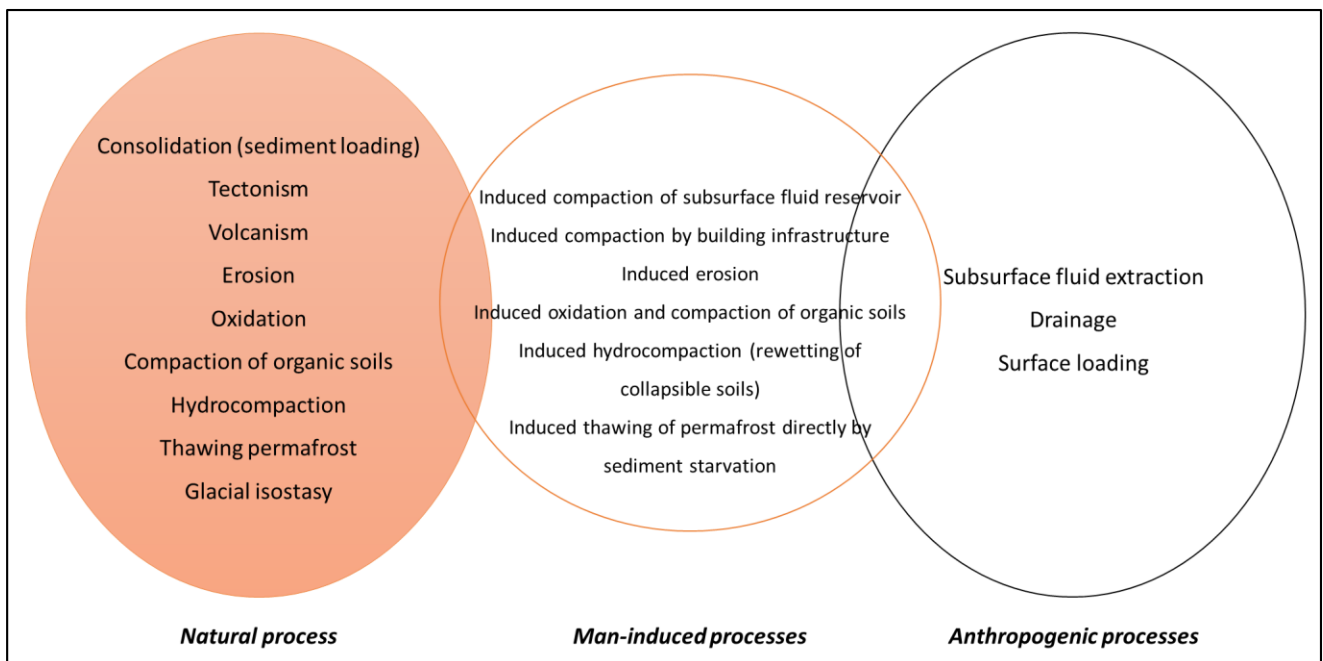

Figure 1.8 - Description of subsidence causes according to Galloway (2014).

Chapter 2

From classical methods to a new multi-component and multi-source approach for studying land subsidence in deltas

The complexity of the subsidence phenomenon described in Chap. 1 points out an essential item in the study approach: the cooperative effort among different disciplines during the phases of data collection, analysis and modelling (cfr. Allen, 1984). For this reason, in the following Chapter, the main focus is devoted to regional scale studies that better integrate aspects regarding different scientific fields (geodesy, geology, geophysics, soil mechanics, hydrology and meteorology).

2.1. Current techniques for measuring subsidence: time series analysis

Most of the subsidence studies can be led to the fundamental relation:

$$S_{meas} = C_n + C_a \, , \tag{1}$$

where S_{meas} indicates the subsidence measured by whatever monitoring tools, C_n and C_a are the natural and anthropogenic components, respectively. Due to the temporal resolution of the geodetic data and the nature of the investigated process (see also Par. 1.1.2.), some studies identify the S_{meas} with a constant rate of ground lowering. This assumption is reasonable when the process that causes subsidence is acting since long time without changing, like the geological processes that take place in thousands or millions of years. Meanwhile, there are some natural and anthropogenic mechanisms that cause non-uniform strains on the ground. For instance, Galloway (2014) states that the geological materials deform in response to natural and anthropogenic perturbations (e.g., natural tidal and atmospheric loading), while anthropogenic loads imposed on the land (e.g. built infrastructure) cause measureable elastic and non-elastic displacements.

In the next section, a brief description of geodetic time series analysis is given, as it allows to measure the subsidence discriminating the main components that contribute to the ground motions.

2.1.1. Interferometry Synthetic Aperture Radar

One of the techniques to detect the Earth's surface displacements is the Interferometry Synthetic Aperture Radar (InSAR). It allows to obtain high resolution images from data acquired by side-looking radar instruments carried by aircraft or spacecraft (Curlander and McDonough, 1991). The basic concept of the interferometry is to combine pairs images, acquired in different dates, for generating a set of differential interferograms that contain information on the interferometric phase (Rosen et al., 2000; Hanssen, 2001). Differential interferograms comprise the ground displacement component, due to the different acquisition times of the two SAR images, plus other terms that contribute to the interferometric phase. According to Hanssen et al. (2001), the interferometric phase (ψ_{int}) can be expressed as:

$$\psi_{int} = \psi_{flat} + \psi_{topo} + \psi_{mov} + \psi_{atmos} + \psi_{noise} \,, \qquad (2)$$

where ψ_{flat} is the flat-earth component related to orbit errors, ψ_{topo} is the topographic phase commonly referred to DEM error, ψ_{mov} is the phase change due to the pixel movement in the satellite Line-of-Sight (LOS) direction, ψ_{atmos} is the difference in atmospheric phase delay between passes due to atmospheric disturbances or artefacts and ψ_{noise} is the phase noise due to both variabilities in scattering and thermal noise. In particular, the effect of the topographic undulation needs to be corrected from the SAR backscatter images (Luckman, 1998; Sun et al., 2002; Soja et al, 2010) and the process of correcting for topography is sometimes referred to as differential InSAR (DInSAR) (Hooper et al., 2012). As shown in equation (2), the interferometric phase contains not only the ground displacement term, but also other components that needs to be isolated during the data processing because they could mask the ground displacement information (Fig. 2.1).
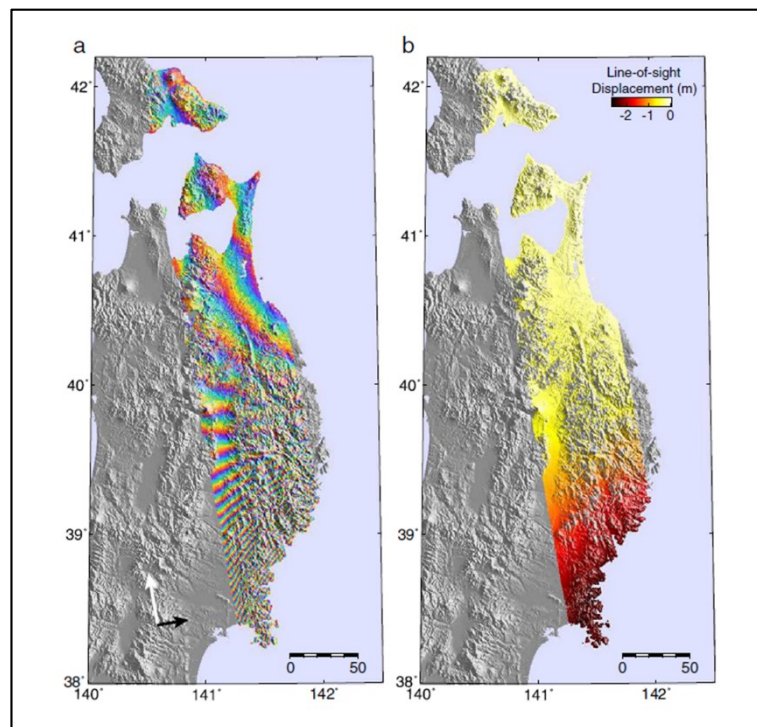
Figure 2.1 - Example of interferogram displaying co-seismic deformation due to Tohoku-oki earthquake – 2011 (Japan): (a) displayed interferometric phase, (b) displacements after processing (from Hooper et al., 2012).

Moreover, the degradation of the interferometric phase quality (decorrelation), which is due to the relative movement of the scatterers (e.g. change in land cover) or to the change in the sight direction of the radar platform, impact not-homogenously on the interferograms (Tomas et al., 2014). This aspect can be improved by selecting more reliable pixels from a set of interferograms, where decorrelation noise is minimised. In addition, signal can be also affected by other effects (e.g., small strain in plate motion), and this aspect can be solved by estimating the non-deformation signal through the combination of synthetic time series obtained from conventionally formed interferograms or by filtering (Hooper et al., 2012). The algorithms for the time series analysis, developed to better address these two aspects, are divided in two categories: Persistent Scatterers InSAR (PS-InSAR) (Ferretti at al., 2001) and Small BAseline Subset (SBAS) (Berardino et al., 2002). The former is based on measuring single and highly coherent permanent scatterers, the latter combines multiple interferograms using small geometric and temporal baselines and considers the sum of many independent small distributed scatterers. In addition, other techniques can be used to estimate the SAR-derived subsidence, such as the Interferometric Point Target Analysis (IPTA) (Werner et al., 2003), which is an implementation of the PS-InSAR technique, the Coherent Pixel

Technique (CPT) (Blanco-Sánchez et al., 2008), the Stanford Method for Persistent Scatterers (SMPS) (Hooper et al., 2004) and the SqueeSAR™ (Ferretti et al., 2011). In general, these techniques provide information on subsidence distribution, magnitude and kinematics, as well as on the data processing quality (Tomas et al., 2014). Furthermore, the InSAR data are measured respect to the LOS and are represented as maps, namely spatial distribution of displacement, either average rates (average displacement respect to the considered time period, expressed in mm/yr or cm/yr) or accumulated magnitude (total amount of subsidence with respect to the first SAR acquisition, expressed in mm or cm). Spatial resolution of the ground displacement data depends on the radar sensor and the processing algorithm: for instance, the amplitude criterion of pixel selection allows to keep the original resolution of the SAR image. The temporal resolution depends on the satellite revisiting period, which determines the availability of SAR images: short revisiting period improves the possibility to identify seasonal patterns (Fig. 2.2a). Data acquired in areas with high subsidence rates can be affected by aliasing effect, which occurs when the sampling frequency is too low and the motion between two dates is greater than the system resolution (half of the radar wavelet, $\lambda/2$). Finally, areas with waters and vegetation disperse the radar-emitted SAR signals and reduce the amplitude of the returned signals, while areas associated to urbanization or rock outcrops provide stable electromagnetic response over time (Fig. 2.2b).
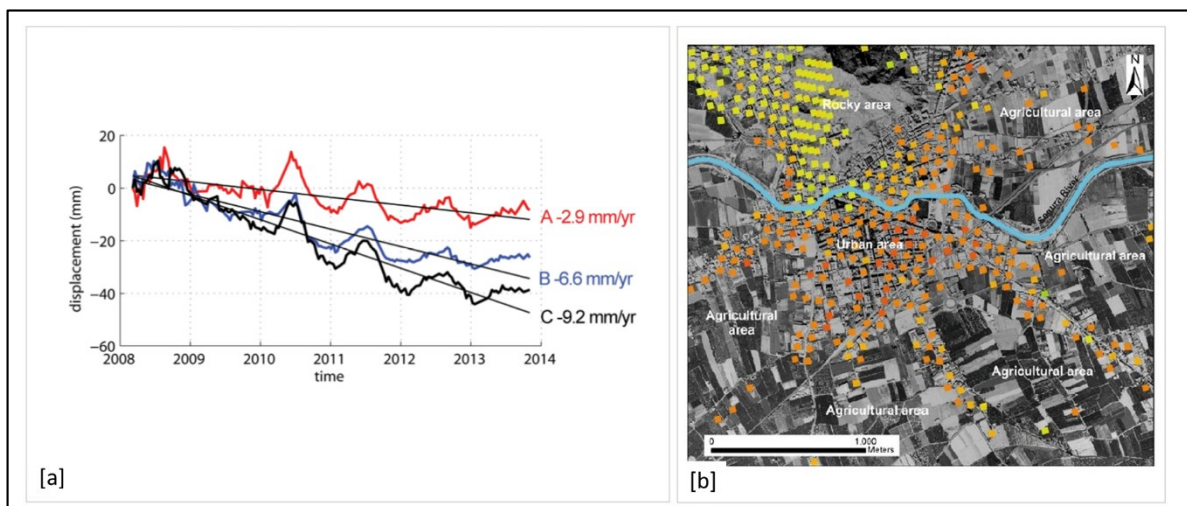

Figure 2.2 – Example of InSAR-derived displacement time-series. (a) Displacement patterns through time and main rates in three different points (A, B and C); InSAR data are from TerraSAR-X interferometry at Jesolo, Italy (modified after Tosi et al., 2018). (b) High and low density of Permanent Scatterers (PSs) in urban/rocky and agricultural areas at Orihuela, Spain (modified after Tomas et al., 2014).

2.1.2. Continuous Global Positioning System

Another crucial monitoring technique for studying solid Earth and atmospheric processes that drive natural hazards, weather and climate on global and regional scales, is the Continuous Global Positioning System (CGPS). CGPS is part of the more generic Global Navigation Satellite System (GNSS), which provides autonomous geo-spatial positioning with global coverage and includes, for instance, the Russian GLONASS, the European Galileo, the Chinese BeiDou and other regional systems (Bock and Melgar, 2016).

During the acquisition stage, GPS data are sampled at a rate of, typically, 15 or 30 s, aggregated into daily files, stored in a standard international format (RINEX) and archived at several global data centers under the auspices of the International GNSS Service (IGS) and other geodetic organizations. During the data processing stage, the GPS data are analysed by two steps to provide station position estimates (X, Y, Z) in daily Earth-centered terrestrial reference frame (ITRF) positions. The first step corresponds to a relative or differential positioning approach, developed for positioning stations with respect to at least one fixed reference station, within a local or regional network. The second one is the precise point positioning (PPP), introduced for individually estimating local and regional station positions directly with respect to a global reference network, the same used to estimate the satellite orbits (Bock and Melgar, 2016). These processing strategies or algorithms are implemented in software packages, such as Bernese (Beutler et al., 2001), GAMIT-GLOBK (Herring et al., 2008) and GIPSY-OASIS (Webb and Zumberge, 1997). The coordinates can be then transformed into more intuitive local topocentric displacements in the North, East and Up directions (ΔN, ΔE, ΔU), with respect to station positions (X_0, Y_0, Z_0) at an initial epoch t_0. Afterwards, the time series analysis can be performed component by component since the correlations between the local displacement components are small (Zhang, 1996).

As suggested by Bock and Melgar (2016), the time series of the individual component of the observed motion, *y(t)*, can be described by the analytical model (Nikolaidis, 2002):

$$y(t_i) = a + bt_i + c\sin(2\pi t_i) + d\cos(2\pi t_i) + e\sin(4\pi t_i) + f\cos(4\pi t_i)$$
$$+ \sum_{j=1}^{n_g} g_j H(t_i - T_{gj}) + v_i \,, \tag{3}$$

where t_i, for i = 1, ..., N, are the daily solution epochs in units of years and *H* is the Heaviside step function. The first two terms are the site position, *a*, and the linear rate, *b*, respectively. Coefficients *c* and *d* describe the annual periodic motion, while *e* and *f* describe the semi-annual motion. The

next term corrects for any number (n_g) of offsets, with magnitudes g and epochs T_g, and v_i is the error term. The data are cleaned using an outlier detection algorithm and modelled to create time series of position residuals, which are then examined for repeatability and noise content (Nikolaidis, 2002). After estimating the correlated noise amplitudes, the modelled time series is re-modelled to attain more realistic uncertainties of model parameters (linear trend, periodic terms, etc.). The noise analysis is based on the power spectral density (PSD) and the maximum likelihood estimator (MLE), while the final parameter estimates are obtained by several iterations through the weighted last squares algorithm. Fig. 2.3 shows an example of simultaneous estimation of linear trend, annual and semi-annual sinusoids with constant phase and amplitude in a CGPS time series. This procedure is generally indicated as the standard model.
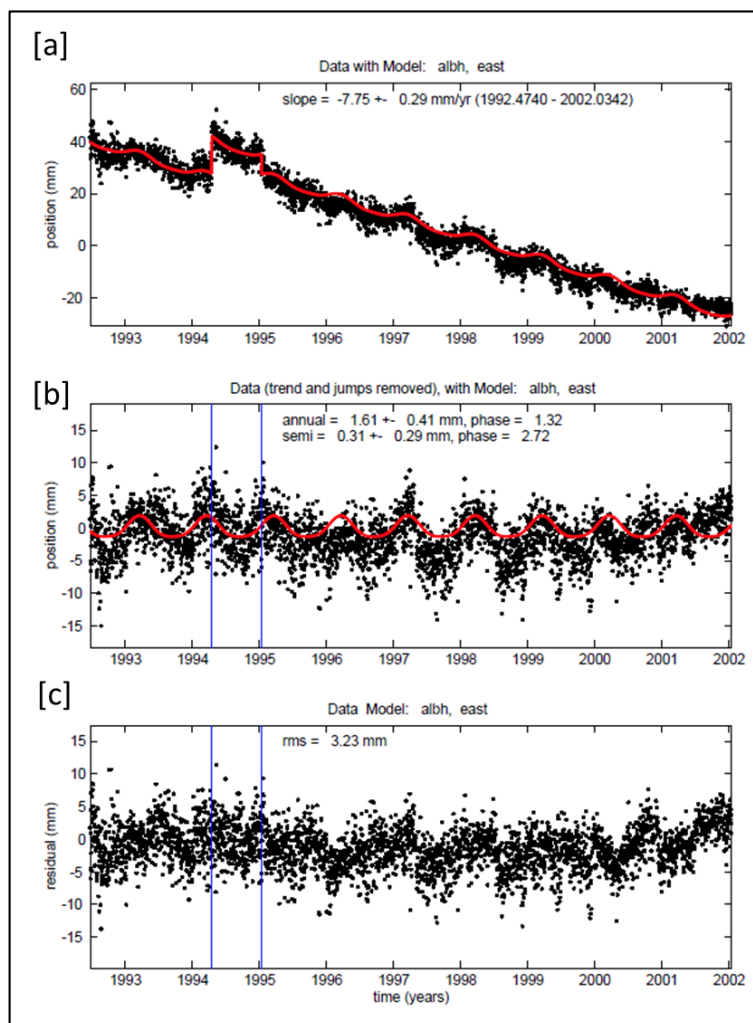
Figure 2.3 - Example of GPS time series analysis along East direction (from Nikolaidis, 2002): (a) standard model (red line includes two instrumental offsets, linear and annual periodic signal), (b) daily solutions after linear trend and offsets removal, (c) final residual (model subtracted from data).

As it regards the physical processes exhibited within the geodetic time series, some of them, which have power mainly at diurnal and semi-diurnal frequencies (e.g. solid Earth tides and ocean tide loading), are modelled and reduced in the processing stage (Teferle et al., 2008). Other periodic terms with annual or semi-annual frequencies (e.g. atmospheric and hydrological loading, human exploitation) or transient (e.g. earthquakes) are partially modelled or are absorbed into the error term during the time series analysis stage. However, in this case the processes-related uncertainty is large or unknown, especially at local scale (Teferle et al., 2008).

The influence of the seasonal signals on the GPS-derived velocity estimates is studied by several authors: for instance, Blewitt and Lavallée (2002) demonstrate that the annual signals affect the velocity uncertainties, and that the velocity bias becomes negligible after ~4.5 years of data time span, while it increases if the time series are extended less than 2.5 years. With respect to the short time series, Bos et al. (2010) suggest estimating the noise properties in order to reduce the trend error. Santamarìa-Gomez et al. (2011) analyse the noise content within time series from 2.5 to 13 years long by testing several noise models and describe the bias velocity decreasing with the increasing of data time span.

With respect to the nature of the observed seasonal variations, Dong et al. (2002) reveal that the joint contributions from surface mass redistribution (atmosphere, ocean, snow, and soil moisture) are the primary causes for the observed annual vertical variations of site positions. Bos et al. (2010) mention the importance of having a methodology to estimate, for any station, how much the accuracy of the linear trend will improve when trying to subtract the annual signal from the GPS time-series by using a physical model. Finally, Davis et al. (2012) highlight that, during the time series analysis, neglecting the stochastic component, as in case of standard model, may significantly affect the velocity estimates and their uncertainties (Fig. 2.4).
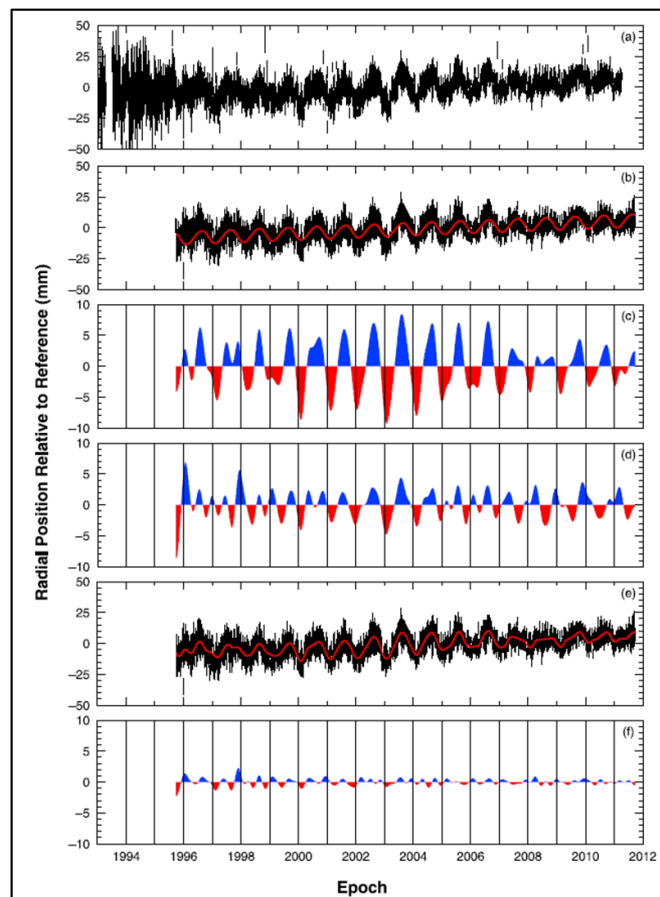
Figure 2.4 – Example of procedures for estimating the seasonal component: (a) original time series; (b) fit using standard model (red line); (c) time series after band-pass filtering; (d) band-pass-filtered residuals to the standard model; (e) fit using stochastic model (linear Kalman filter); (f) band-pass-filtered residuals to the stochastic model (from Davis et al., 2012).

2.2. Classical study approaches

Recent studies have shown similar methodological approaches for understanding the origin of the regional subsidence that occurs in inland and coastal areas. For instance, Raspini et al. (2013) compare the displacement map derived from InSAR data with the geological information, while Higgins et al. (2014) superimpose paleo-river channels on the GPS-calibrated InSAR map, finding clear correlations with soil distribution. Sanabria et al. (2013) present a more quantitative approach by comparing geodetic map with piezometric levels and soft soil thickness. Karegar et al. (2016) use an analytical approach to compare GPS-derived displacements with groundwater and sediment thickness trends, and, in addition, account for Holocene sea level rise and model glacial isostatic adjustment. Smith et al. (2017) innovate the use of InSAR information and formulate a quantitative relation for obtaining hydraulic head from InSAR data and calculating the inelastic deformation due

to groundwater pumping. Therefore, all the most recent studies investigate one or two possible sources of the subsidence through qualitative or quantitative methodologies.

Briefly, the state of the art indicates three main methodological paths for understanding the physical processes (sources) by means of their geodetic measurable effects (data):

1) data to source;

2) residual to source;

3) peering.

These approaches were introduced and shortly described for the first time by Dong et al. (2002) within the pioneering paper that dealt with the seasonal variations observed in the CGPS time series. These authors analysed more than four hundred CGPS stations for retrieving the main natural causes of the annual signals, neglecting the anthropogenic processes. Differently from Dong et al. (2002), the mentioned methods are herein considered three valid procedures for investigating the sources of both periodic and permanent components to land subsidence, i.e. for identifying both natural and anthropogenic causes of subsidence. Specifically, we consider such approaches as a compass to orient the general recognition of strengths and weaknesses of each subsidence study, also within the Po Delta Area. The detailed description of these methods provided in the following paragraph represents the basis for better clarifying the innovative items of the new approach proposed in the current work (Par. 2.3.).

2.2.1. Data to Source

The main issue of this approach is the knowledge of the relevant sources, which means that some of the acting processes are known and monitorable with the geodetic data. Indeed, Dong et al. (2002) state that: "*To explore the nature of the observed seasonal variations, an ideal approach is to compare the observed values with the joint contributions from all relevant sources*". Starting from this statement and extending it also to the permanent trend, the scheme of Approach 1 may be defined and organized in three main steps (Fig. 2.5): the first step corresponds to the time series analysis, which is necessary to recognize the components of the geodetic signal; in the second step, a component is selected according to available data and process comprehension; in the third step, the chosen geodetic component is compared with data or modelling results related to the relevant sources. The quoted authors also highlight some difficulties inherent in this methodology because

many relevant sources are not well understood. Therefore, it is clear that one of the approach limitations is the definition of the criteria for differentiating between relevant and not-relevant processes.
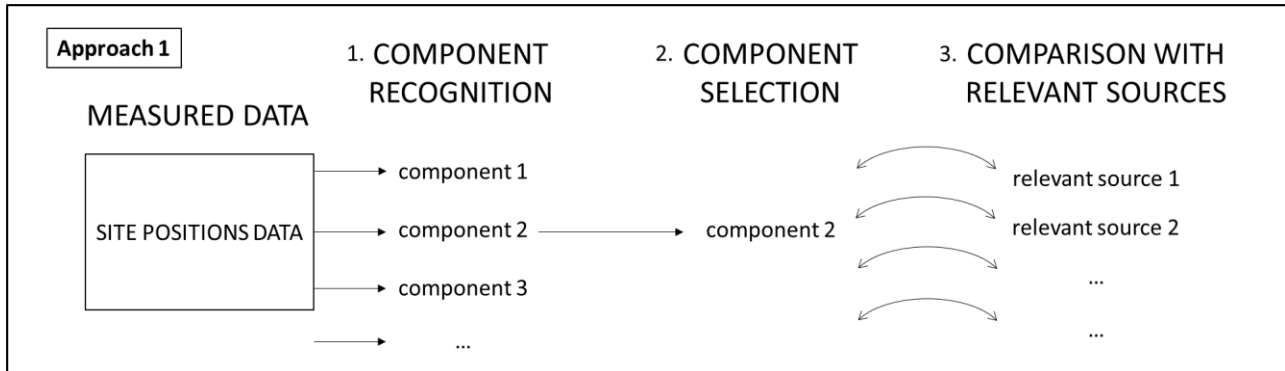

Figure 2.5 – Scheme of Approach 1: Data to Source.

An example of Approach 1 is traceable in the subsidence study proposed by Tosi et al. (2009). They focus on the velocity component of the vertical ground motion and use the subsidence rate derived from SIMS, which stands for Subsidence Integrated Monitoring System (Teatini et al., 2005), by integrating at regional scale five different monitoring techniques: spirit levelling, differential GPS, continuous GPS, InSAR and IPTA. With respect to the relevant processes, Tosi et al. (2009) investigate several sources and modify the following basic relation described by Carminati and Di Donato (1999):

$$V_{tot} = V_t + V_{sl} + V_c + V_{pgr} + V_a \,, \tag{4}$$

where V_{tot} is the measured total subsidence rate, V_t, V_{sl}, V_c and V_{pgr} are the natural contributions related to tectonic, sediment loading, sediment compaction and post glacial rebound, respectively, and V_a is the anthropogenic component. Based on Carminati and Di Donato's findings (1999), Tosi et al. (2009) consider relevant two of the natural terms of the proposed equation (4) (i.e., V_t and V_c) and enlarge the contributions given by the anthropogenic sources (V_a). On the basis of a "weight criterion", they neglect the terms V_{sl} and V_{pgr} because they reach rates around 0.2 - 0.3 mm/yr and 0.1 mm/yr, respectively, while the total natural subsidence rate ranges between 0.9 and 1.6 mm/yr. Moreover, the authors introduce the new equation:

$$V_{tot} = V_t + V_c + V_m + V_{ch} + V_l \,, \tag{5}$$

where V_m, V_{ch} and V_l are due to the anthropogenic component and, in particular, correspond to the compaction due to mechanical processes (water withdrawal), chemical processes (salinization of clay pore fluid and peat oxidation) and load of buildings, respectively.

It is worth to note that in the study of Tosi et al. (2009) the sources of motion differentiate on the basis of the depth, specifically distinguished in deep, medium and shallow causes. The deep causes act at depths generally greater than 400 m (below mean sea level), in relation with the movement of the pre-Quaternary basement. The medium causes act at depths between 400 m and 50 m depending on the compressible clay layers and the groundwater withdrawals. The shallow causes, acting between 50 m and the ground surface, are related to: thickness and compressible behaviour of the Pleistocene-Holocene deposits; geochemical compaction due to the increase of salt concentration in the clayey sediments; oxidation of the outcropping organic soils drained by land reclamation. Therefore, the methodology used by Tosi et al. (2009) and synthetized in Fig. 2.6, although focused only on one component of the ground motion (velocity), can be considered as a reference point for regional studies on land subsidence in coastal areas, especially for the use of displacement data derived from an integrated monitoring system and for the broad investigation of anthropogenic causes. Contrarily, the comparison between measured ground displacements and source-related data needs improvement, since it is based on qualitative descriptions and semi-quantitative procedures. In fact, only the sediment compaction and the peat oxidation processes are dealt with analytical procedures or modelling (Gambolati et al., 2005), while the remaining sources are mainly qualitatively described. Afterwards, Tosi et al. (2009) improve some of the highlighted qualitative aspects: for instance, the subsidence due to primary compaction of Holocene strata is enhanced in Teatini et al. (2011), while the subsidence due to groundwater exploitation and to load of buildings is quantitatively described in Da Lio et al. (2013) and Tosi et al. (2013), respectively.
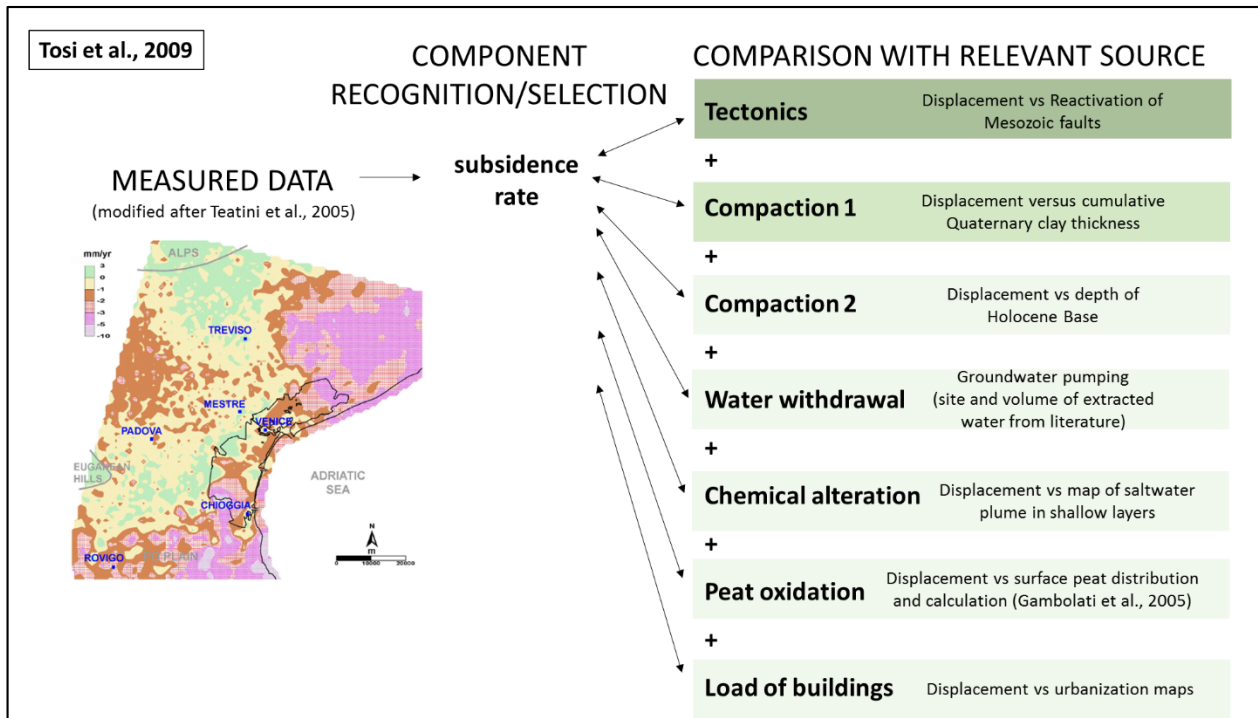
Figure 2.6 – Scheme of Approach 1 applied to the study of Tosi et al. (2009). In the column of relevant sources, the green colour scale represents the depth-dependent processes (deep processes in dark green, shallow processes in light green).

2.2.2. Residual to Source

The main issue of this approach is the possibility to investigate the less known sources, i.e. the remaining ones, after the residual calculation. Indeed, according to Dong et al. (2002), the aim of the approach *"is to subtract the contributions of the well determined or modelled sources from the observation data first, then study the relation between the observed residual seasonal variations with remaining contributors"*. Based on this description, it is possible to draft the scheme of Approach 2 introducing five main steps (Fig. 2.7).

An example of this approach is found in Carminati and Di Donato (1999) and Carminati and Martinelli (2002). According to these authors, the equation (4) can be completed by considering also the two terms of the anthropogenic component, i.e.:

$$V_{tot} = V_t + V_{sl} + V_c + V_{pgr} + V_{cl} + V_{loc} ,\qquad (6),$$

where V_{cl} is the global contribution associated with the sea-level rise, due to climatic warming induced by industrialization, and V_{loc} is the contribution induced by local human activities.

As shown in Fig. 2.8, the geological and the anthropogenic components of the vertical movement act on different time scales (millions to thousands of years and hundreds to tens of years, respectively), and this peculiarity allows one to calculate separately each component.
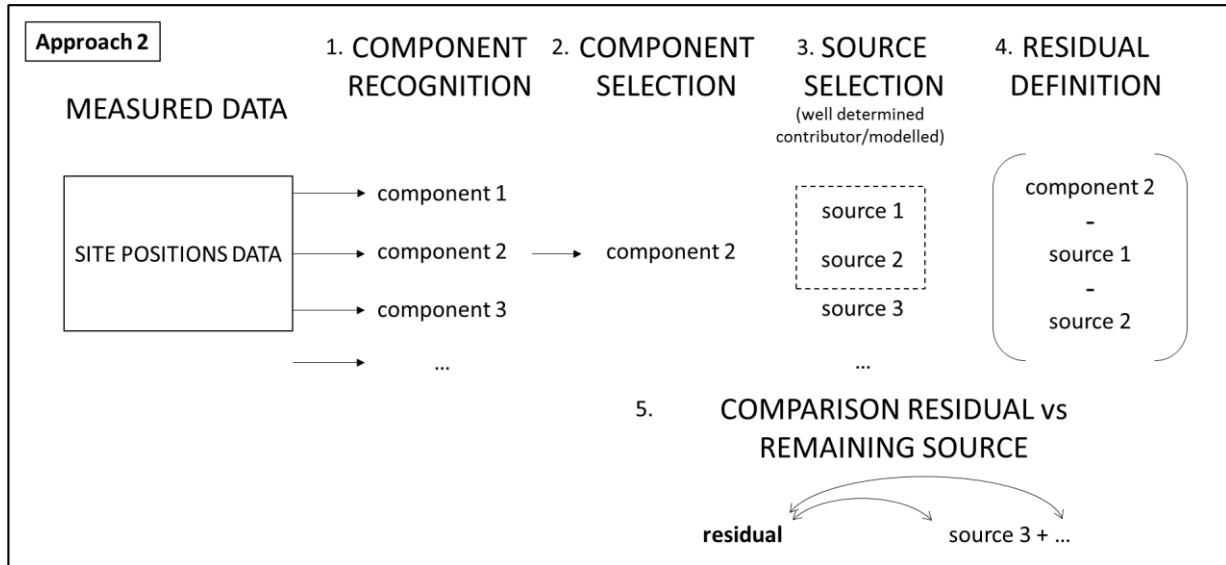
Figure 2.7 – Scheme of Approach 2: Residual to Source.
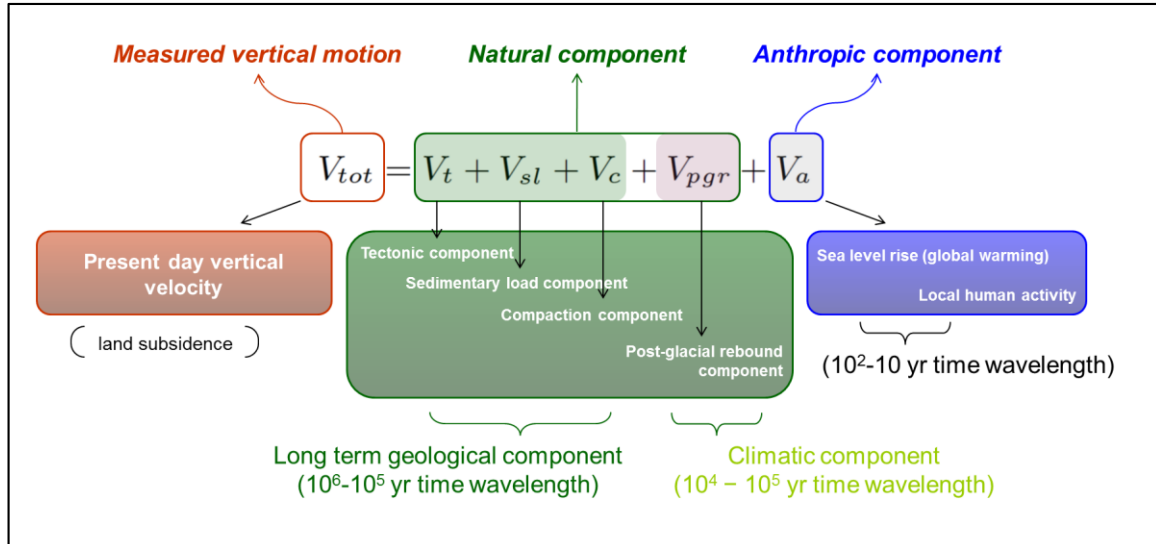
Figure 2.8 – Components and contributions to subsidence according to Carminati and Di Donato (1999).

The methodology behind their study consists in retrieving the local anthropogenic contribution (V_{loc}) by knowing the other terms of equation (6). In particular, the rate of the vertical ground movement is estimated through geodetic data, while the geological and climatic components are modelled by using the backstripping procedure (Sclater and Christie, 1980) and the analytical scheme based on

the normal mode technique (Vermeersen et al., 1997), respectively. The anthropogenic component of sea level rise related to the global warming is calculated by comparing trends derived from a global study with local patterns obtained from tide gauge stations. The results provided by the modelling are validated by using analyses of archaeological, palynological and paleontological data. Finally, the residual is compared with information related to aquifers (dating and chemical composition of groundwater, hydrogeological properties, years and volumes of extracted groundwater) and tectonics (active thrusts). Fig. 2.9 shows the scheme of Carminati and Martinelli's methodology (2002) according to Approach 2.

As the study of Tosi et al. (2009), also the work of Carminati and Martinelli (2002) can be considered as a reference for evaluating regional subsidence through a multidisciplinary approach. The strength of their study is the quantification, through a modelling procedure, of the geological processes acting on the Earth's surface but rooted in the lithosphere, while the limit is the simplified assumptions in the geological model (i.e., stratigraphic model) due to the poor data availability.
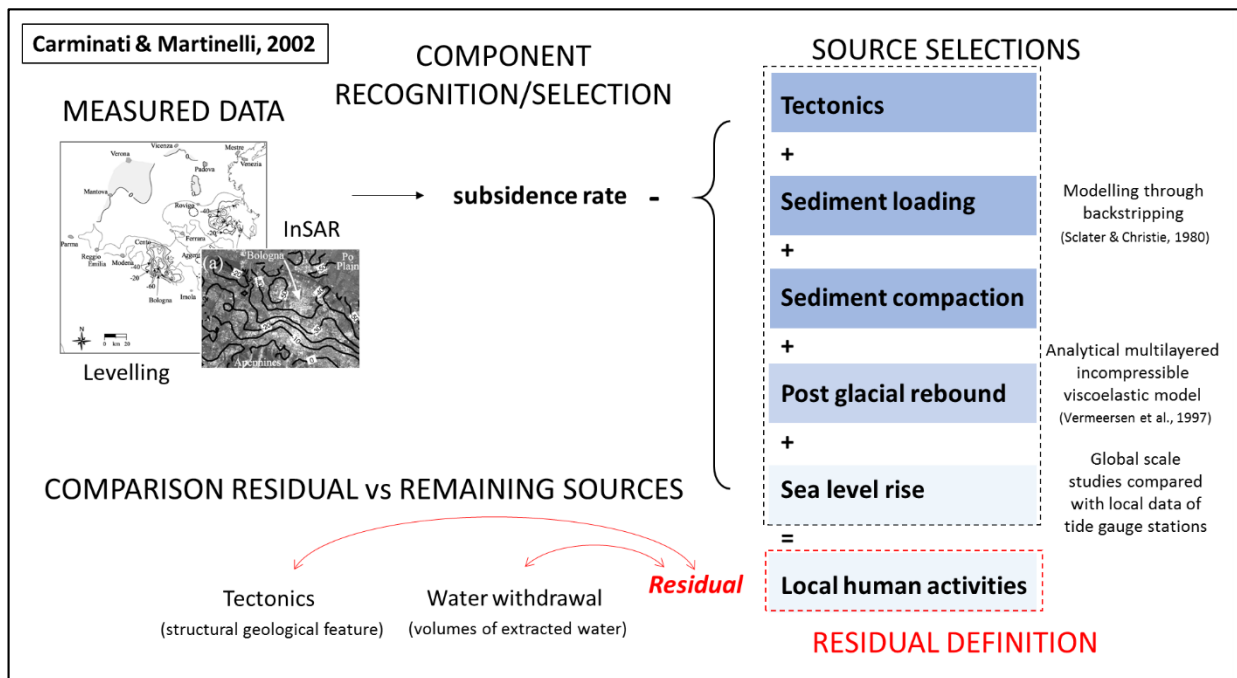
Figure 2.9 - Scheme of Approach 2 applied to the study of Carminati and Martinelli (2002). In the column of source selections, the blue colour scale represents time-dependent processes (geological time processes in dark blue, anthropogenic and recent processes in light blue).

Afterwards, Carminati et al. (2003a; 2003b; 2006) improve the proposed methodology adding other considerations related to glacio-isostatic mechanisms or to geodynamics (subduction and thrusting). It is worth to note that their perspective of separating the time-dependent mechanisms,

is quite similar to the one proposed by Tosi et al. (2009) (see Par. 2.2.1.) concerning the depth-dependent mechanisms. Indeed, the former authors use a simplified model for computing the compaction process (one Quaternary layer) and consequently calculate only the "deep" compaction. The latter authors, by using a more refined stratigraphic geometry, determine the sediment compaction also at medium depth.

2.2.3. Peering Approach

In the third approach, defined by Dong et al. (2002) as *"peering approach"*, *"the observed apparent seasonal variations of site positions include contributions from various geophysical processes, as well as from errors in modeling seasonal effects. There is no single dominant contributor. It is difficult to obtain a clear picture of the observed seasonal variations by analysing the contribution from just a single source"*. Specifically, the authors examine the influence, distribution and magnitude of individual geophysical sources and define this approach "peering" because it is a way to depict the contributions of the comparatively well-known seasonal sources to get insight into the relatively poorly known contributors. In other words, based on the assumption that "a priori" there is no single source playing a dominant role, they compare the joint contribution of these geophysical sources with the observed seasonal variations. Fig. 2.10 shows a schematic representation of the "peering approach", while Fig. 2.11 shows its application to the study presented by Dong et al. (2002). In this study, indeed, the authors evaluate the contributions from pole tide effects, ocean tide loading, atmospheric loading, non-tidal oceanic mass and groundwater loading. They model the pole tide geometrical correction through the formulas adopted by the International Earth Rotation Service (McCarthy, 1996) and calculate the oceanic response to surface pressure variations on the basis of the inverted barometer model (Dickman, 1988; Fu and Pihos, 1994). Furthermore, they compute the mass redistribution from variations of snow cover and soil moisture derived from the assimilated model (Kanamitsu et al., 1999; Roads et al., 1999). It is worth noting that the strength of their study is the quantitative comparison between data and modelling results, while its weakness is the absence of "indicators" driving the source choice before modelling.

After the peering approach, Dong et al. (2002) also apply the Approach 2 by removing the seasonal effects from the observations, in order to investigate the contributions from other sources (e.g., wet troposphere effects, bedrock thermal expansion, errors in phase centre variation models and errors in orbital modelling).
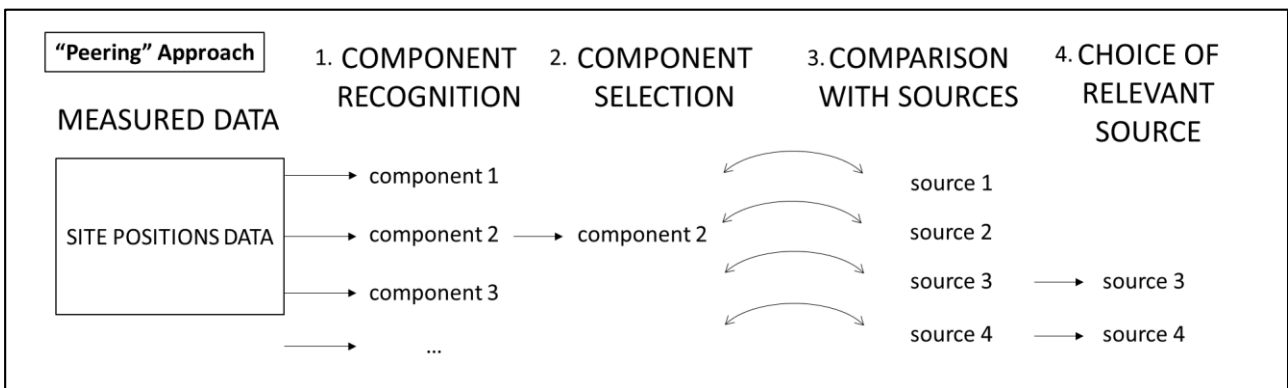
Figure 2.10 - Scheme of Approach 3: Peering Approach.
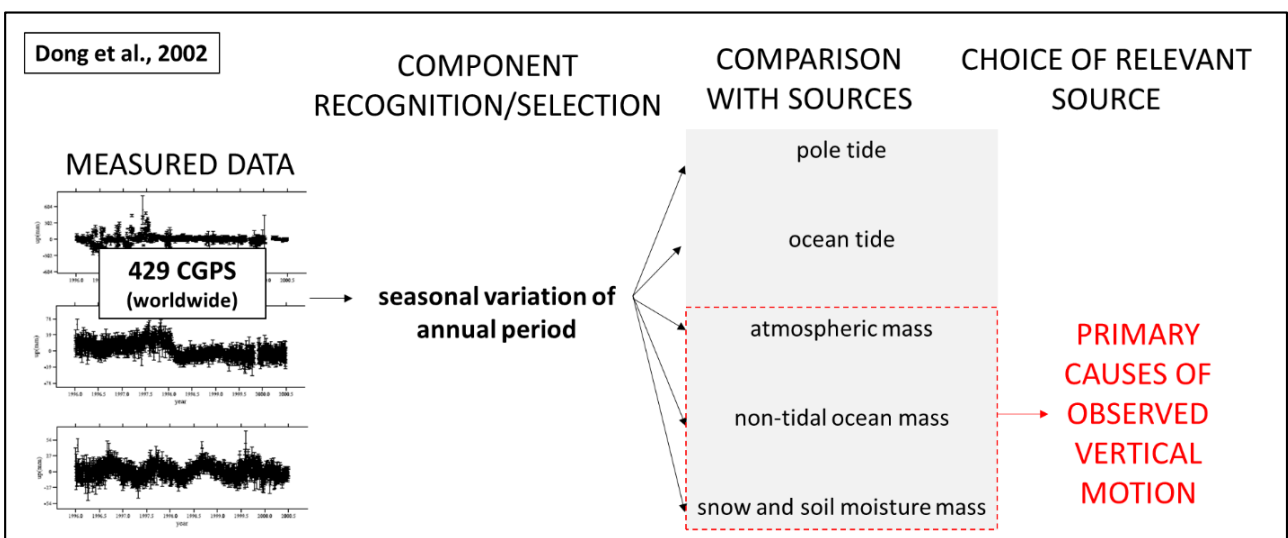
Figure 2.11 - Scheme of Approach 3 applied to the study of Dong et al. (2002).

2.3. A new multi-component and multi-source approach

Deltas and coastal areas are crucial places for life and economic development of a country, harbouring small towns and megacities, feeding agricultural activities and fishing, and hosting important ecosystems. These complex natural systems, although modified over the centuries by human interventions, are founded on a delicate water-land balance that strongly depends on climatic variability. For instance, it is well known that seasonal precipitations changes are spatially variable and depend on climate change over a region (e.g. IPCC, 2001) or that the sediment input to deltaic and estuarine areas is associated with episodic pulsing events climate-related, such as major storms events and river floods (Day et al., 2011). As described in the Par. 1.1.1, it is also clear that climate variability constitutes, as well as subsidence, a hazardous factor of the flooding risk, both in lowlands or coastal regions and in flat inland areas. The seasonal and periodic components of the

water cycle (precipitation, runoff, evaporation) are well studied, but the influence of the hydrological processes on ground dynamics is poorly understood. Moreover, although the periodic components observed in the geodetic signal affect the estimate of the geodetic velocity (see Par. 2.1.2.), studies dealing with prediction and prevention of risks associated to subsidence neglect the periodic component and assess just the permanent component using the "data to source" approach (Par. 2.2.1.) or the "residual to source" approach (see Par. 2.2.2.). Conversely, in the studies targeting tectonics, the seasonal component is removed from the original geodetic data through statistical models or filtering techniques, and, rarely by applying physically-based models, as shown in the case of the "peering" approach (see Par. 2.2.3.).

The new approach herein proposed is aimed at understanding the influence of climate-driven hydrological processes on the dynamics of the Earth's surface and at providing new methodologies that allow to predict more accurate subsidence rates, especially in the most vulnerable delta regions.

2.3.1. Main features and limits of the proposed procedure

Description of the new approach

The multi-component and multi-source approach aims to identify the physical mechanisms that better explain both linear and seasonal signals clearly exhibited by the geodetic time series. The proposed approach is "multi-component", since investigates the permanent component of subsidence apart from the periodic ones, and "multi-source", because it attempts to define the relevant processes causing subsidence (sources). The new approach is structured in three main steps based on multi-methodological and multi-disciplinary analyses, and on modelling of multiple processes (Fig. 2.12). Standard statistical methods and wavelet analysis are first applied to the geodetic time series for extracting the individual components (Step 1). Then, comparative analyses, performed through standard linear and non-linear techniques (e.g. cross wavelet transform and wavelet transform coherence analyses), are used for comparing geodetic data with datasets of different nature (e.g., meteorological, hydrological, hydrogeological, mareographic and weather data), in order to find correlation between land and hydrologic system and to infer possible sources (Step 2). Finally, the latter are validated through physically-based models (Step 3).
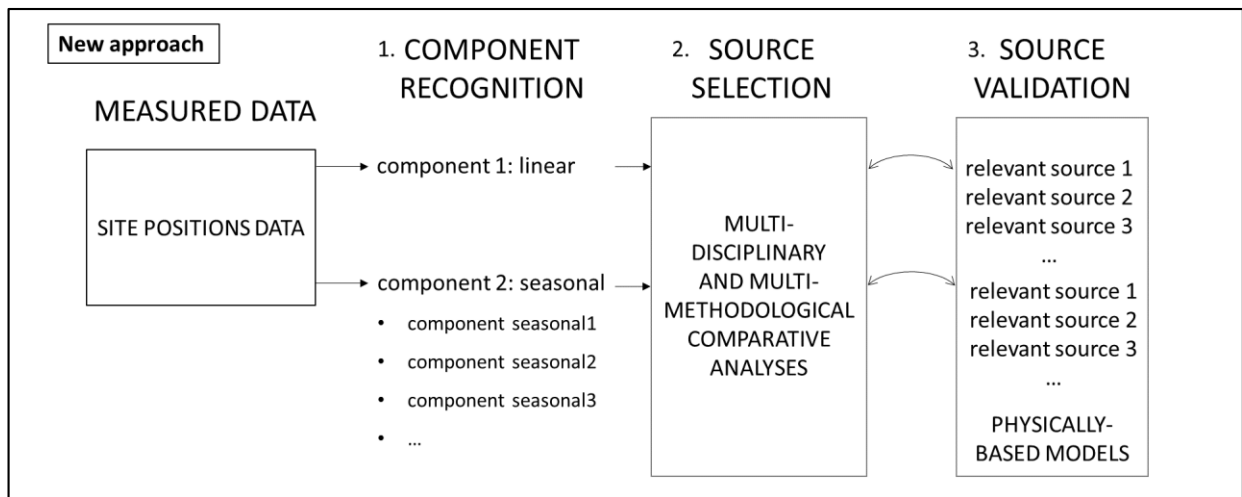
Figure 2.12 – Scheme of the proposed multi-component and multi-source approach.

Different aspects are herein illustrated in order to better explain the proposed procedure.

A first aspect is related to the analytical techniques used for developing the Steps 1 ("component recognition") and 2 ("source selection"). The choice of the most suitable analytical technique depends mainly on the sampling rate of the available data, but also on the scale of the process to investigate. For instance, Wavelet Analyses (WA) require signals with constant sampling rates and allow achieving multi-scale data details by comparing simultaneously local amplitudes, frequencies and phases of the analysed signal patterns (e.g. Grinsted et al., 2004). Other linear statistical techniques, such as the Centered Moving Average (CMA), can be applied to data with inhomogeneous sampling rates for investigating multi-scale dependences. The main drawbacks of this technique is that the obtained trends extend over time length shorter than the original one. The outcomes can be then extended to the original time span, using function estimates. An example of such a kind of function will be presented in Chap. 3, wherein a natural smoothing spline will be used for extending the CMA (the resulting curve it will be named "smoothed CMA").

A second aspect is related to the estimate of the geodetic velocity before and after the Step 3 ("source validation"). As depicted in Fig. 2.13, the permanent component is first calculated by a linear fit analysis of the original data, as it also occurs in the standard procedure of the time series analysis (see also Par. 2.1.2.). The fit is used to residuate the original signal and then the residual signal is analysed for recognizing the seasonal components (Step 1). Afterwards, original data, linear trend and residuals are compared with other databases through multi-disciplinary and multi-methodological analyses for individuating possible sources (Step 2). Finally, linear trend and residuals are compared with the physically-based modelling results (Step 3). If the models match with the seasonal components in term of phase, amplitude and frequency, a final geodetic velocity

is calculated from original data residuated for the computed seasonal signals. The final geodetic velocity, which might be coincident with the subsidence rate, is obtained on a new residual time series, derived removing the physically-based models from the original data.
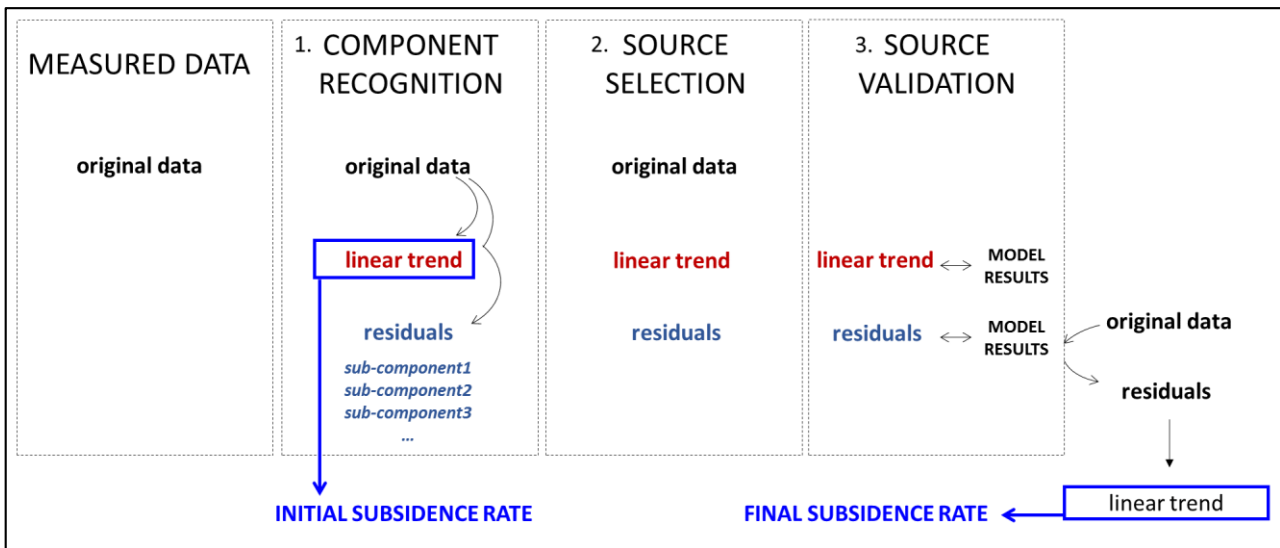
Figure 2.13 – Relation between steps of the proposed approach and calculated subsidence rates.

The third aspect involves mainly the Step 2 ("source selection") and concerns the physical processes responsible for the periodic component observed in the vertical land movement (Fig. 2.14). While the sources responsible of the slow and continuous downward ground movement are less influenced by climate and partially controlled by water movement, the sources that act at shallow depth and/or on the Earth's surface causing the seasonal ground oscillations, may be strongly dependent on climate and water movement. These sources may be grouped in water mass-dependent processes and in water pressure-dependent processes. The former is associated with the elastic response of the Earth's surface to the water mass change (rain, river and sea water), while the latter are related to the elastic compaction and expansion of the fine-grained thin layers within the aquifer, caused by the pore-pressure changes (groundwater).
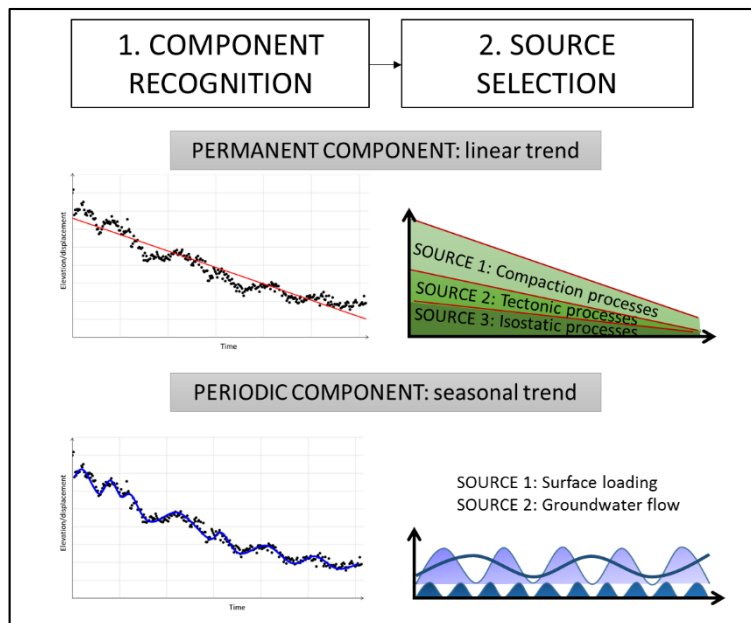
Figure 2.14 – Main physical mechanisms (sources) that may explain the different components of land motion.

In the current work, it is assumed that the occurrence of these processes is mainly driven by the lithological composition of soil (topsoil and subsoil) and shallow sedimentary coverage layers (bedrock): in presence of impermeable soil (e.g. clay-rich soil), water infiltration through the Earth's surface may be inhibited, while water- runoff and loading may be favoured; in case of permeable or partially permeable topsoil, water infiltration may occur changing topsoil moisture weight and thus favouring loading process on subsoil; in presence of permeable soil, rain or river water may reach bedrock by infiltration and generate pressure-dependent mechanisms. In Fig. 2.15 three different lithological compositions of soil and bedrock are presented, with associated mechanisms and ideal ground level rebound to the increase or decrease of water supply. When a permeable and vegetated terrain forms the topsoil, rainfall might change the soil moisture mass in correspondence of the floodplain, causing the occurrence of hydrological loading effects on the Earth's surface (Fig. 2.15a). According to the elastic rebound, a peak of rainwater supply corresponds to a depression in the ground level. Conversely, when impermeable soil extents homogeneously from the floodplain to the sea, the loading effect of the river mass dominates over the hydrological loading (Fig. 2.15b). Riverbanks might be influenced by river oscillations as well as littoral zones by sea level fluctuations (Fig. 2.15b). In this case, a peak in river or sea level corresponds to a ground down lift. In presence of permeable soil and bedrock constituted by permeable layers with interbedded fine-grained sediments, the infiltration of rain, river and sea water might become dominant in controlling the groundwater table variations within the shallow aquifer. Groundwater flow is accompanied by

expansion and contraction of fine sediments and a peak of water supply might be associated to an uplift of ground level (Fig. 2.15c).
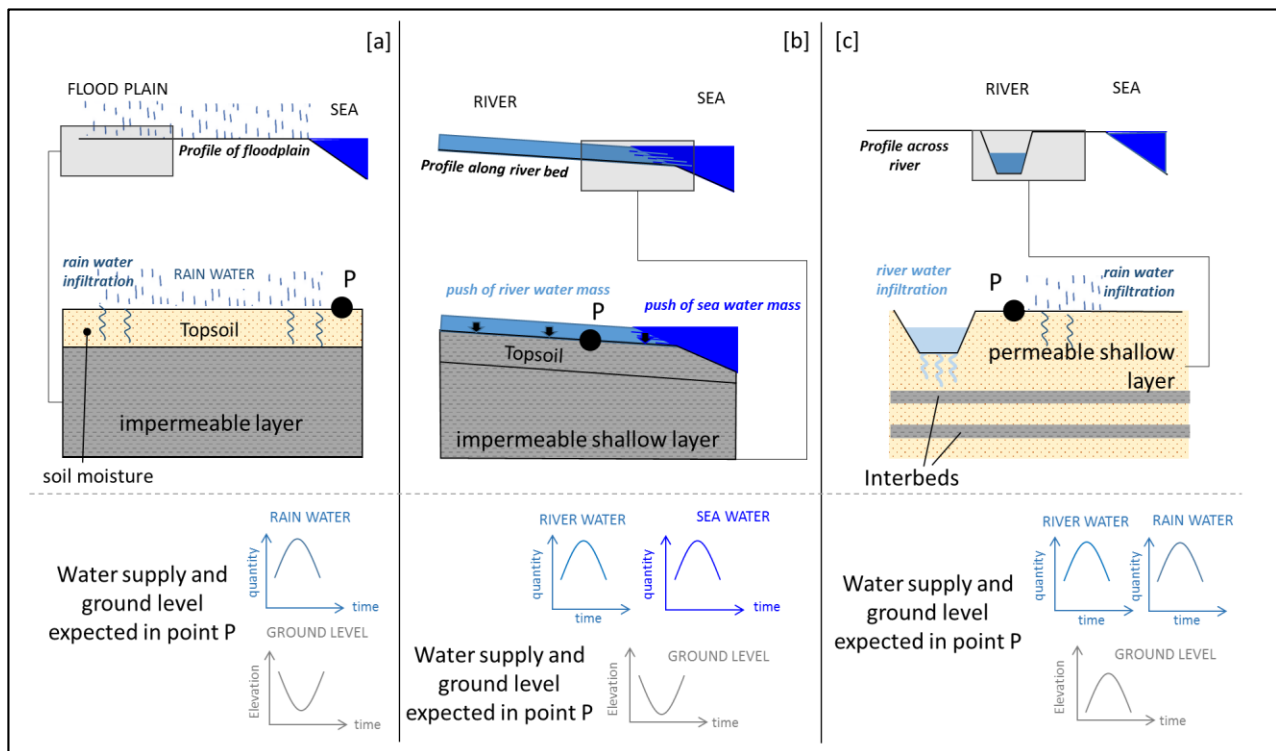
Figure 2.15 – Ground level movement in response to water supply, in presence of: a) topsoil formed by permeable terrain; b) topsoil composed by impermeable terrain; c) soil and bedrock (shallow layer) composed by permeable terrains.

With respect to the permanent component of subsidence, it is worth to note that the long-term geological contributions (see also Par. 2.2.2.) may be evaluated by modelling the geological processes (tectonic subsidence, sediment loading and sedimentary compaction) through the backstripping procedure (Allen and Allen, 2005), which is commonly used in the basin analysis for assessing the burial history of a sedimentary basin in relation to the petroleum generation. In accordance with this procedure, the sedimentary load is progressively removed from a basin and the sedimentary layers are corrected for compaction, paleo-water depth (PWD) and paleo-sea level (PSL) changes, in order to reveal the tectonic contribution driving basin subsidence (Lee et al., 2016). Although most of the studies based on backstripping technique refer to thick sedimentary layers (several thousand of meters), few recent studies validate the possibility to apply this procedure also to thin and shallow sedimentary sequences (e.g. Maselli et al., 2010). In case of thin depositional sequence (tens of meters), subsidence velocity estimates associated to the geo-history reconstruction are strongly influenced by few meters of PWD or PSL changes. Fig. 2.16 shows an

example of different subsidence velocity estimates obtained neglecting PWD and PSL (Fig. 2.16b), accounting for PWD (Fig. 2.16c) and accounting for PWD plus PSL (Fig. 2.16d).
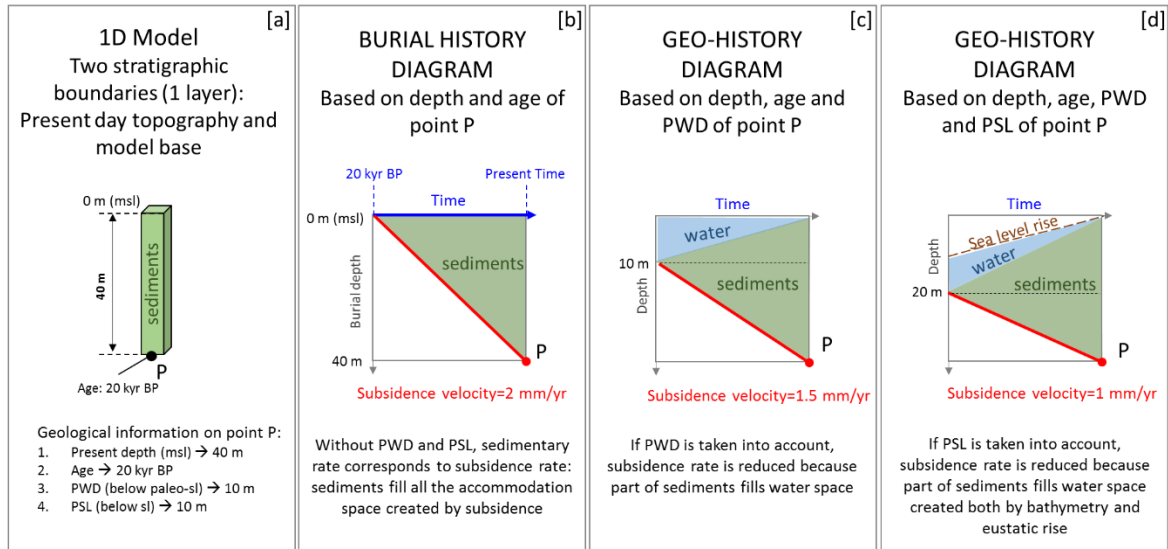
Figure 2.16 – Example of subsidence velocity estimates on 1D synthetic model using geological information: a) 1D model parameters; b) burial diagram obtained taking into account only sedimentation rate; geo-history diagram based on sedimentation rate and PWD (c), on sedimentation rate, PWD and PSL (d). It is worth to note that diagram is called "burial" if sedimentary rate is only used, while it is called "geo-history" if information on bathymetric and eustatic water depths are known.

Fig. 2.17 shows different subsidence velocity estimates obtained not applying and applying the backstripping procedure (Fig. 2.17b and 2.17d, respectively).
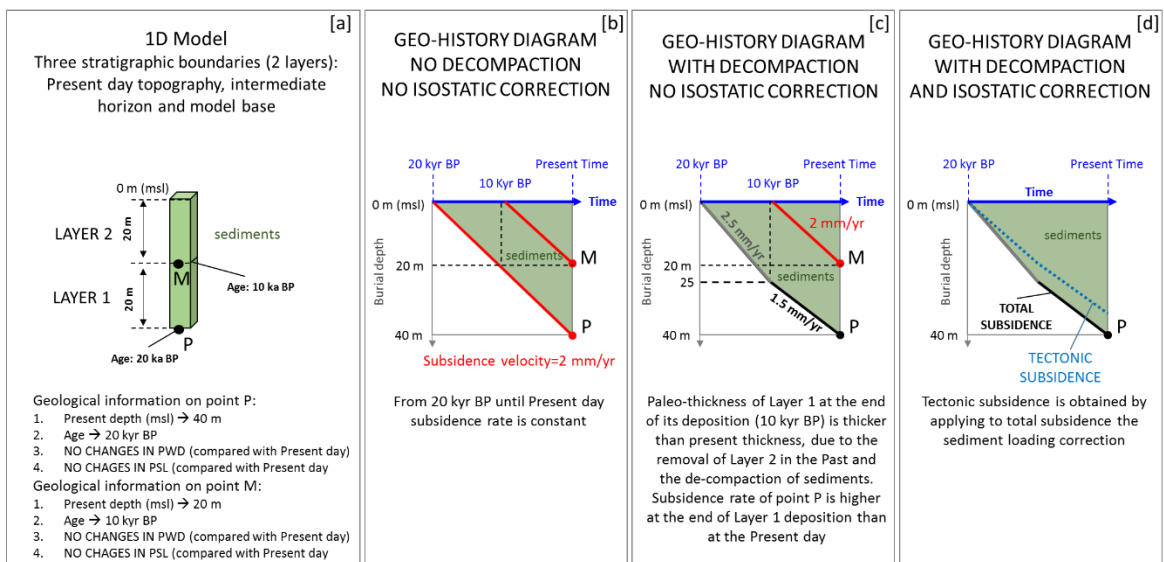
Figure 2.17 – Examples of subsidence velocity estimates on 1D synthetic model: a) 1D model parameters; b) geo-history diagram based only on geological information (sedimentary rate, PWD and PSL); geo-history diagram obtained taking into account the de-compaction process (c) and the sediment-isostatic loading (d).

Advantages of the new approach

Within the panorama of the subsidence studies, the proposed approach introduces three main innovations: i) it breakthroughs the one-component investigation proposed by the other approaches (cfr. Par. 2.2.) and improves the estimate of the geodetic velocity; ii) it fixes the "analyses to modelling" procedure and enhances the qualitative or the semi-quantitative procedures that often characterise the "data to source" (cfr. Par. 2.2.1.) and the "residual to source" (cfr. Par. 2.2.2.) approaches; iii) differently from the "peering approach", wherein no indicators are found for driving the source choice before modelling, the proposed approach attributes the source relevance before the modelling phase, speeding up the source validation step (cfr. Par. 2.2.3.).

Limits of the new approach

The first limit of the proposed approach relies on the component recognition (Step 1). Although several studies emphasize that the noise affects the seasonal signal and it has to be properly recognized and removed to improve the reliability of the assessed geodetic velocity (cfr. Par. 2.1.2.), such kind of analysis is not yet dealt with in the current approach.

The second limitation is related to the source selection (Step 2). In fact, just mechanical compaction of the sediments is accounted for (Par. 2.3.), both in terms of inelastic (permanent component of subsidence) and elastic (periodic component) deformations of the sediments. In addition to these mechanisms, deltas could even undergo other processes that are not yet considered within the proposed approach, such as chemical alteration of the clay due to the saltwater intrusion, and the peat oxidation (cfr. Par. 2.2.1.).

Chapter 3

Application of the proposed approach to the Po Delta

This Chapter shows an application of the new multi-component and multi-source approach for studying the subsidence of the Po Delta (northern Italy), an area historically affected by land subsidence and influenced by climatic changes. After a presentation of the previous studies on subsidence in Po Delta, a description of the geological setting and the land-hydrologic system interplay are shown for a proper interpretation of the results coming from our study.

3.1. Land subsidence in Po Delta

The Po Delta area, located in the northern part of Italy (Fig. 3.1a), is historically affected by both anthropogenic (Bondesan and Simeoni, 1983) and natural subsidence (Carminati et al., 2006; Teatini et al., 2011). Since the end of 1800, measurements of land subsidence started to be collected over the Po Delta area (Salvioni, 1957) and from the second half of 20th century repeated measures of spirit levelling have been analysed in order to individuate the main subsidence causes (Puppo, 1957; Caputo et al., 1970; Bondesan and Simeoni, 1983). Over the last decades, the introduction of new monitoring techniques, such as GNSS and DInSAR (see Parr. 2.1.1. and 2.1.2. for details), and the integration among different tools (Teatini et al., 2005; 2011; Tosi et al., 2010; 2016; Fabris et al., 2014; Fiaschi et al., 2018), favoured a more complete observation of the subsidence phenomenon over the Po Delta and the near coastal areas. In 1950 – 1957 period, the land subsidence reached rates up to 300 mm/yr in the inner part of the Po Delta (Fig. 3.1b), due to the intensive methane extraction from groundwater (Puppo, 1957). During the subsequent years, the subsidence rates diminished because the countermeasures adopted by Limited Government and progressively prevent the water withdrawal (Bondesan and Simeoni, 1983). By integrating spirit levelling, differential GPS, continuous GPS, InSAR and IPTA data (see Par. 2.1. for details) in a subsidence monitoring system, Teatini et al. (2005) mapped the ground displacement in the Venice coastland. After them, Tosi et al. (2010) extended the mentioned system to the central-northern part of the Po Delta detecting rates of vertical displacement over 1992-2002 period that vary from 2 to 10 mm/yr and that increase towards the sea (Fig. 3.1c). Studying the Po Delta Area by IPTA analysis, Teatini et

al. (2011) confirm these values and, in addition, indicate subsidence rates up to 12 mm/yr towards the river mouth (Fig. 3.1d).
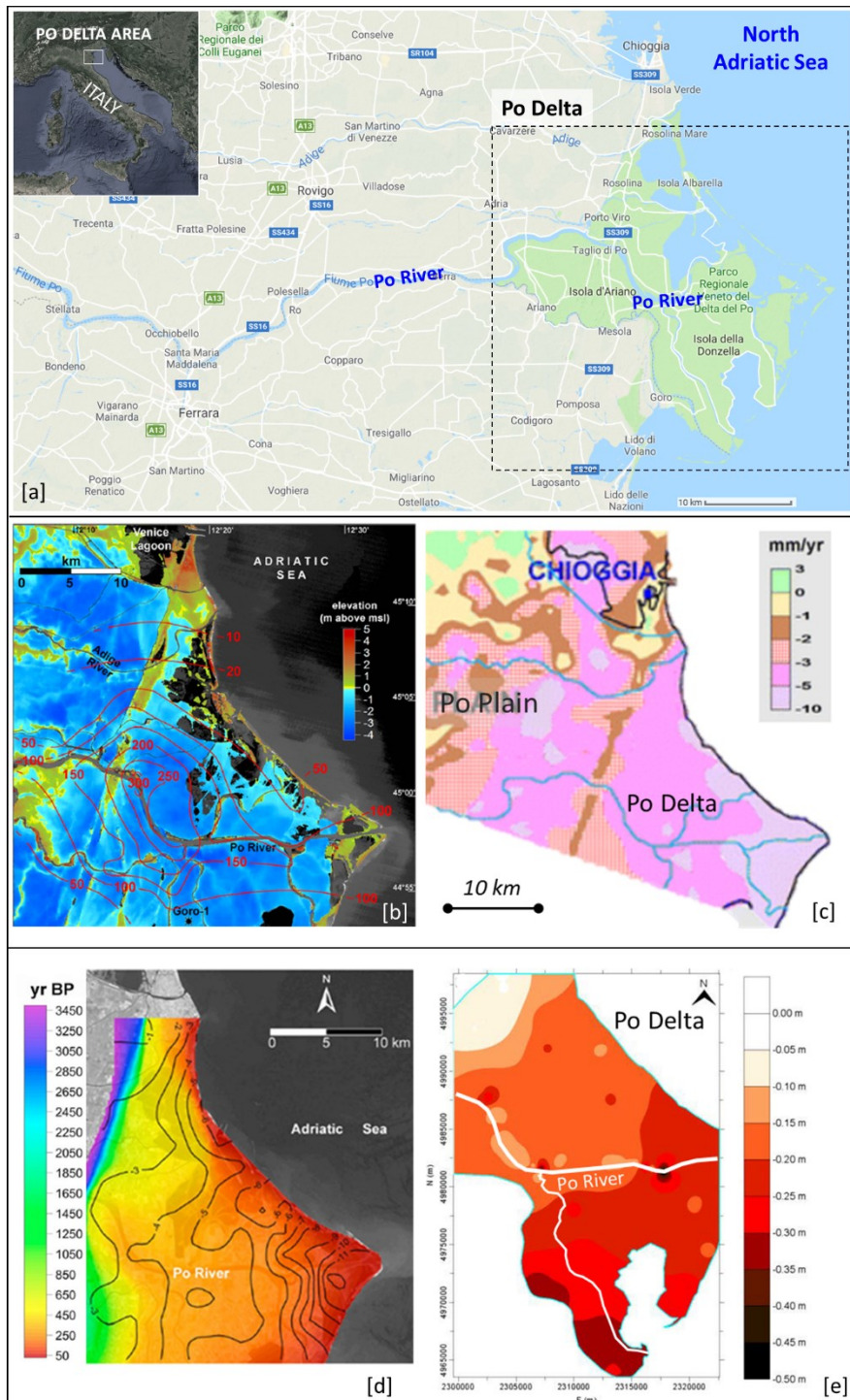
Figure 3.1 – Po Delta and vertical ground motion. a) Po Delta area. b) subsidence rates in mm/yr (red lines) obtained by levelling data and referred to 1950-57 period (modified after Teatini et al., 2011). c) Vertical displacement rates referred to 1992-2002 period and retrieved by using a subsidence integrated monitoring system (modified after Tosi et al., 2010). d) Subsidence rates (black lines) obtained by the map interpolation of IPTA averaged over 1992-2000 period (modified after Teatini et al., 2011). e) Subsidence map reconstructed by using high-precision levelling and multi-temporal GPS data over 1983-2008 period

(modified after Fabris et al., 2014). Note that the values "-0.05 m" and "-0.50 m" used in the map scale of d) sketch are equivalent to -2 mm/yr and -20 mm/yr over 25 years of observations, respectively. The downwards ground motion herein is negative, whereas in the text is positive.

Despite these studies, which show an increase of subsidence eastwards, Fabris et al. (2014) obtain an increase of subsidence to South and to South-East (Fig. 3.1e) by integrating high-precision levelling and multi-temporal GPS datasets over a period of 25 years (1983-2008). With respect to the temporal extension of the InSAR data analysis, Fiaschi et al. (2018) apply the SBAS technique (see Par. 2.1.1. for details) to three different SAR datasets obtaining a temporal span of 25 years: ERS-1/2 from 1992 to 2000, ENVISAT from 2004 to 2010 and Sentinel-1A from 2014 to 2017. Although two time lags occur during 2000-2004 and 2010-2014 periods, these authors provide a more comprehensive view of the ground displacement overcoming the gaps of levelling and GPS data. According to their results, the LOS velocity increases towards East ranging from ±1.5 mm/yr, measured in the stable zone of the sandy ridge, to 30 mm/yr, observed in the high-subsidence zone of the muddy delta tip (Fig. 3.2).
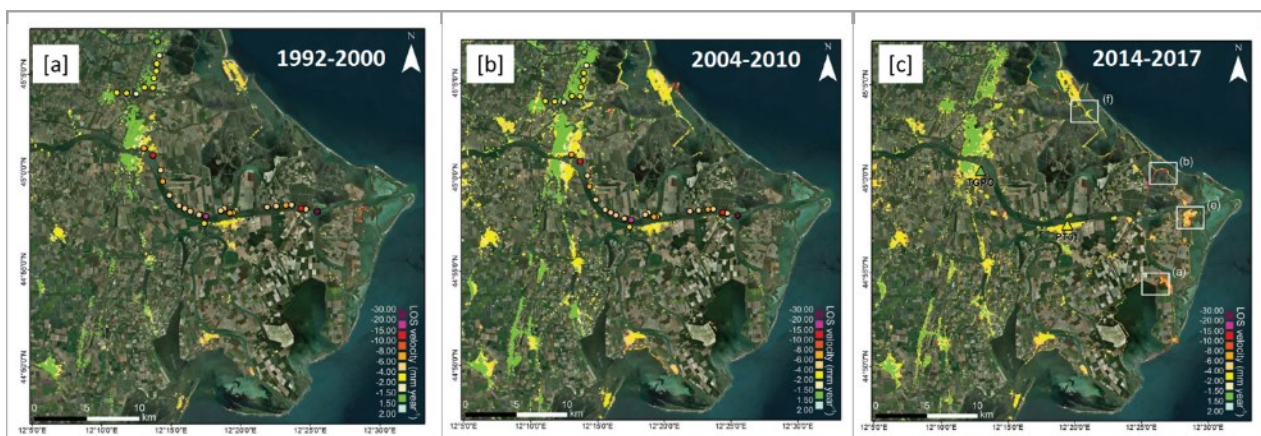
Figure 3.2 – LOS velocity over the Po Delta obtained by using: a) ERS-1/2 data; b) ENVISAT data; c) Sentinel-1A data (modified after Fiaschi et al., 2018). Coloured points of a) and b), and coloured triangles of c) represent high-precision levelling and CGPS data, respectively.

To overcome the low coherence in vegetated areas and the lack of reflectors in presence of farmlands, wetlands and lagoons of the Po Delta, some authors apply a multi-band combination analysis to the DInSAR datasets. In particular, Tosi et al. (2016) improve the spatial coverage by using IPTA and SBAS techniques (see Par. 2.1.1. for details) on two SAR datasets (COSMO-SkyMed and ALOS-PALSAR) over 2007-2010 and 2008-2011 periods. They calibrate the results obtained from the two SAR techniques by continuous GPS data (Figs. 3.3a and 3.3b) and then combine the outcomes in a unique map (Fig. 3.3c), pointing out significant differences between crop and urbanized areas.

According to their study, over 2007-2011 the average displacement rates of the Po Delta range between 5 and 15 mm/yr, being stable in the westernmost part of the delta and increasing towards the River mouth (Fig. 3.3c).
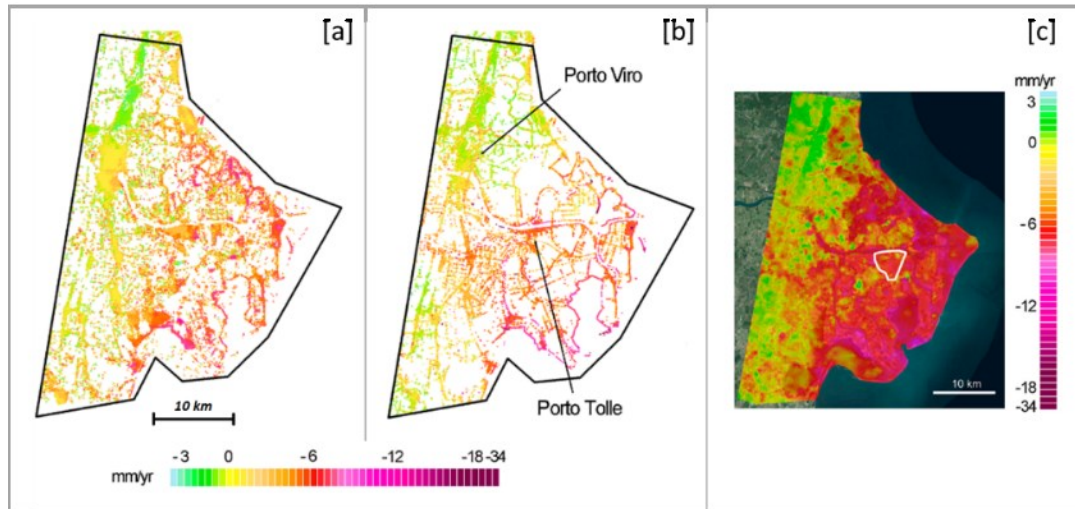
Figure 3.3 – Average displacement rates over the Po Delta (modified after Tosi et al., 2016): a) SBAS technique on ALOS-PALSAR dataset over 2007-2010 period after CGPS calibration; b) IPTA technique on COSMO-SkyMed dataset over 2008-2011 period after CGPS calibration; c) map resulting from the combination of the mentioned techniques over 2007-2011 period.

Table 3.1 shows the ground motion in three different sites of the Po Delta calculated in accordance with the mentioned studies.

Authors	Taglio di Po	Porto Tolle	River mouth	Period	Note
Puppo, 1957[1]	>250	> 200	> 100	1950-1957	
Tosi et al., 2010[2]	~ 3	3 ÷ 5	5 ÷ 10	1992-2002	Increase to E
Teatini et al., 2011[1]	~ 3	4 ÷ 5	11 ÷ 12	1992-2000	Increase to E
Fabris et al., 2014[3]	6 ÷ 8	6 ÷ 8	8 ÷ 10	1983-2008	Increase to S and E
Tosi et al., 2016[4]	~ 4	~ 5	15	2007-2011	Increase to E
Fiaschi et al., 2018[5]	stable; 2÷4	2 ÷ 4	12	1992-2000	Increase to E
Fiaschi et al., 2018[5]	2 ÷ 4	2 ÷ 4	-	2004-2010	Increase to E
Fiaschi et al., 2018[5]	2 ÷ 4	2 ÷ 4	6 ÷ 10	2014-2017	Increase to E

Table 3.1 – Ground motion rates (mm/yr) according to the studies quoted in the text.
[1]Subsidence rate; [2]vertical displacement rate; [3]subsidence rate derived by evaluated subsidence and analysed time interval; [4]calibrated average displacement rate; [5]LOS velocity. It is worth to note that the terms "subsidence rate" or "vertical displacement rate", although different because derived from levelling and SIMS, respectively, are synonymous since indicate movements occurred with respect to a ground-orthogonal plane; "LOS velocity" corresponds to movements occurred in the direction of radar illumination, which is tilted of a certain angle with respect to the ground-orthogonal plane. Moreover, in some cases LOS velocity can be assimilated to vertical displacement rate. For instance, Teatini et al. (2011) assume that only vertical movements contribute to the measured LOS displacements on the basis of geodynamic considerations and due to lack of horizontal strains originated by fluid withdrawals.

Although some of the findings indicated in Tab. 3.1 refer to the same period of analysis (e.g. 1992-2000), the results reveal differences related to both the InSAR techniques used in the analysis phase and the GPS datasets used during the calibration. For instance, Teatini et al. (2011) adopt IPTA technique for the analysis and GPS from American network for the calibration, whereas Fiaschi et al. (2018) utilize SBAS technique and GPS from European network. A data comparison between these two geodetic networks will be done in Par. 3.4.

With respect to the subsidence causes, some authors studied the Plio-Pleistocene sedimentary sequence of the entire Po Basin discriminating the natural short- and long-term components of subsidence (Carminati and Di Donato, 1999; Carminati et al., 2006). They gave particular emphasis to the role of the flexure of the Adriatic Plate beneath the Tyrrhenian Plate (tectonic process), but also quantitatively described the contribute due to the isostatic rebound in relation to the Plio-Pleistocene sediment load and to the Alpine glaciers load after the Last Glacial Maximum (LGM) and the compaction of Plio-Pleistocene sediments (isostatic and sedimentary processes). Other researches focused the attention on the natural short-term component of the subsidence on the basis of the observed correlation between subsidence rate and age of the shallower sediments of the Po Delta (Teatini et al., 2011). In particular, Teatini et al. (2011) indicate the consolidation of the Late Holocene muddy sediments, which rapidly prograded eastwards during the last centuries, as the main cause of the present-day subsidence. Finally, Fiaschi et al. (2018) suggest that over the Po Delta the recent-constructed buildings may locally accelerate the natural subsidence processes causing the settlement of the foundations.

3.2. Geological setting

The Po Delta is located in the northern part of the Adriatic Plate (Fig. 3.4a), a portion of continental lithosphere surrounded by the Apennines, Southern Alps and Dinarides thrust belts and their relative foredeeps (Doglioni, 1993; Carminati et al., 2003a). In the Po Plain and North Adriatic Sea, these systems act at different times and through different tectonic styles (Doglioni, 1993; Fantoni and Franciosi, 2010). Specifically, on the north-eastern margin, the compression of the Dinarides operates from Paleocene to Early Miocene in connection with the frontal thrust belt of a NE-dipping subduction (Fig. 3.4b); on the north-western margin, the Southern Alpine chain acts since Middle Miocene to Pleistocene in relation with the back-thrust belt of the Alps (Fig. 3.4c); on

the south-western margin, the Apennine chain compression is mainly active from Late Miocene to Pleistocene, due to a W-SW-dipping subduction (Fig. 3.4d).
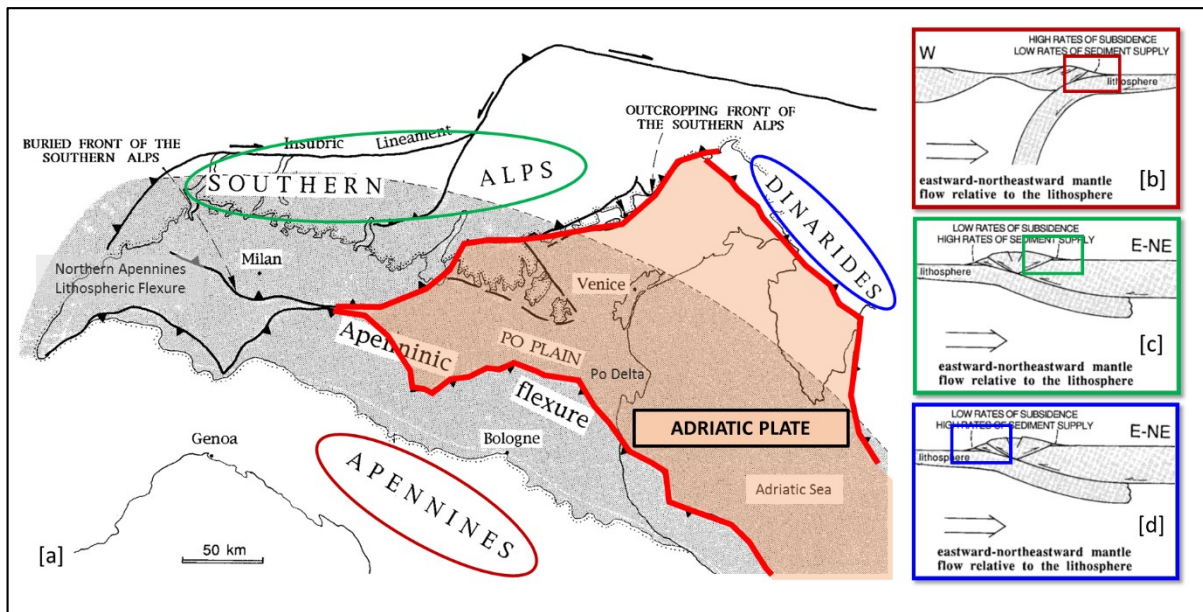
Figure 3.4 – Northern Adriatic Plate and thrust belts: (a) map view of main structural features; (b), (c), (d) section view of the subduction mechanisms and relative thrust belts in the Dinarides, Southern Alps and Apennines, respectively (modified after Doglioni, 1993).

Below the Po Delta Area, the Apennine foredeep basin is filled by the Pliocene-Early Pleistocene aggradational turbidite system, overlapped by the Pleistocene progradation complexes. The aggradational sequences onlap the Pliocene Base both to North-East (Fig. 3.5b), because of the down-flexure of the Adriatic Plate beneath the Apennines (Fig. 3.5a) (Carminati et al., 2003a) and to North-West, due to the presence of a deep regional relief (Fig. 3.6) (Turrini et al., 2014). Moreover, these successions consist in sand-rich turbidite sequences deposed in deep-water conditions, with water depth exceeding 1000 m (Ghielmi et al., 2013). Their depocenters migrate to North-East under the effect of the major tectonic pulses (Ghielmi et al., 2013) and in relation to the eastward rollback of the Apennine subduction hinge (Royden et al., 1987). At the time of turbidite deposits, the basin was affected by high tectonic subsidence rate (> 1 mm/yr), since more than 1500 m of sediments was accumulated during 1.5 Millions of years (Myr) in the same depositional environment (Fig. 3.7).
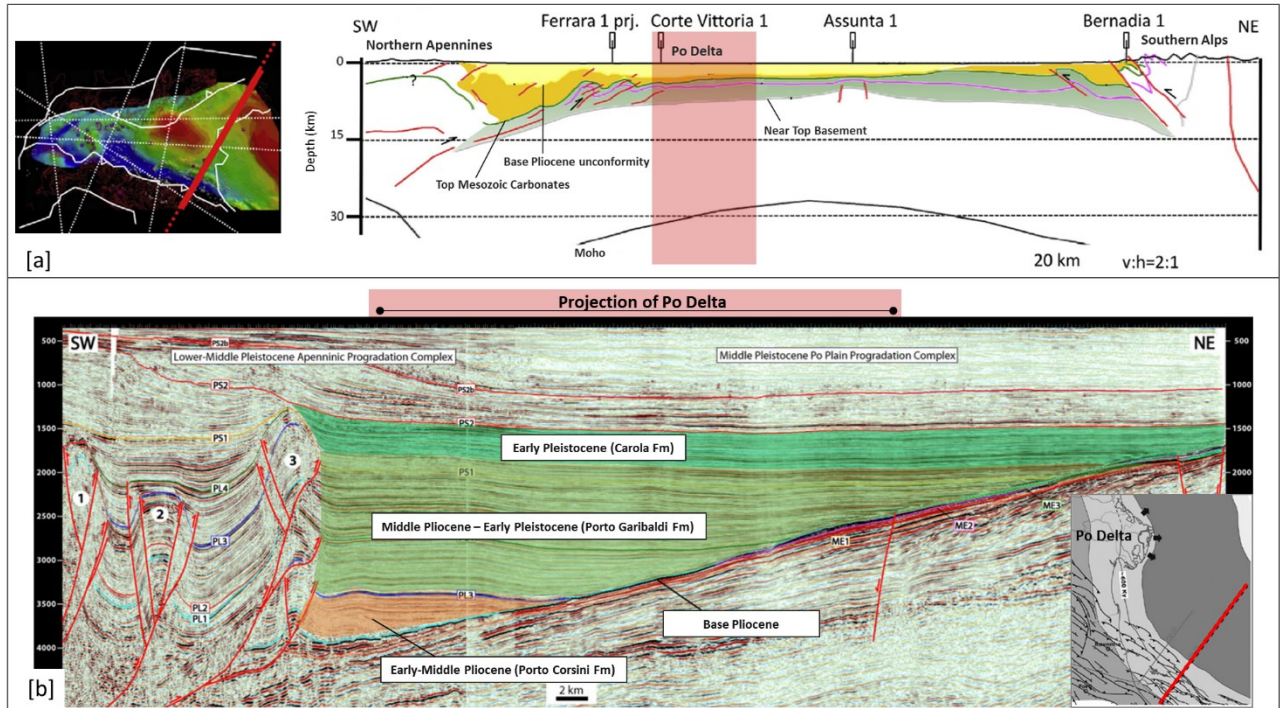
Figure 3.5 – (a) Crustal-scale section through Po Delta Area (modified after Turrini et al., 2014). Yellow sequences represent the Cenozoic succession; top of dark-yellow layer corresponds to the base of Pliocene unconformity. (b) Seismic section through North Adriatic Foredeep showing the Plio-Pleistocene aggradational turbidite system (modified after Ghielmi et al., 2013); location of Po Delta (red shadows in a) and b) sketches); light-brown and light-, dark- green shadows in b) sketch indicate the aggradational sequence.
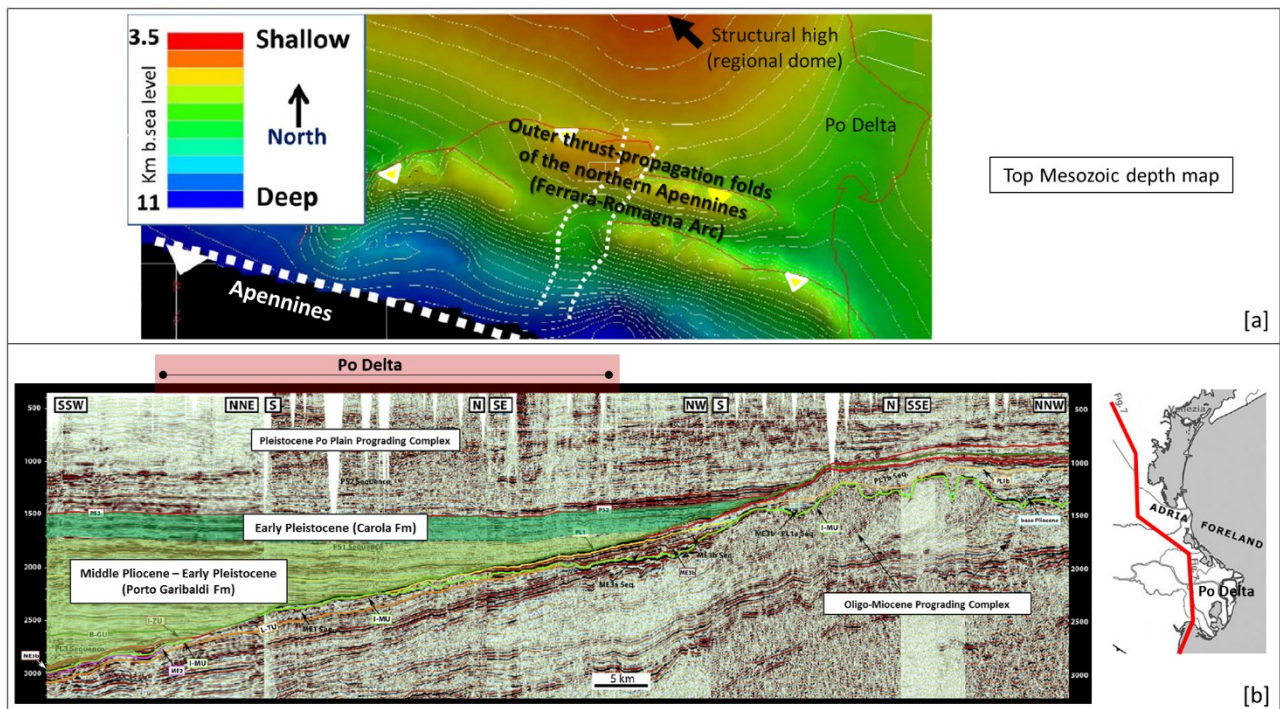
Figure 3.6 – (a) Top Mesozoic depth map and main structural features (thrusts) (modified after Turrini et al., 2014). (b) Seismic section through the eastern part of the Po Plain Foredeep showing the Plio-Pleistocene aggradational turbidite system (modified after Rossi et al., 2015); location of Po Delta (red shadows in a) and b) sketches); light-brown and light-, dark- green shadows in b) sketch indicate the aggradational sequence.

The Pleistocene progradation complexes consist of two major systems formed by slope, shelfal and coastal deposits, which are differentiated for origin of sediment input and direction of progradation. The Pleistocene Apennine prograding system (Early-Middle Pleistocene) is supplied by the southwest side of the basin and moves to North-East, while the Po Plain progradation system (Middle Pleistocene) is nourished from the north-western side and directs to South-East (Ghielmi et al., 2013). Eight transgressive-regressive depositional cycles are identified within the Middle Pleistocene to Holocene vertical stacking strata (Amorosi et al., 2016). These deposits, which lay above the regional unconformity dated 0.9 million of years (Myr) Before Present (BP), correspond to alternating marine and continental sediments formed in response to high-frequency sea-level fluctuations with periodicity of ~100 thousand of years (Kyr), under a predominantly glacio-eustatic control (Amorosi et al., 2004; 2016).
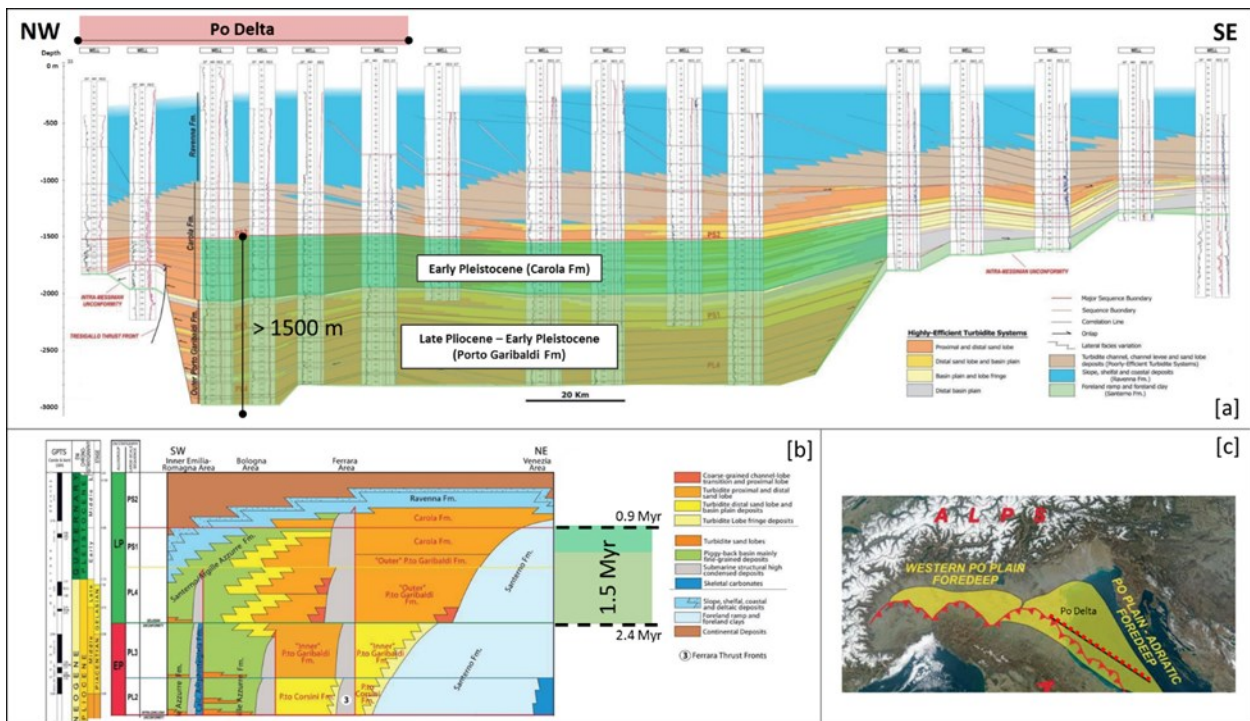
Figure 3.7 – (a) Stratigraphic section based on well data and traced parallel to the main Apennine foredeep axis; (b) chronostratigraphic scheme; (c) stratigraphic section base map (modified after Cazzini et al., 2015). Note that red shadow of a) sketch is overlapped to the image for indicating the location of Po Delta; light- and dark- green shadows of a) and b) sketches indicate the aggradational layer thickness and the time interval of deposition.

The total thickness of the Plio-Pleistocene aggradational and progradation sequences increases toward South (Fig. 3.8a) reaching up to 4000 m of thickness in the Adriatic Sea, to south

of the Po Delta Area (Bigi et al., 1992; Cazzini et al., 2015). These sequences bury also the Conselve-Pomposa fault (Figs. 3.8a, b), a sinistral strike-slip lineament connected to the northern Schio-Vicenza fault (Castellarin et al., 2006; Pola et al., 2014). The entire fault system corresponds most likely to a Mesozoic normal fault, reactivated by the subduction related to Apennines during the Plio-Quaternary (Pola et al., 2014). Although the Conselve-Pomposa fault ends its activity during Pliocene (Fig. 3.8b) (Pola et al., 2014), the historical and instrumental earthquake epicentres collected from national catalogues during 0–2003 period (Tosi et al., 2007), are scattered distributed, thus indicating that seismic activity is still present in that portion of the basin even related to that fault system (Fig. 3.8c).
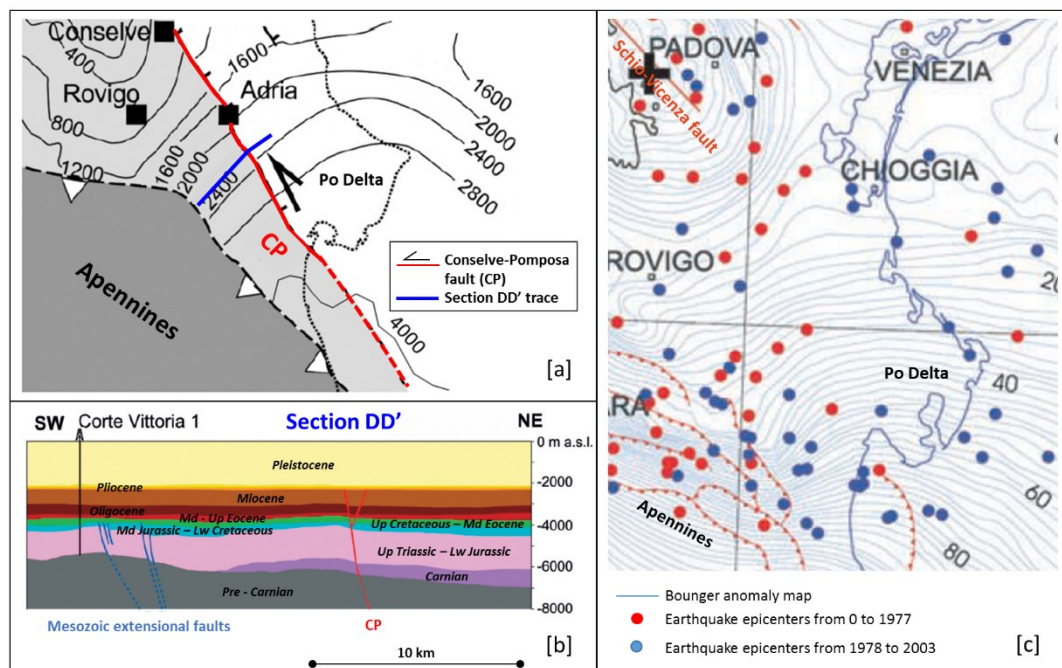
Figure 3.8 – (a) Pliocene Base depth map, in meter below ground level and (b) depth section crossing Conselve-Pomposa fault (modified after Pola et al., 2014). (c) Map of seismicity of Po Delta and near areas showing historical and instrumental events in the period from 0 to 2003 (modified after Tosi et al., 2007). Note that in the a) sketch the contour line '4000 m' is added to the image according to Cazzini et al. (2015).

During the LGM (ca. 20 kyr BP), a broad well-drained alluvial plain covers the north Adriatic area, while the Po River and tributaries reach the central Adriatic basin (Correggiari et al., 2005) (Fig. 3.9a). The climatic condition of the LGM, combined with the sea level fall corresponding to the MIS3-MIS2 boundary, forced the formation of incised valleys (Amorosi et al., 2016). During the early transgressive phase dated 18-14 Kyr BP, thin aggradational continental deposits infill irregularly the latest Pleistocene valley systems (Fig. 3.9b), while after this period, a phase of climatic instability (Younger Dryas) occurred between 13-11 Kyr. Due to this relative cold climatic event, the middle

transgressive unit records extensive paleo-soil and local incisions (Fig. 3.9c). Then, the alluvial plain is progressively flooded due to the Holocene sea level rise and, between 9 and 8 Kyr BP, the fluvial system appears replaced by the estuarine environment, which consists in the back-stepping of barrier–lagoon–estuary systems (Amorosi et al., 2004). The transgressive units are overlain by offshore transition clay–sand alternations, marking the maximum marine ingression (Amorosi et al., 2004). From 5.5-5 Kyr BP, the highstand units, which are characterised by progradational stacking pattern of prodelta, delta front and delta plain sediments, start to be deposited (Amorosi et al., 2004; 2016).
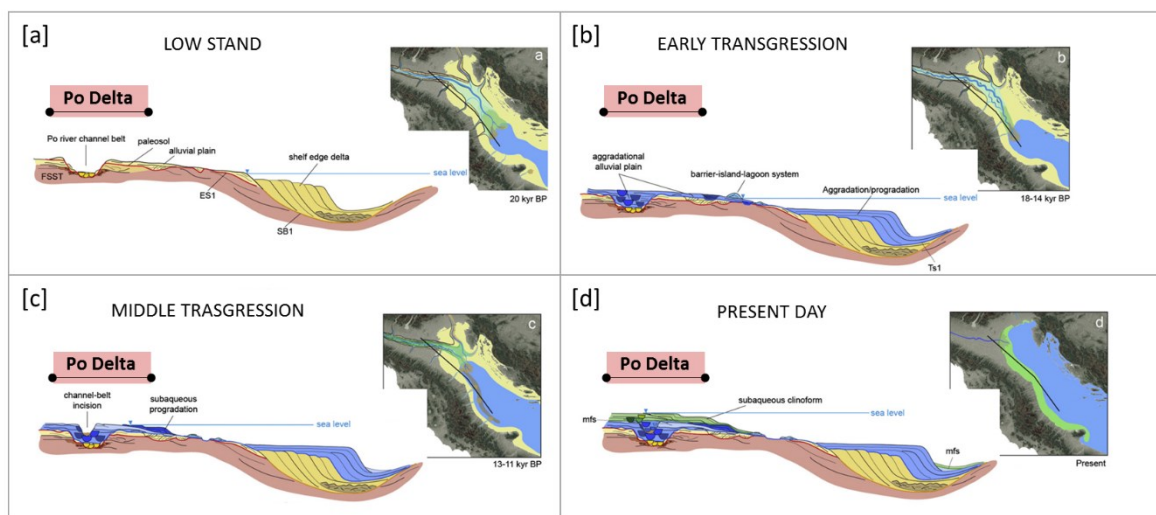
Figure 3.9 –Sedimentary evolution of the Po Plain and Adriatic Basin from Late Pleistocene to Present day (modified after Amorosi et al., 2016). Note that red shadows are overlapped to the images for indicating the location of Po Delta.

The latest Pleistocene–Holocene sediments are constituted by 30-40 m of littoral, deltaic and marine sediments containing sands, silts and clays and locally peats (Fig. 3.10). The sandy deposits also represent the shallow aquifers of the Po Delta basin (Bonzi et al., 2010).
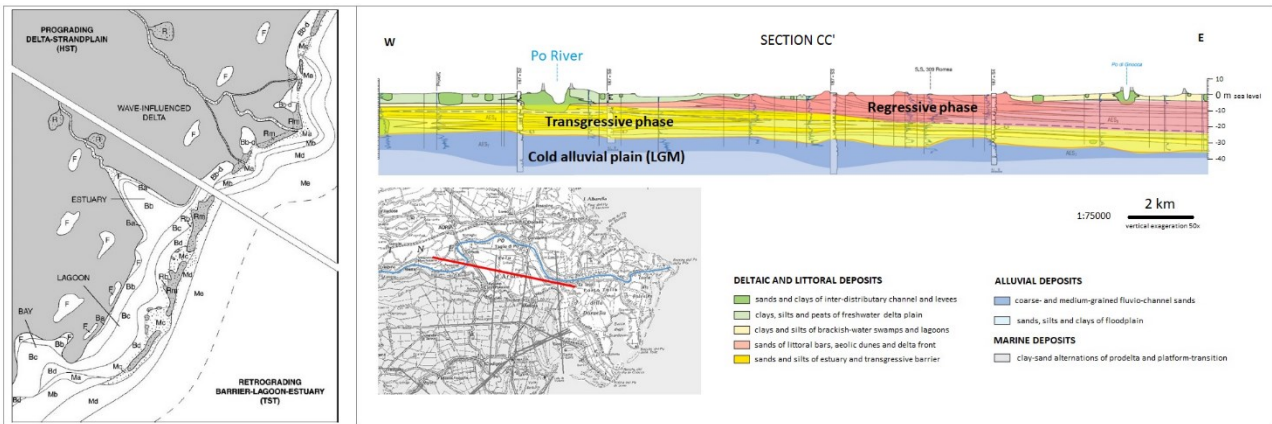
Figure 3.10 – Retrograding and prograding systems of the last transgressive phase: a) paleo-environmental reconstruction based on micro-paleontological studies and facies analysis (from Amorosi et al., 2004); b) geological section passing through the central part of the Po Delta, which shows the last retrograding and prograding sequences. Section is available on Geological Map of Italy F. 187 Codigoro (Geological Survey of Italy, 2009).

The Po Delta Area is today a broad plain of about 400 km² extended seaward for 25 km (Simeoni and Corbau, 2009). Most of the delta plain is below the mean sea level (Fig. 3.11a) and is poorly supplied with sediments because all river branches have major artificial levees, which prevent avulsion and crevassing (Bondesan et al., 1995). The morphology of the eastern part of the Po Delta is characterised by a lower delta plain, with ancient coast, delta fronts (Fig. 3.11b) and lagoons constituted by inter-distributary bay deposits, marsh deposits, beach-ridge and aeolian dune sediments (Correggiari et al., 2005). The modern Po Delta was induced 400 years ago by an artificial fluvial-mouth cut done in Porto Viro (Stefani and Vincenzi, 2005) and it is evolving today towards a wave-dominated and cuspate morphology (Dal Cin, 1983).
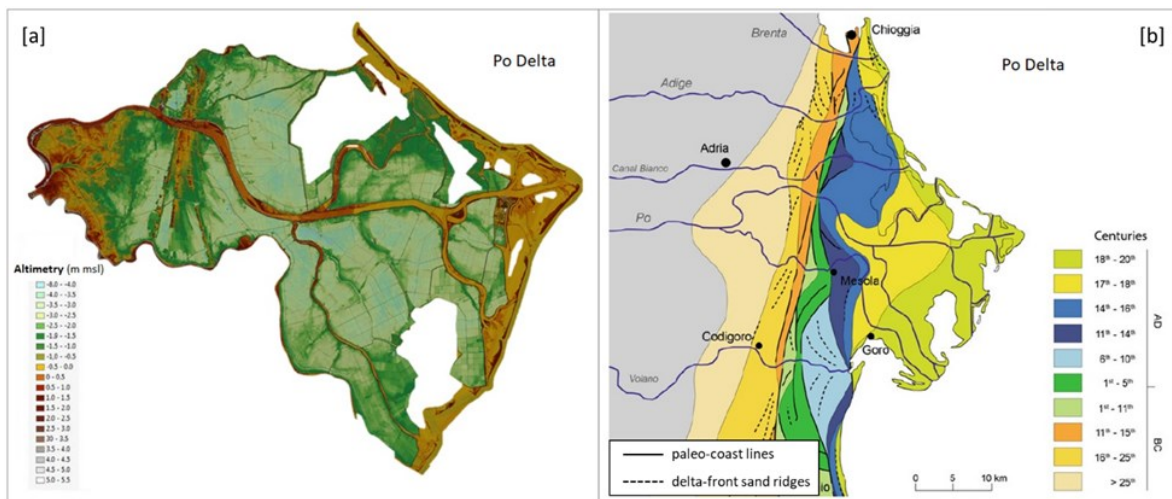
Figure 3.11 – Po Delta: (a) Altimetry derived by LIDAR Survey performed in 2009 (map is available on the website of Consorzio di Bonifica Delta del Po, Veneto Region at http://idt.regione.veneto.it); (b) ancient coasts and delta fronts showing the progradation of Po Delta after maximum marine ingression (5.5 Kyr ago) (modified after Stefani, 2017).

3.3. Interaction between land and hydrologic system

The modern Po Delta is fed by the Po River, the most important Italian river, which is 691 km long and is characterized by a basin's watershed of 74,500 km^2 (Fig. 3.12a) (Cattaneo et al., 2003). At Pontelagoscuro site, about 90 km upstream of the river mouth, the Po River enters the coastal region and flattens its profile (Correggiari et al., 2005) (Figs. 3.12b and 3.12c). The annual regime of the Po River is mainly influenced by the seasonal patterns of temperature, rainfalls and related processes (i.e. runoff, evapo-transpiration and infiltration). Its average annual temperature is strongly correlated to the altitude, being of about 5 °C either on Alps and Apennines, and higher than 15 °C in proximity of the sea (Vezzoli et al., 2015). Minimum temperatures occur in winter season (December to February) and maximum in summer (June to August). The rainfalls of almost the entire Po River basin are characterised by two high-values in spring and autumn, and two low-values in summer and winter. Oglio, Adda and Ticino sub-basins make an exception, since these effluents are lake-dependent (Vezzoli et al., 2015). It is also assumed that about 1/3 of the average annual areal precipitation on Po River basin is lost for evaporation and vegetation interception (Vezzoli et al., 2015). As it concerns the annual regime of the Po River discharge, it shows two high-water periods during spring and late autumn and two low-water periods during summer and winter (Zanchettin et al., 2008), thus indicating the strong meteorological control on the river hydrological pattern. A low-frequency discharge variability is also controlled by groundwater exploitation for human purposes (Zanchettin et al., 2008).
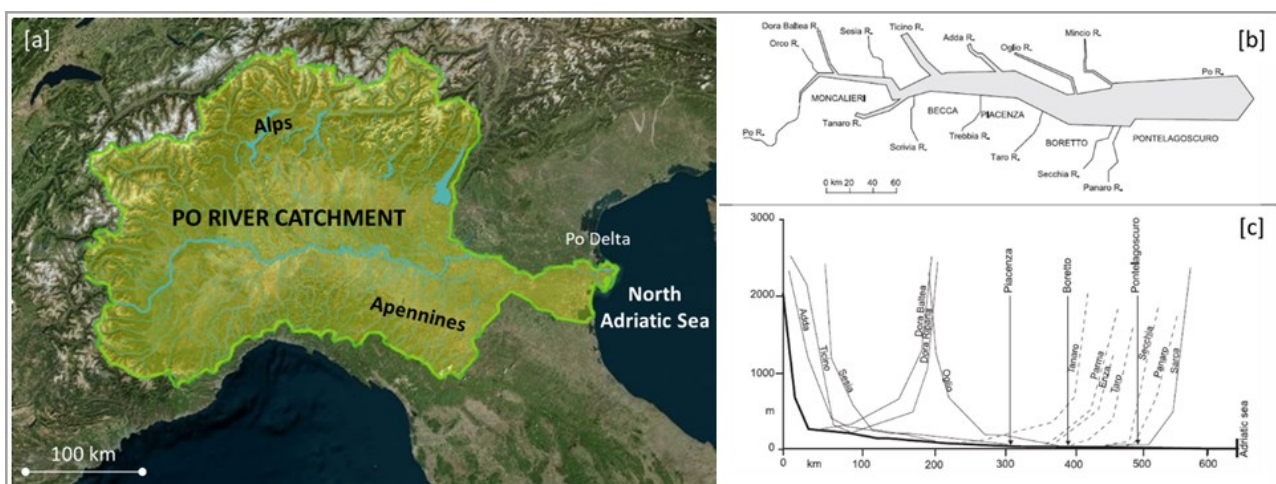
Figure 3.12 – Po River: a) map of the catchment (available on the geoportal of AIPo Interregional Agency); b) and c) scheme and depth profiles of Po River and its tributaries, respectively (modified after Correggiari et al., 2005).

The Po River is also characterised by two distinct peaks of suspended sediments in spring and autumn (Amorosi et al., 2016), clearly unveiling the correlation with the bimodal pattern of the river discharge. Once the Po River flows into the Adriatic Sea, about 15×10^6 t yr^{-1} of sediments are distributed along the coast under the effect of the dense water flow (Cattaneo et al., 2003). Such a kind of current is one of the water masses that interact into the Adriatic Sea and drive the water circulation. The Adriatic Sea is a semi-enclosed basin bounded by a shallow continental shelf, whose water depth does not exceed few tens of meters (Amorosi et al. 2016). It is influenced by micro-tidal regime and waves, and is dominated by a cyclonic circulation dependent on the thermohaline currents (Correggiari et al., 2005). From interaction between wind and sea in enclosed and/or semi-enclosed basin, a peculiar wave, called "seiche", can rise. Seiches are typically caused when strong winds and rapid changes in atmospheric pressure push water from one end of a water body to the other. When the wind stops, the water rebounds to the other side of the enclosed area. The water then continues to oscillate back and forth for hours or even days. Under the wind effects and the freshwater input coming from Po and Apennine rivers, the water circulation of the Adriatic Sea results counter-clockwise directed. This orientation is due to the interaction of the Levantine water, coming from the eastern Mediterranean through the Otranto Strait, the dense water forming in the North Adriatic Sea during the cold-wind of late winter, and the dense water originated in the deep South Adriatic Sea by open-ocean convection (Amorosi et al., 2016). Recently, Benetazzo et al. (2014) described the formation and the spreading of dense shelf waters in the North Adriatic Sea during the winter of 2012 as due to the intense and long cold air outbreak of north-easterly Bora winds (Fig. 3.13).
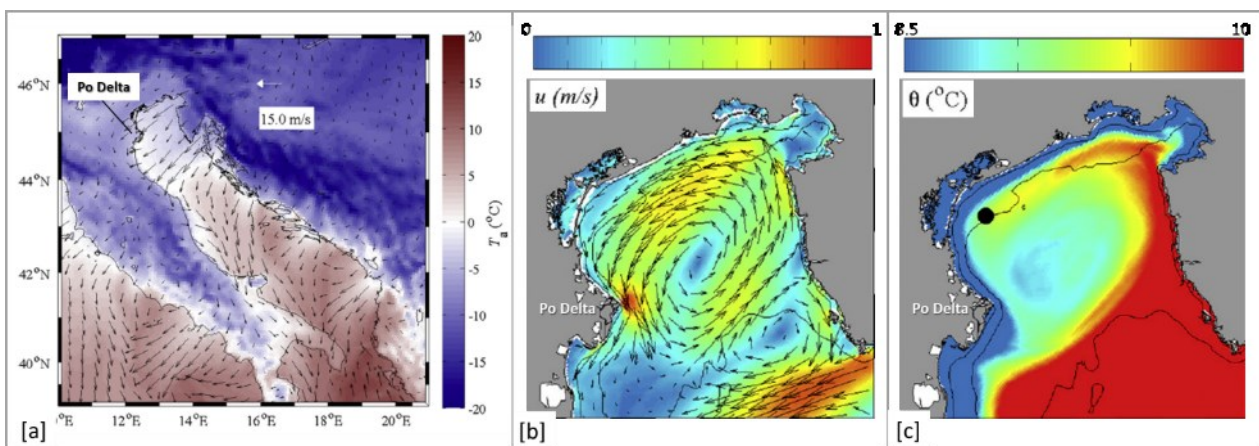
Figure 3.13 – Example of water circulation-related factors in Adriatic and North Adriatic Sea (modified after Benetazzo et al., 2014): a) 10-m height wind field provided by the COSMO-I7 atmospheric model on February 2, 2012 during a cold air outbreak; wind is overlapped to the ground air temperature (T$_a$). b) Average sea

surface current speed and c) average sea temperature calculated by circulation models during January-February 2012.

The sea water density of the North Adriatic Sea, as well as the sea level oscillations, impact also on the groundwater of the Adriatic coastal aquifers in terms of localization of the sea-land interface and water table oscillations, respectively. South to the Po River, the sea-land interface controls the groundwater salinity, especially in the areas placed below the sea level (Antonellini et al., 2008). The sea level fluctuations, which depend on lunar and solar gravitational attractions (astronomic causes) and on wind, barometric pressure, seiches and storm surges (atmospheric causes), combined with the rainwater infiltration, clearly control the water table changes within the phreatic aquifers (Balugani and Antonellini, 2011). In addition to the mentioned mechanisms, Teatini et al. (2006) demonstrate that the past extensive water withdrawal from the Emilia-Romagna coastal aquifers causes the delayed compaction of the clay aquitards comprised between depleted aquifers and determines, as consequence, the recent land settlement.

The amplitude of the sea level fluctuations transmitted through the aquifer decreases moving to the inland, becoming indiscernible in the water head variations at a certain distance from the sea. In the central part of the Po Basin (Boretto area) and near Ferrara (Emilia-Romagna Region, northern Italy) (see Fig. 3.1a), the shallower phreatic and confined aquifers may be connected to the river-bed and influenced by the river level variations. Severi et al. (2012) show that the water table oscillations, measured in a piezometer located close to the Po river-banks in the phreatic aquifer, has similarities with the rainfall patterns and well correlate with the river discharge fluctuations (Fig. 3.14a). The piezometer located close to the Po river-banks in the confined aquifer shows the same trend as the Po River level (Fig. 3.14b). Conversely, another piezometer located more than 1.5 km far from the river and in the confined aquifer, does not show similarities with the river trends, thus indicating that the river water does not charge directly the permeable sands (Fig. 3.14c). Herein the shallow aquifers located in the alluvial permeable strata are juxtaposed also to the alluvial fans of the Alpine rivers and separated by the colluvial sediments accumulated at the base of the Apennine hillslopes, thus receiving additional groundwater contribution from the north side of the river basin (Severi et al., 2012).
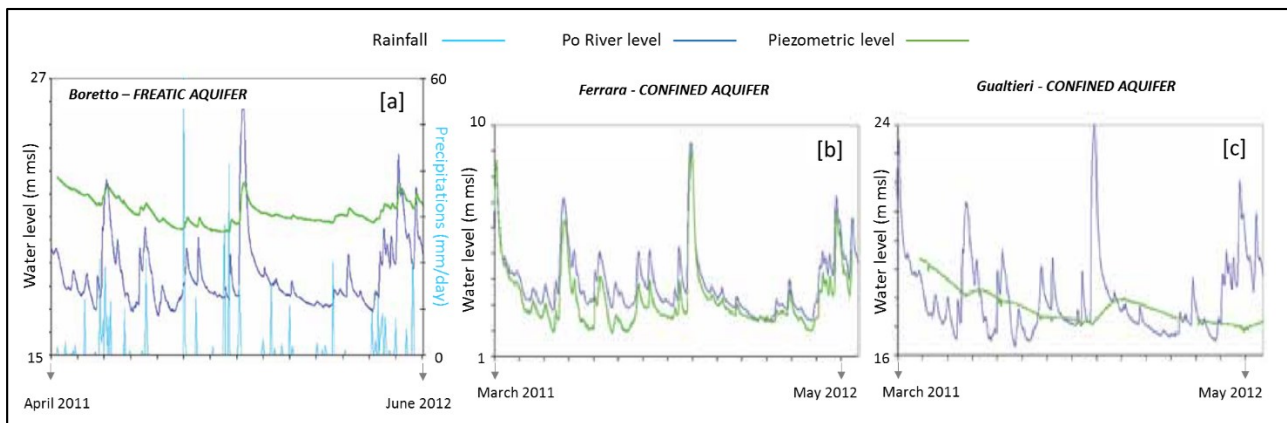
Figure 3.14 – Groundwater levels of phreatic and confined shallow aquifers of the Po Basin around Ferrara and Boretto areas, from 2011 to 2012 (modified after Severi et al., 2012): a) piezometer in the phreatic aquifer and close to the Po river; b) piezometer in the confined aquifer and close to the Po river; c) piezometer in the confined aquifer and located 2.5 km far from the Po river.

As it concerns the river-aquifer interaction in the Delta Area and especially moving towards the sea, the hydrometric stage is higher than the groundwater head even during dry periods, since the river bed elevation is higher than the floodplain elevations, thus expecting that the water flow is only directed from river to near aquifers (Severi et al., 2012).

3.4. Multi-component and multi-source approach

The multi-component and multi-source approach proposed in the Chap. 2 for studying the land subsidence in the deltas has been applied to the Po Delta Area. The workflow of this methodology and the main results derived from its application are herein described step by step. As the main goal of this study is the subsidence of the Po Delta, the hereafter analyses are focused just on the vertical component of the available geodetic data. Moreover, as it concerns the modelling phase, the computation of ground displacement due to the hydrodynamic flow and to the hydrological loading processes have been evaluated in collaboration with Dr. L. Piccinini (University of Padua) and Dr. J-P. Boy (IPGS, Strasbourg), respectively.

3.4.1. Step 1: Geodetic time series analysis

The analysis of the geodetic time series (step 1) has been performed using two sets of site-position time series (CGPS data) and one set of displacement time series (DInSAR data). The CGPS data come from three permanent stations located close to Po and Po di Volano rivers, specifically at Taglio di Po, Porto Tolle and Codigoro villages, while the DInSAR-derived data cover the central-southern and

the easternmost parts of the Po Delta, near Albarella, Boccasette, Pila and Scardovari sites (Fig. 3.15).
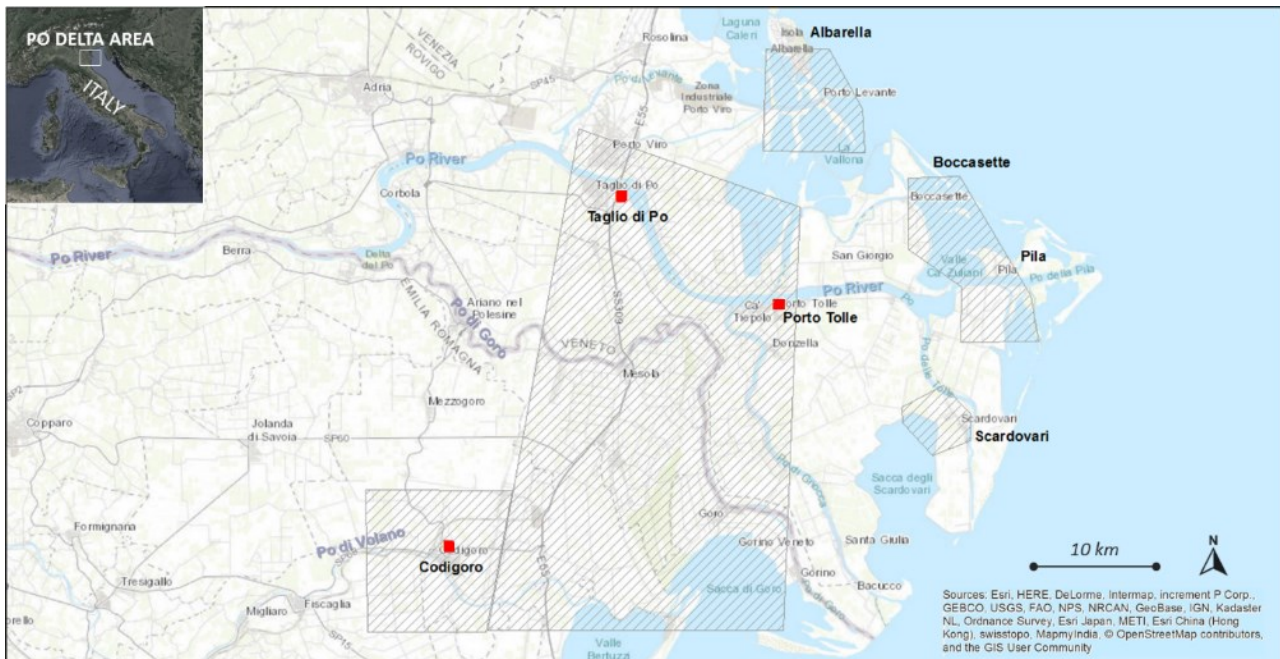
Figure 3.15 –Location of the geodetic data in the Po Delta Area: CGPS stations (red squares) and DInSAR data coverage (striped areas).

The first set of CGPS data, hereinafter referred to as "American dataset" (Am dataset), comprises three site-position time series, which are available as daily solutions produced by Nevada Geodetic Laboratory (MAGNET) and refer to Taglio di Po (TGPO), Porto Tolle (PTO1) and Codigoro (CODI) stations (http://geodesy.unr.edu/magnet.php). TGPO and PTO1 belong to Veneto Region GPS network, while CODI belongs to Emilia Romagna GPS network. The Analysis Centre of Nevada Geodetic Laboratory (University of Nevada, Reno) processed the primary RINEX data by using GIPSY/OASIS-II software and obtained station 3D positions in the International Terrestrial Reference Frame 2008 (Altamimi et al., 2011). It provides "cleaned data", which consist in time series whose outliers have been removed, and information about earthquake and equipment events are given. The GPS stations are placed on the roof of a barn (TGPO), of a three-floors (PTO1) and one-floor (CODI) buildings, whose foundations do not exceed 2 m in depth and lay on deltaic, littoral and marine sediments of the last regressive sequence (see also Fig. 3.7).

The second dataset, hereinafter referred to as "European dataset" (Eu dataset), comprises two site-position time series from TGPO and PTO1 stations, which are available as weekly solutions

produced by University of Padua, using Bernese software. The station positions of this dataset are obtained in the European Terrestrial Reference Frame 1989 (ETRF2000).

The third dataset consists in displacement time series derived from Sentinel-1A DInSAR data, using the SBAS technique (Fiaschi et al., 2018). The data consist of 54 (track 95) SAR images, acquired in C-band (5.6 cm of wavelength) with vertical co-polarization and in descending geometry. The SAR images were acquired with the Interferometric Wide swath mode from 17 November 2014 to 17 May 2017 and have a revisit time of 12 days, a look angle of 39.0° and a ground resolution of about 15 m × 15 m by adopting a multi-look of 4–1 in range and azimuth directions (Fiaschi et al., 2018). The processing workflow is structured in progressive steps: generation of connection graph, interferograms generation, phase unwrapping, refinement, first estimation of velocities, final estimation of velocity and atmospheric contribution removal, displacement time series estimation. The final outputs are imported in a Geographic Information System (GIS) for being classified and interpreted. During the processing a temporal baseline of 110 days and a perpendicular baseline of 2% have been chosen. The satellite's orbit geometry was estimated using precise orbits data available from European Space Agency (ESA), while topographic phase residuals were removed using the Shuttle Radar Topographic Mission (SRTM) DEM with a ground resolution of around 30 m × 30 m (pixel size) (Fiaschi et al., 2018). The obtained DInSAR results are not calibrated but compared and validated with in-situ observations provided by previous high-precision levelling surveys and GPS data (TGPO and PTO1 European dataset) (Fiaschi et al., 2018).

The available geodetic time series exhibit different time span lengths during which several seismic events and an equipment change occurred (Fig. 3.16). Moreover, the series clearly exhibit non-tidal loading effects (i.e. atmospheric pressure, ocean bottom pressure and hydrological). In case of large earthquake (Mw>6.9) occurred near enough to the CGPS stations, the background trends of the American datasets are corrected during the time series analysis phase. Herein a data check on both the American and the European CGPS time series has been done for verifying if any displacement variation occurs in relation to the disturbing events (Fig. 3.17). From 2012 to 2016, in the Northern and Central Apennines three seismic events occurred: Mw 6 earthquake of May 20, 2012, Mw 5.8 earthquake of May 29, 2012 and Mw 6.5 earthquake of October 30, 2016. These events are reported on the log-files. In addition, other two seismic events of Mw 6 and Mw 5.9, although not indicated in the log-files, occurred during August 2012 in the Central Apennines.
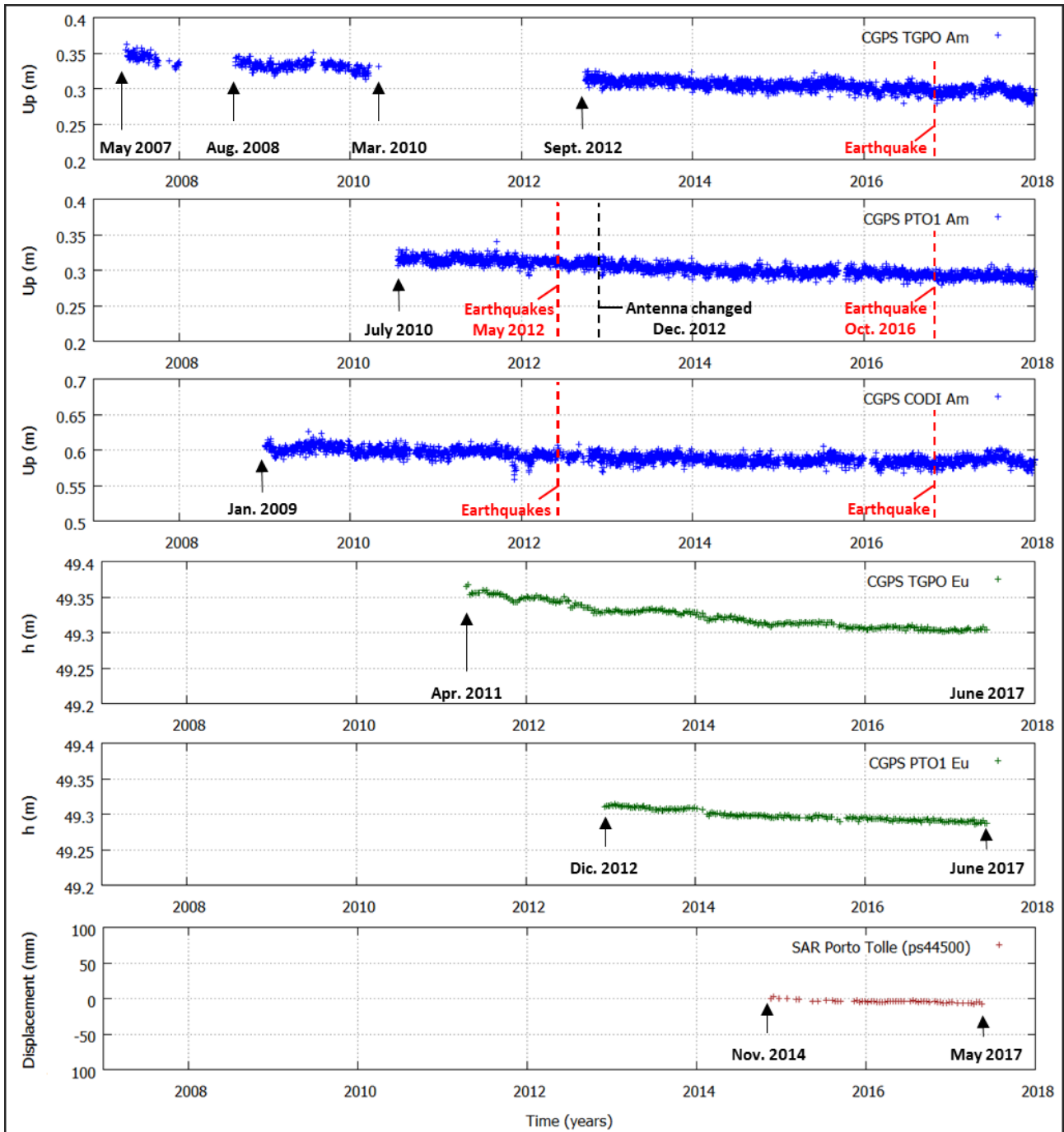
Figure 3.16 – Time span lengths of the available geodetic time-series: daily CGPS data of American Network (blue points), weekly CGPS data of European Network (green points) and DInSAR-derived data (brown points). Occurrence time of nearby earthquakes and equipment change are marked with red and black vertical dashed lines, respectively.

Figs. 3.17a and 3.17b depict the CGPS time series (Up component) around three of the main seismic events over 5-months period and show unaffected displacement trends on the occasion of the earthquakes. Fig. 3.17c presents the equipment change event of PTO1 station over a 2-months data period and shows that the displacements are undisturbed too.
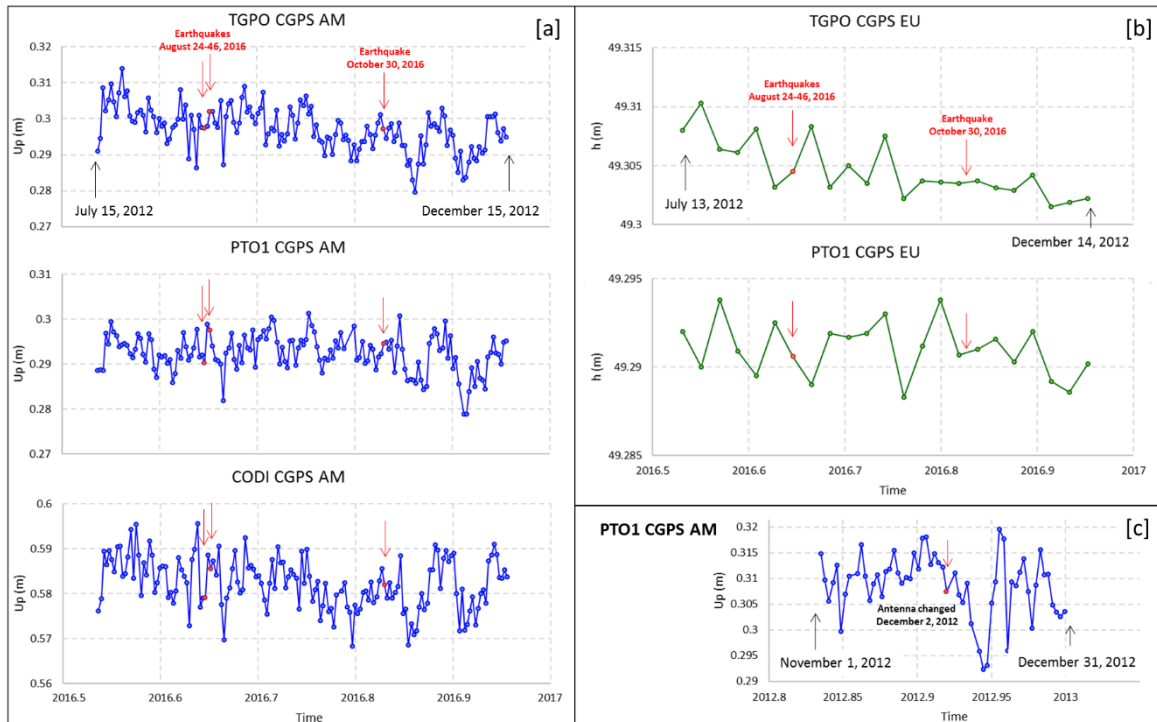
Figure 3.17 – Example of CGPS time series (Up components) before and after: a), b) seismic events on American (AM) and European (EU) CGPS time series, respectively; c) equipment change on the American time series.

In order to quantify the subsidence rates, to delineate the seasonal patterns of each station and to compare the trends of different stations, several time intervals have been considered during the analytical phase of Step 1 (Tab. 3.2). The studied intervals have been chosen on the basis of the data time span, including also the uncertainty on the data correction in relation to the seismic events indicated within the GPS log-files.

N°	Time interval	Analysis type	Dataset	Station/site	Analytical technique
1	September 2012 – December 2015 July 2010 – December 2015	Intra-dataset	(daily data)	TGPO PTO1	12-months CMA, WA
2	October 2012 – December 2015	Intra-dataset	(daily data) American CGPS	TGPO, PTO1	Linear function Polynomial function
3	January 2009 – December 2017 July 2010- December 2017 January 2009 – December 2017	Intra-dataset	(daily data) American CGPS	TGPO PTO1 CODI	12-months CMA 12-months CMA 12- and 6-months CMA, WA
4	June 2012 – October 2016	Single (inter-seismic deformation period)	(daily data American CGPS	CODI	Linear function 6-months CMA
5	October 2012 – October 2016	Intra-dataset (Inter-seismic deformation period)	(daily data) American CGPS	TGPO, PTO1, CODI	Linear function 6-months CMA WA
6	December 2012 – October 2016	Inter-datasets (period not affected by seismic events and equipment changes)	(daily data) American CGPS (weekly data) European CGPS	TGPO, PTO1	Linear function
7	December 2012 – June 2017	Inter-datasets	(daily data) American CGPS (weekly data) European CGPS	TGPO, PTO1	Weekly mean Linear function 12-months CMA and SST 6-months CMA and SST 3-months CMA and SST
8	April 2012 – April 2017 October 2012 – April 2017 April 2012 – April 2017	Intra-dataset	(daily data) American CGPS	TGPO PTO1 CODI	24-months CMA and SST 18-months CMA and SST 12-months CMA and SST 6-months CMA and SST
9	November 2014 – May 2017	Inter-datasets	(daily data) American CGPS (weekly data) European CGPS DInSAR-derived data	TGPO (GPS), PTO1 (GPS), Taglio di Po and Porto Tolle areas	Linear function 12-months CMA 6-months CMA 3-months CMA
10	November 2014 – May 2017	Intra-dataset	DInSAR-derived data	Albarella, Boccasette, Pila (ENEL) and Scardovari areas	Linear function Polynomial function 6-months CMA

Table 3.2 – Time intervals, station/site and analytical techniques used in the current study.

The data pre-processing has been performed taking into account the adopted analytical techniques and the calculation tools (see also Par. 2.3.1.). For instance, the Wavelet Analysis (WA) has been developed by using a Matlab package software (Grinsted et al., 2004), which requires data with constant sampling rate and non-nihil values, while the linear and polynomial functions, as well as the smoothed Centered Moving Average (CMA) (see also Par. 2.3.1. for details), have been calculated by Gnuplot, an interactive plotting program, which loads data with original sampling rate. The main analyses and results are first described in relation to the single database and then illustrated for comparing the different datasets. Three time intervals are proposed herein for describing data analysis and results:

1) October 2012 - October 2016 for the American dataset;

2) December 2012 - June 2017 for the European CGPS dataset;

3) November 2014 - May 2017 for the SAR-derived dataset.

Then, other time intervals are used for showing the correlation among different datasets.

American CGPS time series: permanent and periodic components of subsidence

As it concerns the American daily time series, the subsidence rates estimated using the linear fit over 4-years period of inter-seismic deformation, range between 1.7 and 3.4 ± 0.1 mm/yr (Fig. 3.18), being minimum in the southern part of the Delta (CODI) and maximum in the central part (TGPO). Moreover, the velocities calculated in TGPO (3.4 ± 0.1 mm/yr) and PTO1 (3.3 ± 0.1 mm/yr) stations are quite similar.
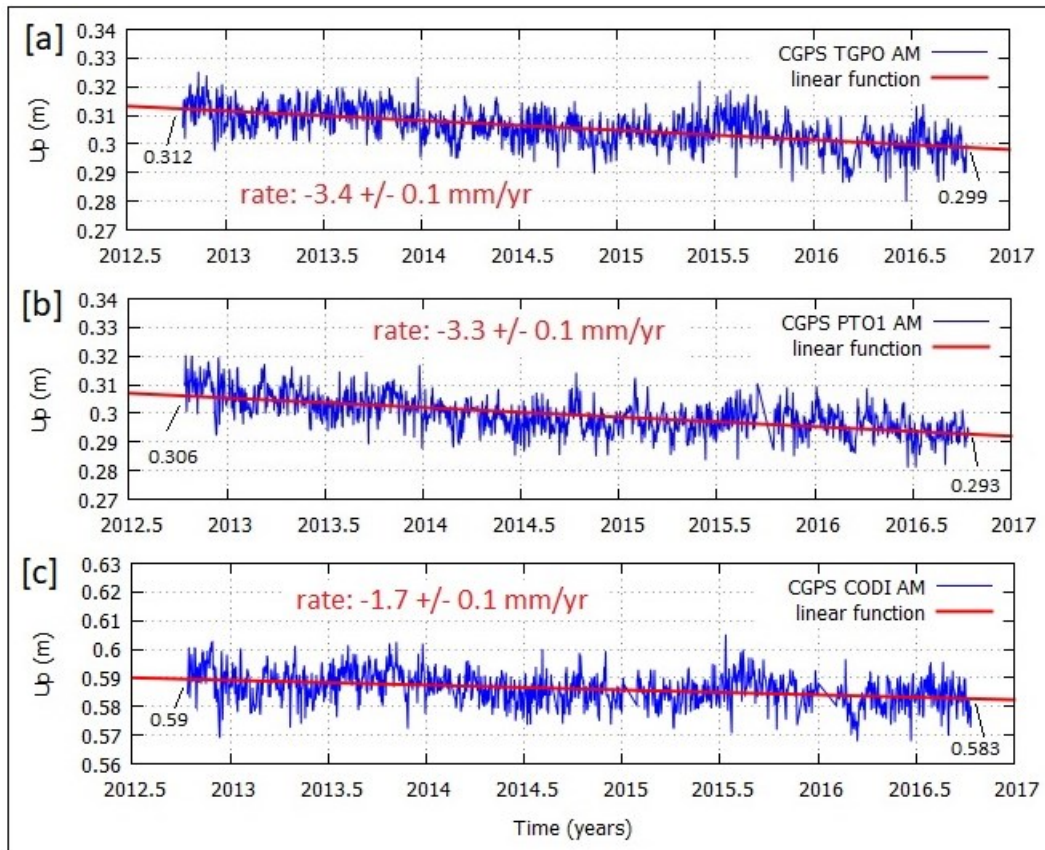
Figure 3.18 – Linear fit on American CGPS data (AM) spanning October 2012 – October 2016 period: a) TGPO, b) PTO1 and c) CODI stations.

It is worth noting that the subsidence rates change in relation with the analysed time interval (Tab. 3.3), thus indicating the occurrence of non-uniform processes controlling the ground motion.

SUBSIDENCE RATE (mm/yr) – American CGPS time series			
TIME INTERVAL	TGPO	PTO1	CODI
October 2012 – December 2015	2.9 ± 0.2	4.0 ± 0.2	-
October 2012 – October 2016	3.4 ± 0.1	3.3 ± 0.1	1.7 ± 0.1
June 2012 – October 2016	-	-	1.9 ± 0.1
November 2014 – May 2017	4.1 ± 0.3	2.5 ± 0.2	

Table 3.3 – Analysed time intervals and mean subsidence rates estimated by daily time series of American dataset.

With respect to the seasonal patterns, the smoothed 12-months CMA applied on the residuals (linear trends removed by original data) reveals a quite regular narrow oscillation characterised by an inter-annual period (~ 2 years), especially in TGPO and CODI CGPS data (Figs. 3.19a – 3.19c). The WA performed at CODI over 9-years of data period enhances the occurrence of these two stronger power peaks at about 1-year and 2.1-years scales. The smoothed 6-months CMA

points out the presence of a clear annual signal with variable amplitude, also confirmed by the WA. In particular, Figs. 3.19d, 3.19e and 3.19f show the continuous wavelet power spectrum of TGPO, PTO1 and CODI CGPS time series, respectively. In the images, the thick black contour designates the 5% significance level against red noise, while the black contoured shading is the cone of influence where edge effects occur (Grinsted et al., 2004). All the three records clearly exhibit a strong power peak at 12-month scale (period=1 year) and a weaker intra-annual oscillation at about 6-month scale (period = 0.5 year). PTO1 and CODI CGPS time series are also characterised by an oscillation at 3-month scale (period = 0.25 year).
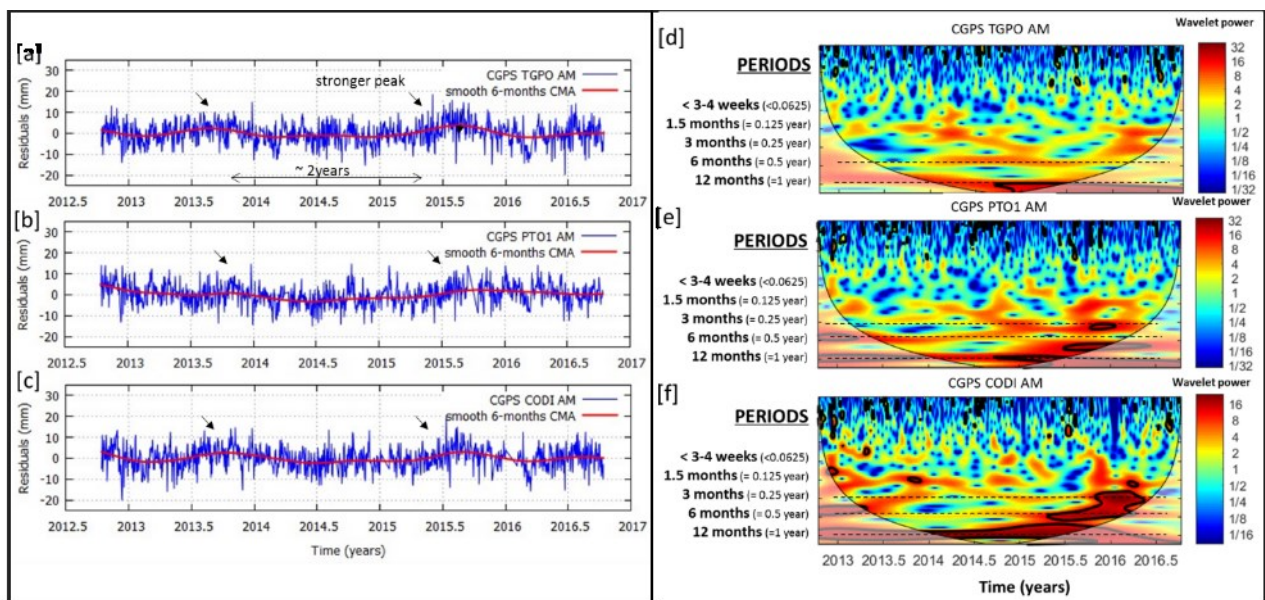
Figure 3.19 – Time and frequency behaviour of the American (AM) dataset during October 2012 – October 2016 period. Smoothed 6-months CMA (red curve) at: a) TGPO, b) PTO1 and c) CODI stations; WA at: d) TGPO, e) PTO1 and f) CODI stations.

European CGPS time series: permanent and periodic components of subsidence

The subsidence rates estimated from the European weekly time series, in the time span December 2012 - June 2017 in the central part of the Delta, range between 5.2 ± 0.1 and 7.2 ± 0.2 mm/yr at PTO1 and TGPO stations, respectively (Figs. 3.20a and 3.20d).
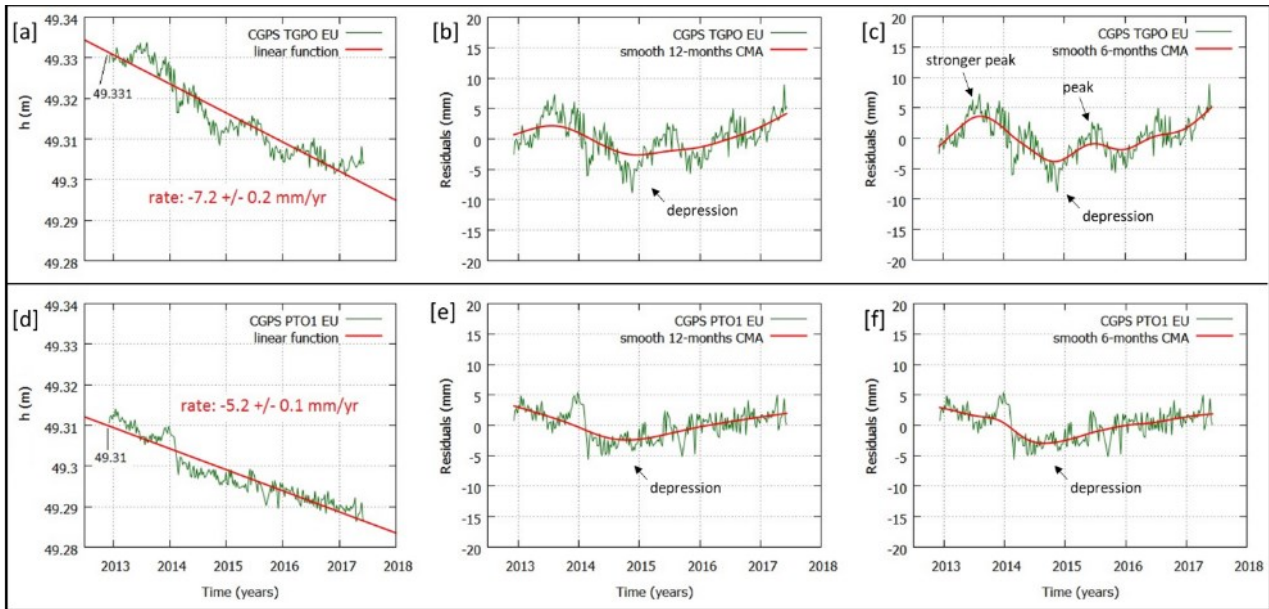
Figure 3.20 - Linear fitting and moving averages on European CGPS data (EU) during December 2012 – June 2017 period: a), b) and c) TGPO CGPS station; d) e) and f) PTO1 CGPS station. a) and d) linear fit on TGPO and PTO1 stations, respectively; b), e) smoothed 12-months CMA and c), f) smoothed 6-months CMA on residuals of TGPO and PTO1 CGPS data, respectively.

Moreover, the geodetic velocities resulting from the European data are systematically higher than those obtained by the American data during the same time intervals, as it is shown in Tab. 3.4.

SUBSIDENCE RATE (mm/yr) – American versus European time series			
STATION	December 2012 to October 2016	December 2012 to June 2017[1]	November 2014 to May 2017
TGPO AM	3.3 ± 0.2	3.4 ± 0.2	4.1 ± 0.3
TGPO EU	7.8 ± 0.2	7.2 ± 0.2	4.8 ± 0.3
PTO1 AM	3.0 ± 0.1	3.0 ± 0.2	2.5 ± 0.2
PTO1 EU	5.6 ± 0.2	5.2 ± 0.1	3.4 ± 0.2

Table 3.4 – Mean subsidence rates estimated using American (AM) and European (EU) time series. [1]Note that within this interval, the velocity values are calculated from American weekly time series, obtained applying statistic mean on daily data.

With respect to the seasonal patterns, the smoothed 12-months CMA applied on the residuals, reveals an evident transient subsidence (hereafter called "depression") during 2014 in both the CGPS stations (Figs. 3.20b and 3.20e). In addition, the smoothed 6-months CMA points out the clear occurrence of an annual signal only in the time series of TGPO station and confirms the presence of the mentioned depression in both the stations (Figs. 3.20c and 3.20f). The transient subsidence occurred during 2014 is still present in the American dataset, even smoothed (Figs.

3.19a, 3.19b and 3.19c). It appears on both the datasets as an "hinge zone" by applying the 12-months CMA on the original data (Fig. 3.21).
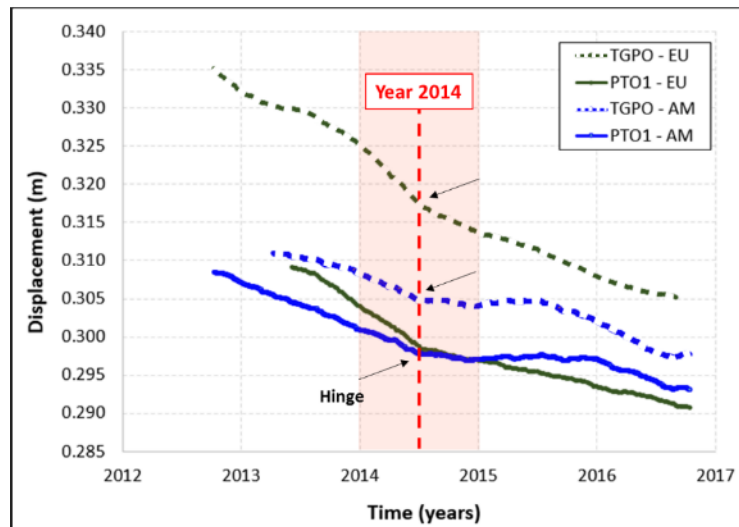
Figure 3.21 – Comparison between American (AM) and European (EU) datasets through 12-months CMA over April 2012 – April 2017 data period. Red dashed line indicates the "hinge zone" in 2014.

InSAR-derived time series: permanent and periodic components of subsidence

In order to estimate the LOS velocity rates from the SAR-derived time series, several permanent scatterer points (PSs) have been chosen around the CGPS stations on the basis of the proximity to the GPS antenna and to the PSs coherence values. In particular, 25, 26 and 19 PSs placed at lesser than 150 m of distance from TGPO, PTO1 and CODI stations, respectively, and characterised by high coherence (> 0.80) were chosen. The base maps of Fig. 3.22 depict the location of the GPS stations and the analysed PSs. The selected PSs have been averaged for obtaining one single time series representative of each area around the GPS stations (black points in the graphs of Fig. 3.22). Since some of these PSs are very close (< 50 m) to the GPS stations, another averaged time series have been calculated using the more proximal points (red points in the graphs of Fig. 3.22). The polynomial fits applied on both the averaged time series (black and red lines, respectively, in Fig. 3.22) show some discrepancies only in CODI area (Fig. 3.22c). Herein, the PSs time series appear more dispersed, although the high coherence. The LOS velocity rates obtained by using the averaged time series (more proximal PSs) range between 0.9 and 2.3 ± 0.2 mm/yr, being minimum in the southern part of the Delta (CODI) and maximum in the central part (PTO1). Moreover, the velocities calculated around TGPO (2.1 ± 0.2 mm/yr) and PTO1 (2.3 ± 0.2 mm/yr) stations are quite similar (Figs. 3.23a and 3.23c).
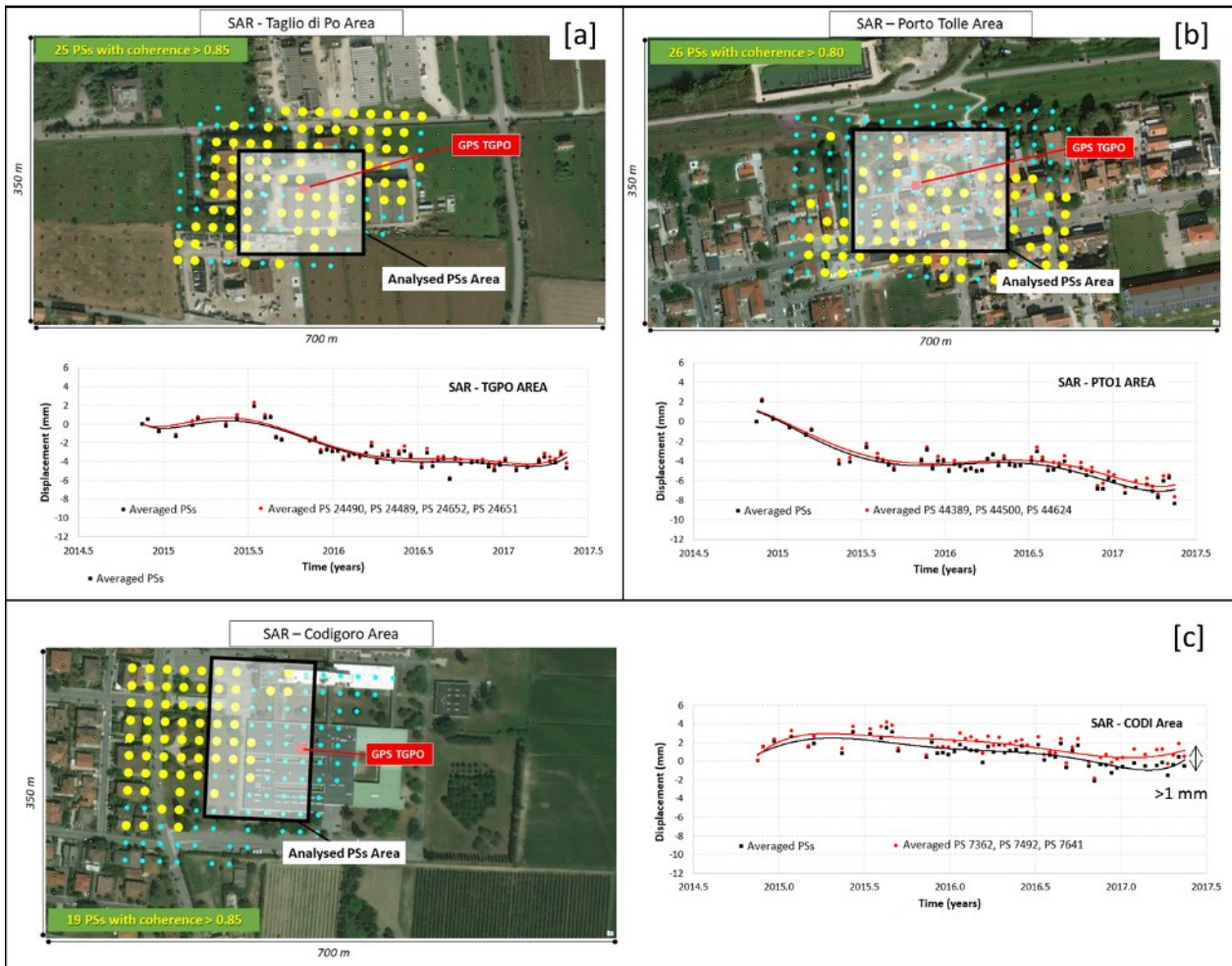
Figure 3.22 – PSs of Sentinel-1A DInSAR data and related displacement time series around: a) TGPO, b) PTO1 and c) CODI CGPS stations.
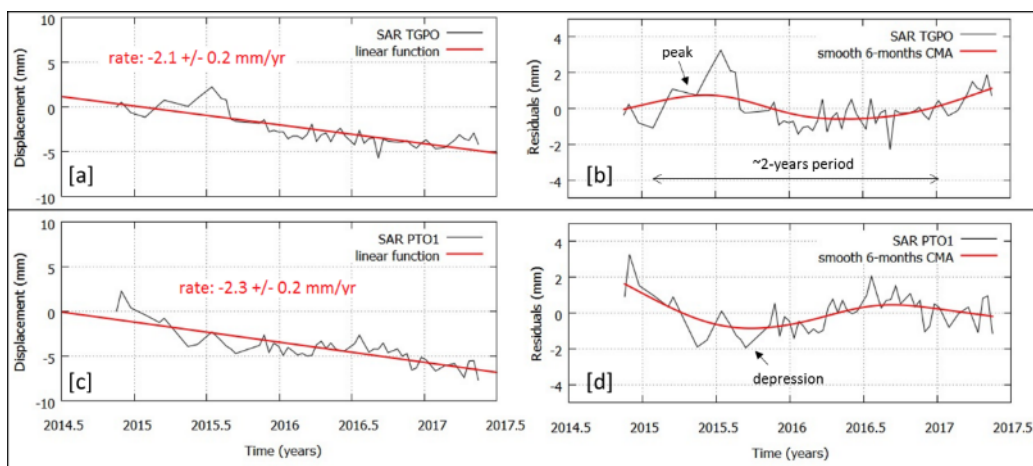
Figure 3.23 - Linear fitting and moving averages on SAR-derived data during November 2014 – May 2014 period: a) and c) linear fit on TGPO and PTO1 areas, respectively; b) and d) 6-months CMA on residuals of TGPO and PTO1 data, respectively.

In order to properly compare results from CGPS and DInSAR, the vertical component of the CGPS vectors has been projected into the SAR LOS using the simplified relationship (from Tosi et al., 2016):

$$GPS_{LOS} = \cos \theta * Up,$$

where θ corresponds to the ground track angle of SAR satellite and Up is the GPS vertical displacement. Then, the LOS velocities have been estimated from projected time series. Tab. 3.5 collects the LOS velocities derived from InSAR and projected European datasets within the same time interval, November 2014 – May 2017. It points out the quantitative differences among them and, in particular, shows that the SAR-derived velocities underestimate the CGPS linear rates, especially in TGPO area.

LOS VELOCITY RATE (mm/yr) November 2014 - May 2017		
STATION	DATASET	RATE
TGPO	European CGPS - LOS	3.7 ± 0.2
	SAR-derived time series	2.1 ± 0.2
PTO1	European CGPS - LOS	2.6 ± 0.1
	SAR-derived time series	2.3 ± 0.2

Table 3.5 – Mean LOS velocity rates estimated from American, European CGPS and SAR datasets.

The LOS velocity rates have been also estimated using SAR-derived time series in the eastern part of the Po Delta. Differently from the above mentioned procedure, the PSs selected around the Albarella, Boccasette, Pila (Enel thermoelectric power plant) and Scardovari sites, have been mainly selected on the basis of the location to analyse, within a circular radius up to 75 m long. Tab. 3.6 summarises some information on the PSs and illustrates that the LOS velocity rates are higher than the ones obtained using the same technique in the central and southern parts of the Delta.

LOS VELOCITY RATE (mm/yr) November 2014 - May 2017			
SITE	Number of analysed PSs	PSs mean coherence	RATE
Albarella	15	0.74	6.3 ± 0.2
Boccasette	15	0.65	7.8 ± 0.4
Pila (Enel)	29	0.61	10.8 ± 0.4
Scardovari	11	0.56	9.5 ± 0.5

Table 3.6 – Mean LOS velocity rates estimated using SAR dataset in the eastern part of the Po Delta.

With respect to the seasonal oscillations, the smoothed 6-months CMA applied on the residuals, highlights the occurrence of inter-annual scale signals with period of about 2 years in all the analysed series. In particular, around TGPO GPS station the residual data exhibit a peak during 2015, followed by a depression in 2016, while in PTO1 site the data show a depression in 2015, followed by a peak in 2016 (Figs. 3.23b and 3.23d). Data results thus indicate that the seasonal signals of these series are in opposition of phase.

Inter-datasets comparison and further analyses

In order to verify similarities in the seasonal trend of CGPS and SAR datasets, CMA analyses have been applied on the original time series during November 2014 – May 2017 period. The results indicate that over the Delta, the SAR-derived time series provide different trends with respect to the CGPS-derived time series, especially in PTO1. This achievement enhances the idea shared by several authors that the SAR-derived data need more accurate calibrations through the GPS data.

As it concerns the comparing between CGPS datasets coming from Am and Eu databases, similarities are found only in TGPO station. Since the CGPS data provide more accurate information on the land motion and are crucial for understanding the size of the subsidence phenomenon, it will be very important deepening into the differences derived from these analyses and likely due to the different data processing carried out by the two agencies with different softwares (Gipsy/Oasis II and Bernese). Fig. 3.24 depicts an example of statistical analysis for comparing the three datasets (CGPS Am/Eu and DInSAR) using the smoothed 6-months CMA. The figure illustrates the main features mentioned above.
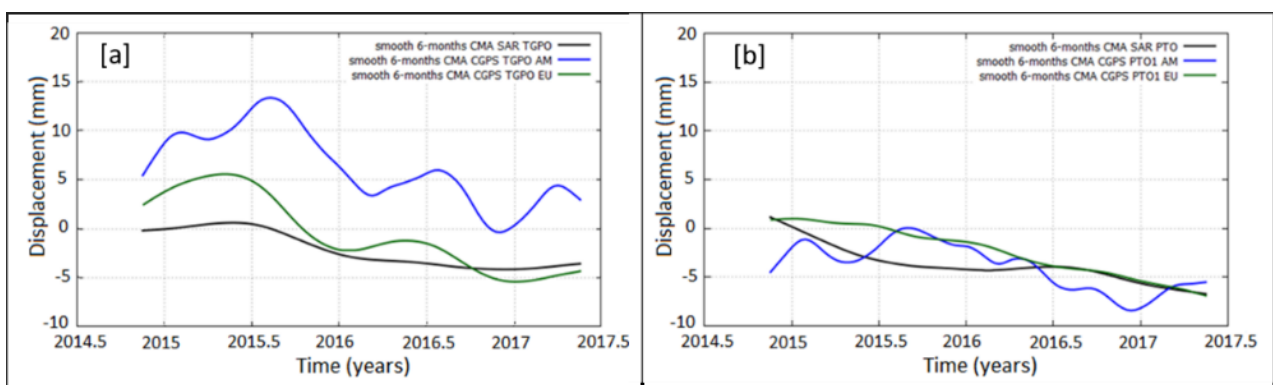
Figure 3.24 – Moving averages applied on the three available geodetic datasets over November 2014 – May 2017 period. Displacement time series at: a) TGPO site and b) PTO1 site.

Finally, the improvement in accuracy of the subsidence velocity estimate by removing the periodic intra-annual variations with statistical models is carried out. Several tests by applying 3-, 6-, 12-months Stable Seasonal Component (SSC) filters have been performed on the European CGPS dataset. The subsidence rates are calculated on the residuated time series (seasonal component removed from original data) according to the periodicity of the removed seasonal component. Tab. 3.7 shows an example of subsidence rates and bias reduction calculated using the SSC filters.

SUBSIDENCE RATE (mm/yr) - European CGPS time series	
FILTER	RATE
No filter	7.2 ± 0.16
12-months SSC	7.0731 ± 0.000152
6-months SSC	7.1092 ± 0.000163
3-months SSC	7.1524 ± 0.000161

Table 3.7 – Subsidence rates calculated using several SSC filters on the European CGPS TGPO data between December 2012 and June 2017.

3.4.2. Step 2: Multi-disciplinary and multi-methodological comparative analysis

In order to properly detect the main physical processes (step 3) responsible for the land subsidence in the Po Delta Area, as well as to explain the permanent and the periodic components clearly exhibited by the geodetic time series (step 1), multi-disciplinary and multi-methodological comparative analyses have been performed. The results of this phase provide useful indications for selecting and modelling the main physical mechanisms active over the Delta.

Permanent component of subsidence: geodetic versus geological data

With respect to the permanent component of subsidence, the step 1 allowed to recognize that the rates of vertical land motion vary over the Delta, being lower in the southern part (CODI site) and higher in the eastern one (Albarella, Boccasette, Pila and Scardovari sites), while low and intermediate values are observed in the central part (TGPO and PTO1 sites). Although the DInSAR data seem to underestimate European CGPS data-derived subsidence, especially at TGPO station (see Tab. 3.5) and need further checks on the raw data processing, among the available geodetic datasets, the SAR-derived time series offer a better covering over the Po Delta. This is the main reason why the SAR-derived LOS velocities are selected for validating the proposed study approach and to get insights into the geological processes controlling the subsidence. In particular, the LOS-

velocities have been compared with the thicknesses of the geological strata, following a procedure already used by other authors (e.g. Tosi et al., 2009). Differently from them (see also Par. 2.2.1.), herein the comparison between geodetic and geological data has been finalised to individuate and model the main active processes. With respect to the comparative procedure, the considered thicknesses correspond to the Plio-Pleistocene, Late Pleistocene-Holocene and Late Holocene sequences, which have been obtained from stratigraphic information available in literature and from Geological Map of Italy F. 187 Codigoro (Geological Survey of Italy, 2009). The comparative analysis reveals that the best correlation between velocity and thickness is obtained with the prograding sequences of Late Holocene (Fig. 3.25).
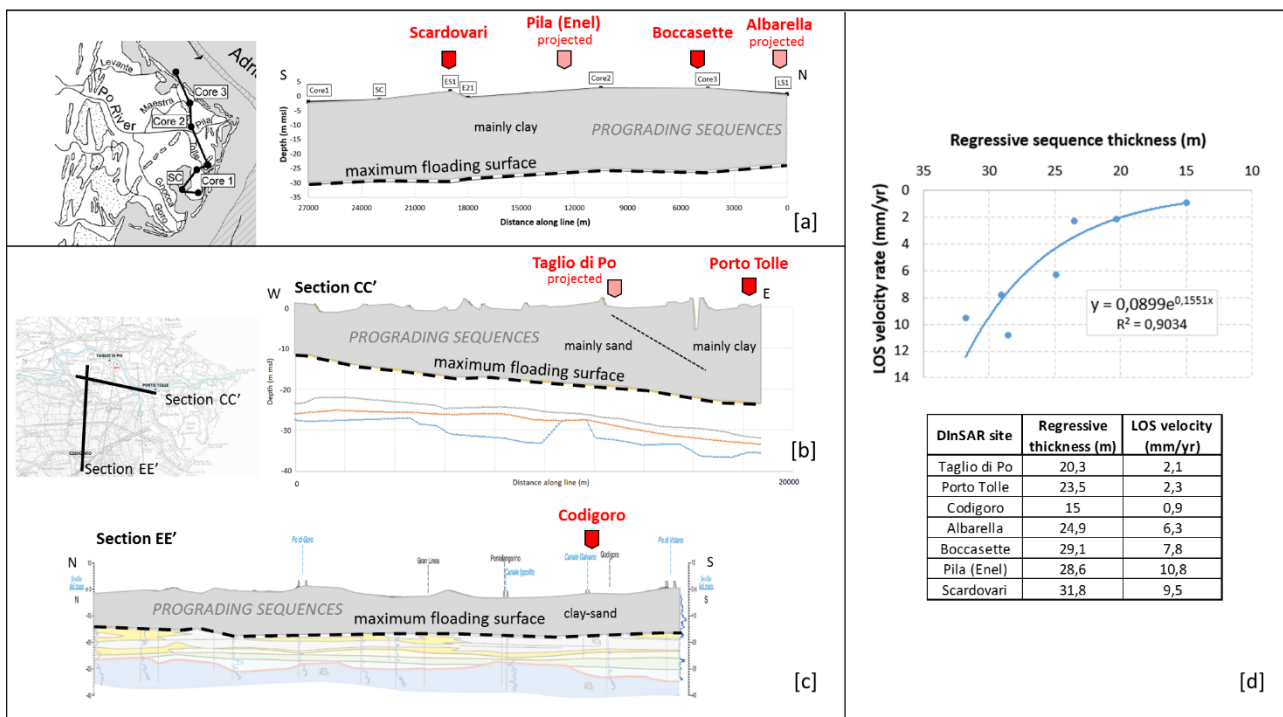
Figure 3.25 – Thickness of prograding sequences of the last transgressive phase over the Po Delta and correlation with the LOS-velocities: a) NS geological section passing through the easternmost part of Delta (modified after Amorosi et al., 2008); b) and c) CC' and EE' geological sections passing through central and southern parts of Delta; original sections are available on Geological Map of Italy F. 187 Codigoro (Geological Survey of Italy, 2009); d) exponential function describing the relation between LOS velocity and sedimentary thickness.

As suggested by other authors (e.g. Teatini et al., 2011), this result confirms that the compaction process of the shallow sedimentary layers and, in particular, of the clay-rich strata, control the subsidence rates over the Po Delta. In addition to this observation, in the following paragraph (Par.

3.4.3.) the compaction process will be modelled on the basis of the exponential porosity-depth relation and in accordance with the back-stripping procedure (see also Par. 2.3.1.).

Periodic component of subsidence: hydro-meteorological data

With respect to the seasonal components, the Step 1 highlighted that the oscillations of the geodetic time series are characterised by periodicities at inter-annual (24-months), annual and intra-annual (6, 3-months) scales, and that the data trends significantly change during 2014. Since these periodicities are typically found in the rainfall patterns (Montanari, 2012) and are generally related to climate-depending meteorological processes, herein hydro-meteorological data (meteorological, hydrological, hydrogeological, mareographic data) have been analysed for recognizing the trend patterns. The analysed measurements, available on open source websites or by request to the producing institutions, refer to 12 different meteo/hydro parameters collected from 57 stations. Most of the analysed data are located in the Po Delta Area (Fig. 3.26).
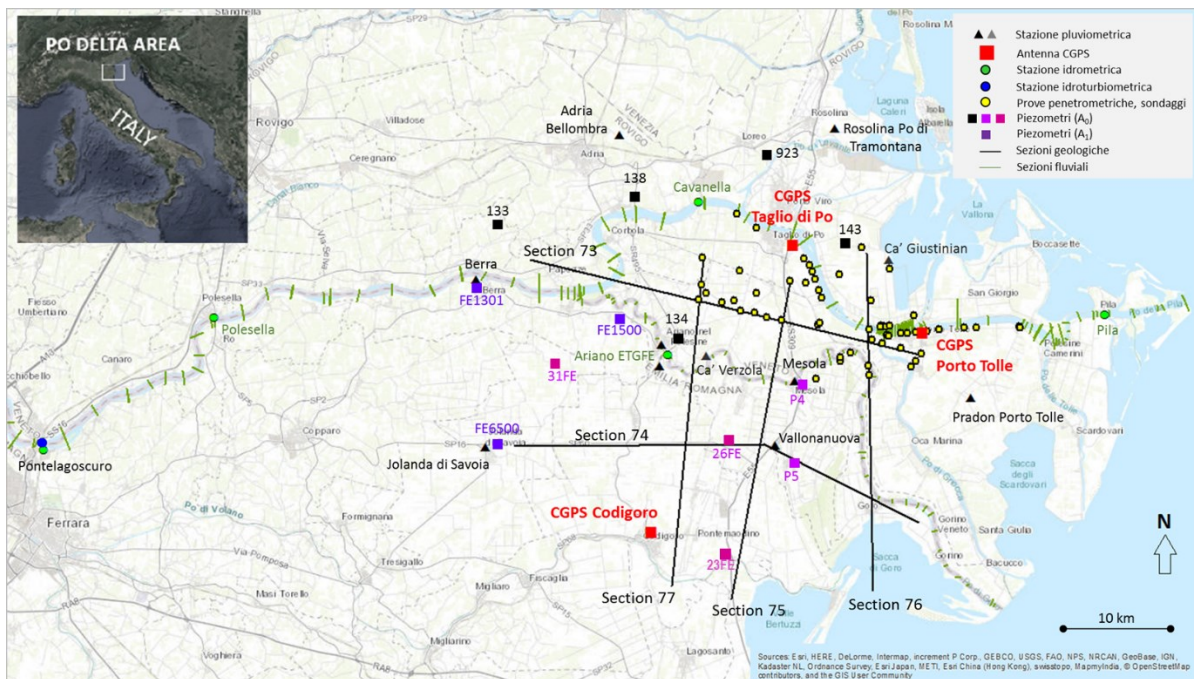
Figure 3.26 – Location of measurement sites: CGPS stations (red squares), pluviometric stations (grey triangles), hydrometric stations (green circles) and piezometers (pink squares). In addition: geological sections (black lines); fluvial sections (green lines) and standard piezocone tests or lithological boreholes (yellow points).

Since the data coming from each station are inhomogeneous in terms of sampling rate and time span length, different pre-processing procedures have been applied. Tab. 3.8 summarizes the studied parameters, provider websites, time intervals and adopted analytical methods.

Data type	Original sampling rate	Source	Station	Time interval	Analytical technique
Rainfall	Daily data	www.bonificadeltadelpo.it	Cà Giustiniani, Goro Cà Verzola	January 2008 – December 2017 June 2012 – December 2017	Mean on 1-month and on 6-, 7.5-, 9-, 12-months; 12-, 6- and 3-months CMA
		www.scia.isprambiente.it www.arpa.veneto.it	Pradon Porto Tolle, Rosolina Po di Tramontana, Adria Bellombra	January 2009 – December 2017	
			Copparo, Volano	January 2008 – December 2017	
			Berra, Mesola, Jolanda di Savoia, Vallonanuova, Ariano ETGFE	January 2012 – December 2015	
			Codigoro	January 2013 – December 2015	
		cloud.consorziocer.it/FaldaNET	31FE, 26FE	January 2008 – December 2015	
River discharge	Daily data	www.adbpo.gov.it	Pontelagoscuro	January 2009 – December 2015	Mean annual values; 12- and 6-months CMA; WA
River hydrometric level	Hourly data	www.agenziapo.it	Pontelagoscuro SIAP, Polesella SIAP, Cavanella SIAP, Ariano SIAP, Pila SIAP, Castelmassa SIAP	January 2012 – December 2017	Mean daily values; mean on 12- and 7.5 months; 12-months CMA; WA
Piezometric level	4 values/year	http://dati.veneto.it	Loreo 923, Porto Viro 143, Adria 138, Villanova Marchesana 133	January 2009 – December 2015	Mean annual values; 6-months CMA
			Ariano nel Polesine 134	January 2009 – December 2017	Mean annual values
	12-36 values/year	cloud.consorziocer.it/FaldaNET	23FE, 26FE, 27FE, 31FE, 35FE	January 2009 – December 2017	Mean annual values; 12-and 6-months CMA
Sea level	Hourly data	www.mareografico.it	Venezia, Ravenna, Ancona, San Benedetto del Tronto	January 2012 – December 2017	12-months CMA
Pumped water volumes	Monthly data	Consorzio di Bonifica Delta Po	Cà Zen, Cà Verzola, Conca, Pisana	January 2011 – October 2017	6-months CMA
Sea water conductivity	Hourly data	www.mareografico.it	Venezia	January 2011 – December 2017	Mean daily values; 3-months CMA
Air temperature	Monthly data	www.scia.isprambiente.it	Adria Bellombra, Rosolina Po di Tramontana, Pradon Porto Tolle	January 2011 – December 2017	Mean annual values
Air pressure	Monthly data	www.scia.isprambiente.it	Pradon Porto Tolle, Rovigo	January 2011 – December 2017	Mean annual values; 3-months CMA
Air humidity	Monthly data	www.scia.isprambiente.it	Adria Bellombra, Rosolina Po di Tramontana, Pradon Porto Tolle	January 2011 – December 2017	Mean annual values; 6-months CMA
Evapotranspiration	Monthly data	www.scia.isprambiente.it	Adria Bellombra, Rosolina Po di Tramontana, Pradon Porto Tolle	January 2011 – December 2017	Mean annual values
Water balance	Monthly data	www.scia.isprambiente.it	Adria Bellombra, Rosolina Po di Tramontana, Pradon Porto Tolle	January 2011 – December 2017	6-months CMA

Table 3.8 – Analysed parameters, measurement sites, time intervals and analytical techniques performed in the current study.

Moreover, some tests have been also performed in order to quantify the bias introduced by resampling data through simple statistical mean. For instance, the error introduced within the resampled series by neglecting the aliasing effect is lower than 1%. If other specific corrections are neglected, such in case of Bloomfield filter on tidal level measurements, the bias on the resampled series is higher than 1%. Thus, such kind of errors may be still present in the time series used in the current study.

As expected, the analyses of the mean annual and annual cumulative values have shown some correlations among river water level, rainfalls and sea water level (Fig. 3.27). All the time series show rising trends until 2014 and an evident common peak in 2014 (Figs. 3.27b, d and f). After that time, rainfalls keep quite stable high values (Fig. 3.27b), excepted for pluviometric data of Cà Giustiniani station, while Po River levels decrease (Fig. 3.27f). The sea level measured at Venice station indicates higher values during 2014 and 2016, and lower values in 2012, 2015 and 2017 (Fig. 3.27 f).
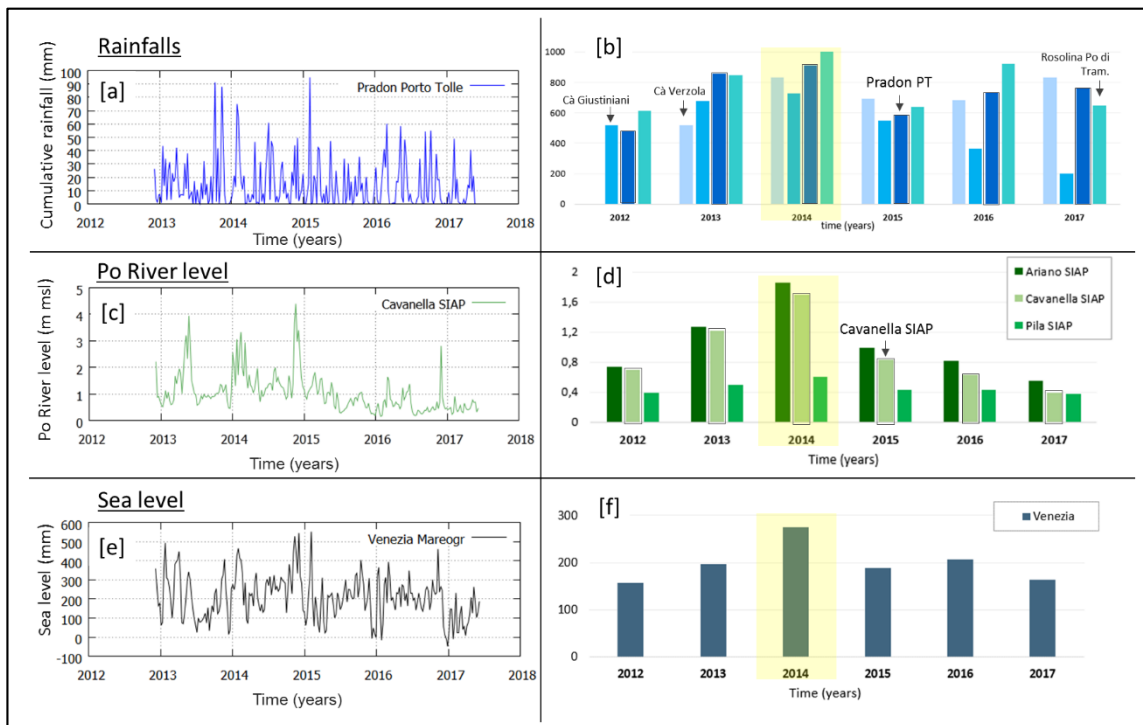
Figure 3.27 – Daily meteorological, hydrological and mareographic data and relative histogram of mean annual values, during December 2012 – June 2017 period: a) rainfalls and b) rainfalls histogram at Pradon Porto Tolle station and Pradon Porto Tolle, Rosolina Po di Tramontana, Cà Giustiniani and Cà Verzola pluviometric stations, respectively; c) Po River hydrometric level and d) hydrometric level histogram at Cavanella SIAP and Cavanella SIAP, Ariano SIAP and Pila SIAP stations, respectively; e) sea level and f) sea level histogram at Venice mareographic station, respectively. Yellow shadow depicts the peak during 2014. See also Fig. 3.26 for sites location.

The annual CMA applied on the same database points out the high correlation among the geodetic data, Po River and sea levels during 2014 (Fig. 3.28). Trend in the river level shows also strong similarities with the sea level in the period 2013-2015 (Figs. 3.28c and 3.28d). After 2015, the river level trend lowers, while the sea level trend arches in relation to an increase of local rainfalls (Fig. 3.28). Moreover, the Po river-water table trend does not change at wider scale, as demonstrated by applying the annual CMA on other measurements collected out of Delta area (Pontelagoscuro SIAP and Castelmassa SIAP river hydrometric stations, located more than 80 km upstream of the river mouth). Conversely, Venice sea level trend, although similar to the one observed in other mareographic stations located out of Delta area (Ancona and San Benedetto del Tronto, positioned more than 200 km southwards to the river mouth), shows also small differences, likely due to local effects (e.g. Po River and local rainfalls).
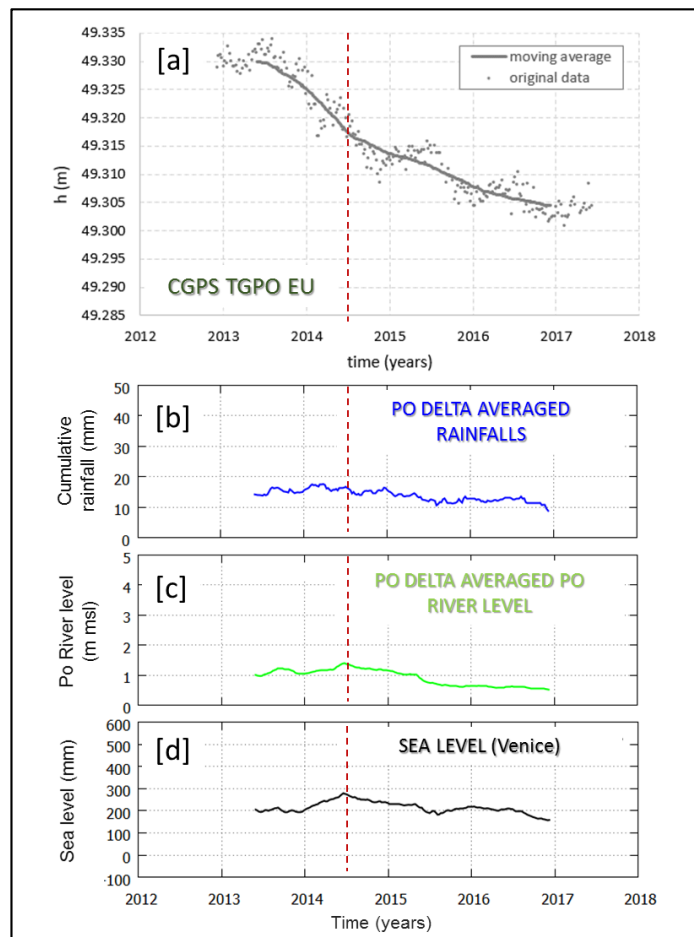
Figure 3.28 – Example of annual CMA applied on geodetic, meteorological, hydrological and mareographic data during December 2012 – June 2017 period: a) CGPS time series of TGPO station; b) daily cumulative rainfalls corresponding to the mean values of 4 stations (Cà Verzola, Cà Giustinian, Pradon Porto Tolle and Rosolina Po di Tramontana); c) daily Po River level corresponding to the mean values of 3 hydrometric stations (Cavanella SIAP, Ariano SIAP and Pila SIAP stations); d) daily sea level at Venice station. See also Fig. 3.26 for sites location.

As regards the groundwater level, several piezometers located within the Po Delta Area reach the shallower unconfined aquifer (phreatic water) and the soil water (vadose water) located few meters below the ground level. These two groundwater zones could play a key role in the seasonal oscillations recorded in the CGPS data, since the GPS antennas are monumented on buildings characterised by shallow foundations (up to 2 m b.g.l.), which might be affected by the groundwater table oscillations and relative capillary fringes. Although only few measures are available from each piezometer, such data allow to reconstruct the shallow aquifer trend and to delineate the main correlations with the other parameters. In particular, the measures collected in the central and northern parts of the Delta by Veneto Region, describe only oscillations with annual period due to the lack of data (Fig. 3.29a). The evident peaks of the Fig. 3.29a fall in spring and are related to one of the two peaks of the wet periods of rainfalls. This correlation with the rainfalls is also confirmed by the smoothed 6- and 9-months CMA applied on the rain data collected in the south-eastern part of the Delta and on the more frequent piezometric measures collected by FaldaNET, a public network of Emilia Romagna Region, over the central and southern parts of the Delta (Figs. 3.29b and 3.29c).
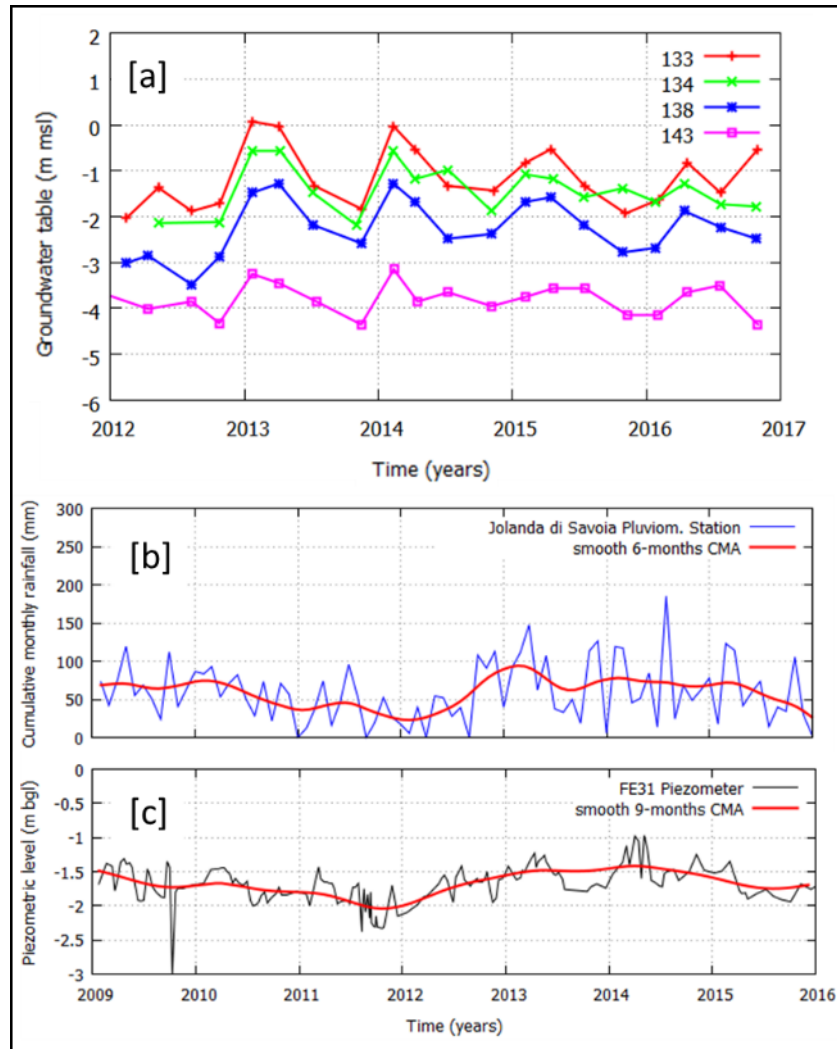
Figure 3.29 – Groundwater levels and correlation with rainfalls in the northern and central parts of the Po Delta: a) groundwater table during 2012-2016 period from Villanova Marchesana 133, Ariano nel Polesine 134, Adria 138 and Porto Viro 143; b) rainfalls during 2009-2015 period at Jolanda di Savoia pluviometric station (red line indicates smoothed 6-months CMA); c) piezometric level during 2009-2015 period at FE31 piezometer (red line indicates smoothed 9-months CMA). See also Fig. 3.26 for sites location.

In addition to the rainfall correlation, the histogram analysis of mean annual and cumulative annual values applied on both rainfalls and river water level, reveal that somewhere the groundwater better correlates with the river, especially in proximity of the main river courses (Fig. 3.30). According to Fig. 3.30, the main difference between river- and rain- water trends is individuated during 2015-2017 period, wherein the river stage elevation decreases, meanwhile the rainfall profile keeps high and quite constant values. The groundwater levels reflect more or less these two different trends.
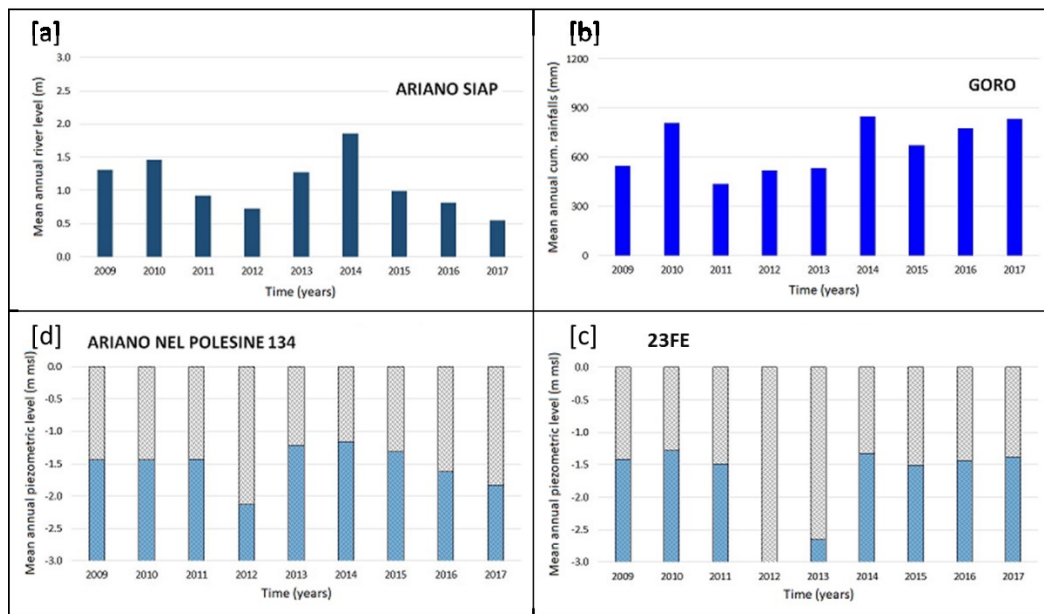
Figure 3.30 - Histograms of mean annual values: (a) hydrometric level of Po di Goro River measured at Ariano SIAP hydrometric station; (b) cumulative rainfall at Goro station; (c) and (d) piezometric levels at 23FE and Ariano del Polesine 134, respectively. See Fig. 3.26 for sites location.

Periodic component of subsidence: geodetic versus hydrological data

In order to characterize possible common features between Po River hydrological data and CGPS data, frequency analyses based on Cross Wavelet Transform (XWT) and Wavelet Transform Coherence (WTC) have been also performed (Grinsted et al., 2004). The analyses have been done first within the time interval from October 2012 to December 2015, between Po River discharge records, measured at Pontelagoscuro hydro-turbiometric station, and daily CGPS data of TGPO and PTO1 stations (Vitagliano et al., 2017). Then, within the same time interval, the Po di Goro River stages, measured at Ariano SIAP hydrometric station, have been compared with the daily CGPS data of TGPO, PTO1 and CODI stations. Some results of the performed analyses are presented in Fig. 3.31, which shows diagrams obtained by comparing each CGPS time series with Po River patterns. In particular, the XWT analysis (Figs. 3.31a, 3.31c and 3.31e) finds regions in time-frequency space where two simultaneous time series show high common power, while the WTC analysis (Figs. 3.31b, 3.31d and 3.31f) finds regions in the time-frequency space where time-series covary but without having necessarily high power. The red areas of the XWT diagrams (Figs. 3.31a, 3.31c and 3.31e) reveal that the geodetic trends compared to the hydrological patterns share strong power peaks at scales of about 12 and 6 months. In addition, PTO1 and CODI time series, in pairs with Po River discharge and hydrometric level at Pontelagoscuro and Ariano stations, respectively, have also a common spectral power at 3-months scale (see also Figs. 3.19c and 3.19e). In the red areas

74

surrounded by the black curves, the signals are more relevant with a 95% confidence level, while the black contoured shading is the cone of influence, where edge effects occur (Grinsted et al., 2004). All the diagrams of Fig. 3.31 include arrows depicting the local phase shift between CGPS records and hydrological patterns for each period; phase differences of 0°, 90°, 180° and 270° are indicated by arrows pointing toward right, up, left and down, respectively. The cross-correlation in the wavelet domain (XWT) shows that the TGPO CGPS and the Po River discharge data are usually out of phase by 180° (Figs. 3.31a and 3.31b) where coherence is more significant (red areas), and this means that when the Po River discharge is higher the ground level is lower and vice-versa. This opposition of phase occurs at periods of about 12- and 6-months. Similar results are obtained also comparing PTO1 CGPS data and Po River discharge (Figs. 3.31c and 3.31d). In this case, however, the two records are found out of phase by 90° at 12-months period, indicating that when the Po River discharge is higher, the ground level at Porto Tolle has a response delayed by about 3 months. Comparing CODI CGPS with Po di Goro River level data, the highest coherence is found for period of annual scale (Figs. 3.31e and 3.31f), when the two series result out of phase of 135°, thus indicating that the land motion is between the TGPO and PTO1 stations. Significant regions in the XWT and WTC spectra are identified using the Monte Carlo method illustrated by Grinsted et al. (2004).

The comparative analyses herein used for studying the periodic component suggest that the ground level may be involved in water mass-dependent processes (Vitagliano et al., 2017; 2018). This item, with other results of the analytical phase, will be better clarified and properly modelled in the next section (Par. 3.4.3.).
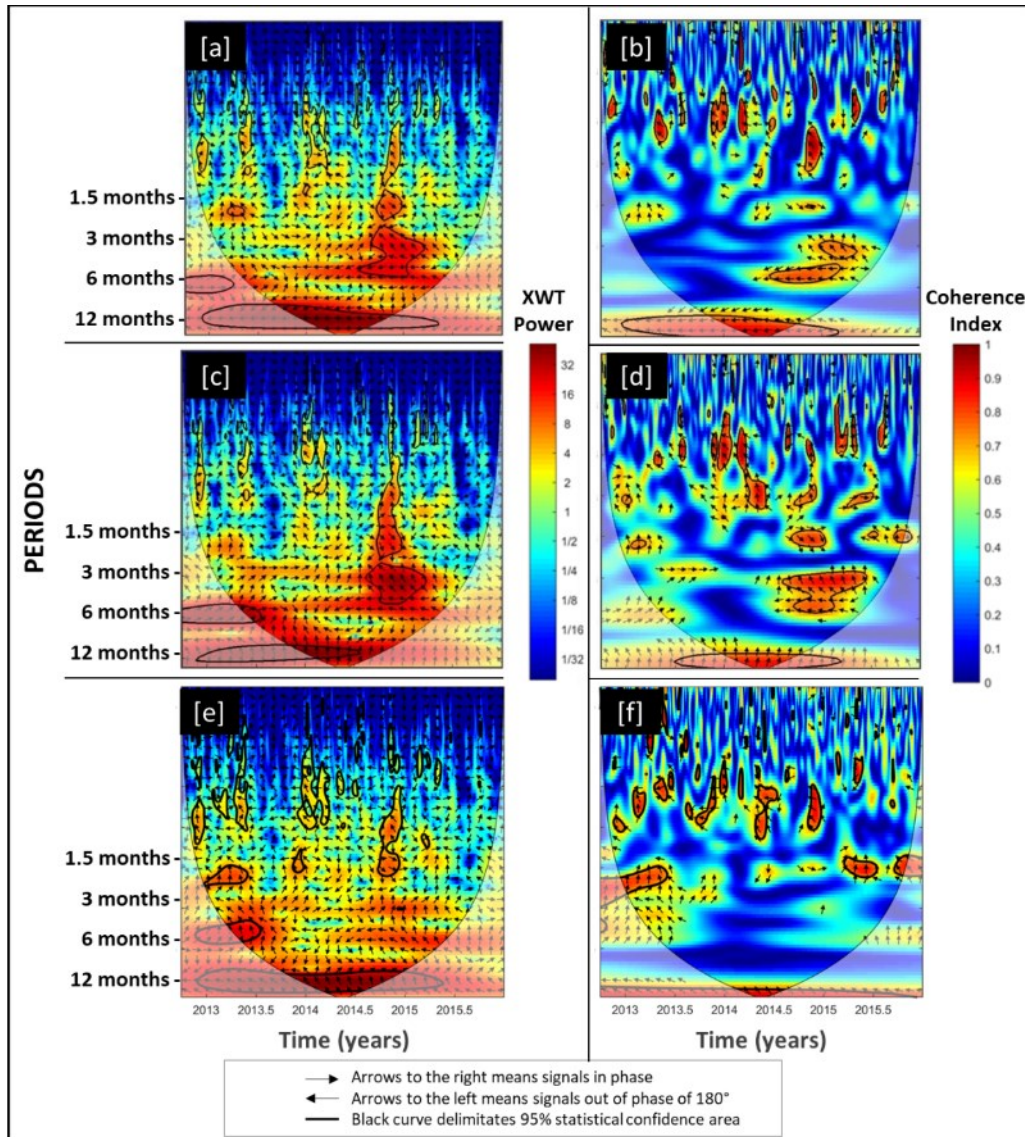
Figure 3.31 – Cross Wavelet Transform (XWT) and Wavelet Transform Coherence (WTC) analyses: a), b) XWT and WTC, respectively, between TGPO CGPS and Po River discharge data at Pontelagoscuro hydro-turbiometric station (modified after Vitagliano et al., 2017); c), d) XWT and WTC, respectively, between PTO1 CGPS and Po River discharge data at Pontelagoscuro hydro-turbiometric station (modified after Vitagliano et al., 2017); e), f) XWT and WTC, respectively, between CODI CGPS and Po di Goro level at Ariano SIAP hydrometric station. See also Fig. 3.26 for site locations.

3.4.3. Step 3: Modelling of the main physical processes

The multi-disciplinary and multi-methodological analyses (Step 2) have been focused on the relationship between ground surface, shallow sedimentary layers and water system (rain-, river-, sea- and ground-water) and unveiled the role of specific processes for explaining the permanent and the periodic components of the land subsidence in the Po Delta. These processes, mainly described in the Chap. 2, have been herein simulated through several physically-based models. Before illustrating the setup of the models and the main results, the findings derived from the

analytical phase are also re-proposed. More details on some of the models equations are provided in Appendix.

Processes related to the permanent component of subsidence

As it concerns the permanent component of the land subsidence, that is the long-term component of subsidence (cfr. Carminati and Di Donato, 1999), the exponential relation found between the mean SAR-derived LOS velocity and the thickness of the last prograding deposits (see also Fig. 3.25), pointed out the key role of the sedimentary compaction process with respect to the spatial distribution of the subsidence rates. Although some authors already highlighted the importance of the consolidation process within the shallower strata (e.g. Teatini et al., 2011; see also Par. 3.1.), or in the deeper strata (e.g. Tosi et al., 2009; see also Par. 2.2.1.), other authors argued the occurrence of tectonics- and isostasy-depending processes in addition to the sediments compaction (Carminati et al., 2006; see also Par. 2.2.2.). In order to validate these processes over the Po Delta and to explain the subsidence rates derived from the analysed geodetic datasets (3.4.1), a 2D geological model has been set up along part of a geological section belonging to the Geological Map F. 187 (Geological Survey of Italy, 2009) (see also Fig. 3.10). The modelled line is WE trending and passes through the central part of the Delta, deepens down to about 35 m and extends up to 18.8 km (Fig. 3.32a). Since the eastern margin of the line ends near Porto Tolle village, while the central part is likely correspondent to Taglio di Po area, these two sites along the line become significant for validating the computed subsidence with the observed one. The line comprises 10 horizons dated from 18 kyr BP to Present time, simulates continuous depositional events (not erosive events) and one hiatus between 11 and 14 Kyr (Fig. 3.32b). The layer geometry has been built by merging the horizons depicted in the geological sections AA' and CC' belonging to the shallow and deeper sheets of the Geological Maps F187 (Geological Survey of Italy, 2009), respectively. Although the two original sections are traced along the same profile, partially share the same horizons and differ for the basal depth (section AA' reaches a depth of about 20 m, while section CC' arrives at about 40 m of depth), these transects present large depth discrepancies with respect to the shared horizons. In addition, these sections show incongruences with other data, like geological sections, lithological boreholes and piezocone tests, available in literature (Cibin and Stefani, 2006). In order to overall such problems and to define a reliable 2D model geometry, the shallow horizons of the modelled line have been derived from the section AA', more refined in the shallowest part of the sedimentary sequence, while the deepest horizons have been depicted on

the basis of the section CC'. Furthermore, a wider and thorough geological database (Tab. 3.9) was necessary for solving the found incongruences and for better selecting the input parameters (ages and litho-types). Although these efforts to improve the model input, data uncertainties on layer geometries and paleo-environment indicators are still present and affect, joint with the lack of in-situ information (e.g. depth-porosity data), the reliability of the modelling results, as it is shown at the end of this section (Tab. 3.11).
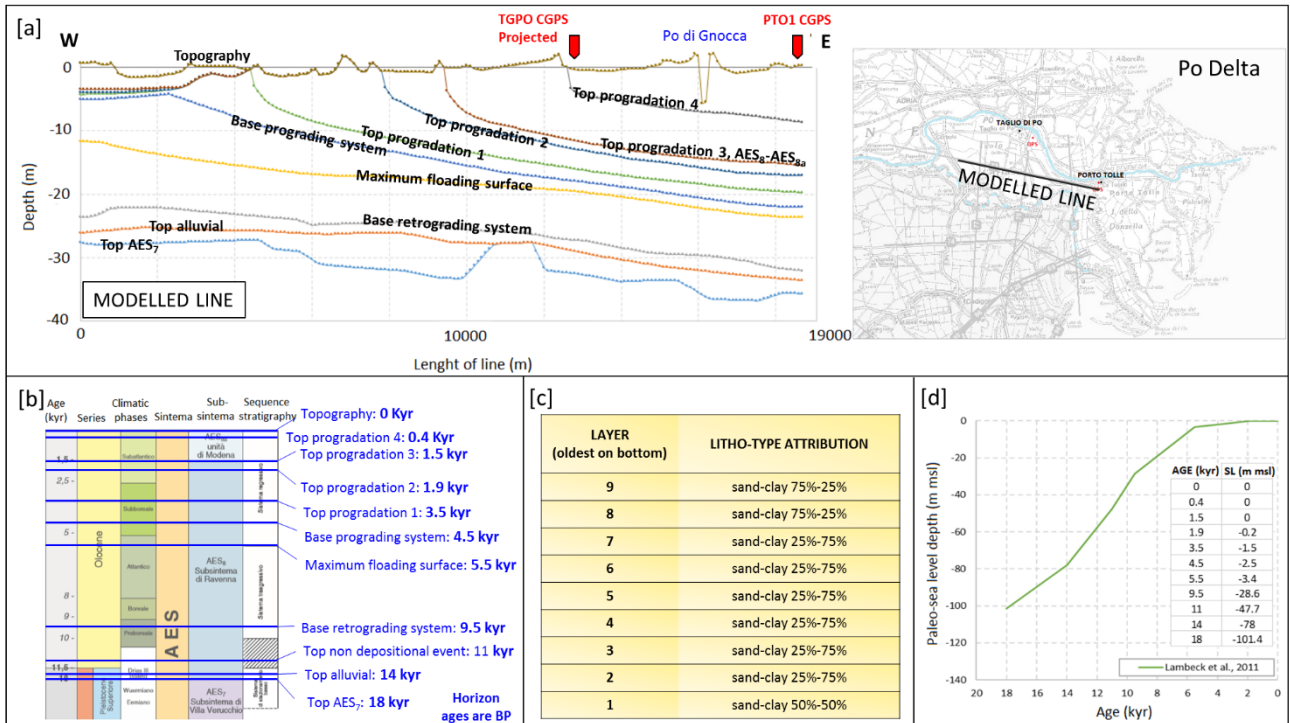
Figure 3.32 - Modelled line and main input parameters: a) horizons geometry; b) horizons age over chronostratigraphic scheme of Po Delta (modified after Cibin and Stefani, 2006); c) litho-types; d) paleo-sea level values.

MAIN INPUT OF GEOLOGICAL MODEL	DATABASE	DATA SOURCE
HORIZONS GEOMETRY	Line AA' – Geological Map F187 (surface sheet) Line CC' – Geological Map F187 (deeper sheet) 5 Cross sections – Geological Map F187	Geological Map 1:50000 (www.isprambiente.gov.it)
HORIZONS AGE	Chronostratigraphic scheme Chronological evolution of Po Basin and Adriatic Sea Measures of radiocarbon age	Cibin and Stefani, 2006 Amorosi et al., 2016 Cibin and Stefani, 2006
PALEO-TOPOGRAPHY	Geological Map NL-33-7-Venice	Geological Map of the Italian Sea 1:250000 (www.isprambiente.gov.it)
PALEO-BATHIMETRY	Core 1 and Core S1 micro-paleontological study Micro-paleontological study on 187-S1 Borehole Paleo-coast lines Environmental and sedimentological data Pro-delta and shallow marine bathymetry Dune system profile Foraminifer depth distribution	Rossi and Vaiani, 2008 Cibin and Stefani, 2006 Antonioli et al., 2009 Cibin et Stefani, 2006 Correggiari et al., 2005 Donadio et al., 2017 Aiello et al., 2012
PALEO-SEA LEVEL	Depth of paleo-sea level	Lambeck et al., 2011; Lambeck et al., 2014
GLACIAL REBOUND	Isostatic correction due to ice melt	Carminati et al., 2003b; Carminati and Di Donato, 1999
LITHOTYPES	Lithological boreholes (187-S4 and 187-S3) Penetrometer tests: 187080U50 (4 sites), 187020U50 (4 sites), 187NEU5 (7 sites) Environmental and sedimentological data Sedimentological and lithological study Geological Maps: F187, F77, F65	Lithological logs; Cibin and Stefani, 2006 Geoportal ER-Region (http://ambiente.regione.emilia-romagna.it/geologia/cartografia) Cibin and Stefani, 2006 Cibin and Stefani, 2006 Geological Maps 1:50000 and 1:100000 (www.isprambiente.gov.it)
PETRO-PHYSYCAL PARAMETERS	Porosity Bulk density shallow sequences	Sclater and Christie, 1980; Dickinson, 1953; Maselli et al. 2010 Tornaghi and Perelli, 1985; Maselli et al. 2010
LITHOSPHERE ELASTIC PROPERTIES	Elastic thickness, flexural wavelength Mantle density	D'Agostino et al., 2001; Carminati et al., 2010 Gvirtzman et al., 2016; Maselli et al., 2010; Carminati and Di Donato, 1999

Table 3.9 – Main input and information for constraining the 2D geological model.

The line is characterised by sand-clay paralic sediments, which reflect the last retrograding and prograding depositional sequences (see also Par. 3.1.1.). The litho-types attributed to the modelled layers reflect also the increasing of clay-content to the East, due to occurrence of prodelta-transition to marine environments during the prograding phase. The compaction process and the sediment-isostatic mechanism have been modelled using the 2D De-compaction module of Move^{TM}, a structural geology software developed by the Midland Valley Ltd. Company. The change of rock volume due to the porosity loss associated with the burial depth, is calculated according to the depth-porosity curve and to the sand-clay content attributed to the modelled layers (Fig. 3.32c) (see Appendix for details). In particular, two depth-porosity curves have been used: the under-compacted shale curve of Dickinson (1953) and the sandstone curve of Sclater and Christie (1980). The former is congruent with the shallower portion (muddy layer) of a curve obtained from the depth-porosity data, which refers to a borehole of the Central Adriatic Sea, considered as an analogue (cfr. Maselli et al., 2010). The latter curve presents a quasi-vertical trend within the first 40 m of depth. Therefore, it is expected that the sand-rich strata will be not affected by compression. The model calculates the decompacted thickness at the end of each depositional event, and these values are then used for calculating the compaction and the sedimentation rates (Figs. 3.33a and 3.33b). It is worth to note that both these parameters do not correspond directly to the subsidence rates (see also Par. 2.3.1.). In particular, Fig. 3.33a shows the compaction rates of the Holocene-Late Pleistocene sequences, computed on the sites along line that correspond to the CGPS stations (see Fig. 3.32a for location). The different compaction rates, which at PTO1 are higher than at TGPO site, are likely due to the computed paleo-thickness and to the clay-content, which increases eastward. The Fig. 3.33b depicts the sedimentation rates in TGPO and PTO1 sites from Late Pleistocene. Both the sites show an increase in depositional rates after the maximum marine ingression occurred about 5.5 kyr BP. Especially during the prograding phase, the lower-thickness layer alternates with greater-thickness sequence (Fig. 3.33c), but without any evident correlation with the last climatic phases (Fig. 3.33d). In Fig. 3.33d, the climatic phase of Subboreal and Subatlantic periods have been reconstructed on the basis of literature (Denton et Karnel, 1973; Mayewsky et al., 2004; Simeoni and Corbau, 2009; Piovan et al., 2010).
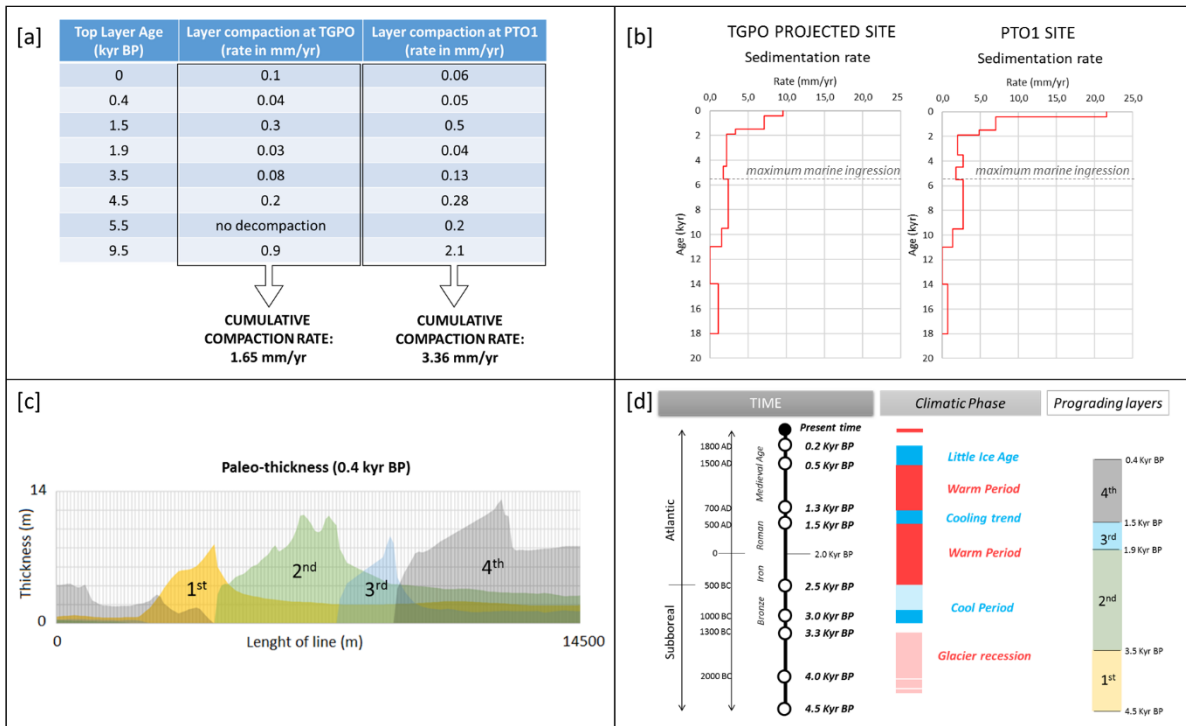
Figure 3.33 – Parameters based on the de-compacted thicknesses computed by modelling: a) Holocene-Late Pleistocene compaction rates in TGPO and PTO1 sites along line; b) Late-Pleistocene and Holocene sedimentary rates in TGPO and PTO1; c) paleo-thickness of the prograding layers calculated at 0.4 kyr BP; d) comparison between climatic periods and ages of the modelled prograding layers.

With respect to the isostatic mechanism, 2D Move™ accounts for the effects of the flexural isostatic deflection of the lithosphere due to the sedimentary load, according to the methodology proposed by Turcotte and Schubert (1982) (see Appendix for details). Since the elastic parameters of the lithosphere below the Po Delta are not well defined, a sensitivity analysis on these variable have carried out by using values associated to the lithosphere below the Central Apennine (D'Agostino et al., 2001) and the Southern Alps (Carminati et al., 2010). The results are shown in the Tab. 3.10 and indicate that greater elastic thickness combined with larger flexural wavelength produce lower mean subsidence rates. The obtained results are in accordance with the value of about 0.4 mm/yr proposed by Carminati and Di Donato (1999), who assume the Airy isostatic compensation relative to the thicker Plio-Pleistocene sediments over the Po Delta.

TEST	REFERENCE	MANTLE DENSITY (kg/m³)	ELASTIC THICKNESS (km)	FLEX. WAVELENGTH (km)	RATES submarine (mm/yr)	RATES subaerial (mm/yr)	MEAN RATES (mm/yr)
1	D'Agostino et al., 2001; Gvirtzman et al., 2016	3225	4	15	0.22	0.36	0.29
2	Carminati et al., 2010	3300	15	250	0.13	0.22	0.18
3	Carminati et al., 2010	3300	10	250	0.13	0.21	0.17

Table 3.10 – Main model input, references and calculated subsidence rates from 18 kyr BP to Present day due to sediment-isostasy.

Moreover, since the modelled layers are deposited after the LGM, the area may be also affected by a double surface effects related to the ice melting: the isostatic rebound due to the reduction of ice thickness in the Alps, and the water load, due to the increase of sea water after deglaciation. The uplift rates associated to the post-glacial rebound amounting to about 0.15 mm/yr, derive from the results of the land and ice models provided by Carminati and Di Donato (1999) and is also confirmed by other authors (e.g. Lambeck et al., 2011). With respect to the paleo-bathymetry, the water depths have been reconstructed at the end of each depositional event following the methodology proposed by Kjennerud (2001) and using the geological information collected over the area (Tab. 3.9). With respect to the paleo-sea level, levels have been obtained using the curves of the North Adriatic Sea, corrected for the glacial-hydro isostatic effects (Lambeck et al., 2011) (Fig. 3.32d). The geological evolution of the line has been reconstructed from 18 kyr BP to Present time according to the backstripping procedure (Allen & Allen, 2005), and accounting for sediment compaction, sediment-isostatic load, glacial-isostatic rebound, paleo-sea level and paleo-bathymetry (see Appendix for details). The geological history of the line is depicted in Fig. 3.35: subaerial conditions are simulated until 9.5 kyr BP (beginning of retrograding system deposition), then shallow marine environment takes place until 5.5 kyr BP (maximum marine ingression) and gradual infilling is assumed up to the present-day (prograding sequences). According to the geological evolution, the total subsidence rates have been calculated in correspondence of the CGPS sites. The computed values of about 0.4 mm/yr at TGPO site and 0.8 mm/yr at PTO1 site, underestimate the LOS velocities derived by DInSAR in Par. 3.4.1. (2.1 ± 0.2 and 2.3 ± 0.2 mm/yr, respectively). The modelled rates depend on present topography and paleo-water depth, both affected by great uncertainty since the discrepancy among the original geological data and the lack of information for better constrain the reconstruction of the paleo-bathymetry (e.g. micro-paleontological study). Tab. 3.11 outlines the wide range of computed subsidence rates obtained varying the Present-day topography

or the PWD at 5.5 kyr BP and enhances the importance of using reliable input to improve modelling results.

	Present-day topography depth (m msl)	PWD at 5.5 Kyr (m msl)	Computed land subsidence (mm/yr)
TGPO	0	-18.2	0.38
	-1	-18.2	0.56
	-2	-18.2	0.75
	0	-15.5	0.82
PTO1	0	-21.8	0.76
	-1	-21.8	0.95
	-2	-21.8	1.13
	0	-19	1.25

Table 3.11 – Influence of present-day topography and paleo-water depth (at 5.5 kyr BP) on computed land subsidence.

Figure 3.35 – Reconstruction of the geological evolution along the modelled line (see Fig. 3.32a for location). Paleo-depths have been obtained considering decompacted thickness, glacio-sediment isostatic corrections, paleo-water depths and paleo-sea levels.

Processes related to periodic components of subsidence

As it concerns the periodic components of the subsidence, our analyses indicated that the geodetic data are characterised by oscillation with 6-months, annual and intra-annual periods, commonly found in the rainfalls (Montanari, 2012) and by inter-annual variations, which are likely associated to other weather- and climate-related fluctuations, such as the quasi biennial oscillation

and the North Atlantic oscillation (Baldwin et al., 2001; Scafetta, 2014). The comparative analyses (see also Par. 3.4.2.) showed that the local rain water trend controls the piezometric level within the shallowest and unconfined aquifer of the Delta, especially in the sites located far from the river or not connected through permeable strata (fluvial and littoral sandy deposits) with the main river courses. This evidence suggests that the process of rain water infiltration within the soil might be active over the Delta, being predominant far from the river courses. Conversely, some piezometers located near the main river courses, revealed that the groundwater variations correlate with the river trends, and thus indicate that the process of river water infiltration might be even active. Since the GPS antennas are monumented on buildings characterised by foundations depths comparable with the unconfined aquifer depths, the geodetic stations might be affected by groundwater table oscillations. In order to verify this hypothesis two models have been performed for simulating the groundwater flow combined with the soil elastic strain. Such kind of mechanism refers to water pressure-dependent processes (see also Par. 2.3.1.). Moreover, the cross-wavelet analysis outcomes the occurrence of opposite trends between the ground level measured at the three CGPS sites and the river level recorded for instance at Ariano SIAP station, thus suggesting a coupled elastic response of the ground level with respect to the river level variations. The river level measured in the Po Delta is mainly related to the rainfalls and to the snowmelts collected in the wide catchment of the Western and Central Alps and Norther Apennines (see also Par. 3.3.). Meanwhile, the North Adriatic Sea receives the contributions from both the Po River and the local rainfalls, as shown in Fig. 3.28 and also supported by the bit differences observed among the sea level trend recorded at Venice mareographic station respect to those localised more than 200 km southwards. In order to verify the hypothesis of an elastic coupling between the rain/river water and soil surface, three models based on surface water loading have been performed. Such a kind of mechanism refers to water mass-dependent processes (see also Par.2.3.1.).

The simulations of water-pressure relating processes have been started at TGPO site, that is an area close to the main Po River course (less than 300 m of distance from river). In TGPO the CGPS data analysis on both the American and European datasets provided similar trends (see also Par. 3.4.1.). Before to start the modelling, new geological and hydrogeological information have been collected within a region comprises between Pontelagoscuro and Pila villages, for better define some hypotheses on the groundwater flow and on the stratigraphic configuration below the CGPS site. In particular, 76 cone tip resistance logs and 52 water-pressure profiles derived from the standard piezocone tests, 18 lithological boreholes, 8 exploration wells, 15 fluvial sections and 4 piezometric

holes that reach the confined aquifer (aquifer A1-I, according to Emilia-Romagna Region, RER classification at http://ambiente.regione.emilia-romagna.it/geologia/temi/acque/idrogelolgia-della-pianura-emiliano-romagnola), have been collected. As it concerns the water charging mechanisms, it is assumed that the water supply reaches the sandy deposits of the phreatic aquifer (aquifer A0, according to RER classification, see above for web reference) or, eventually, the coarse alluvial deposits of the aquifer A1, through entry points located along the river path (Fig. 3.36). In accordance with this mechanism, the regional groundwater flows and the rain water infiltration are considered not relevant with respect to the river water supply. In addition, since the TGPO CGPS station is located out of the Geological Map F187 that collects most of the available information on the Po Delta (Geological Survey of Italy, 2009), the attribution of the lithological content and the definition of the strata geometry is largely affected by uncertainty. In order to overcome this uncertainty, two main hypotheses on the lithological composition of the subsurface terrains have been tested using two different models: Model 1 assumes that the GPS site is located on a clay-rich layer, while in Model 2 the geodetic station is situated on a silty layer.
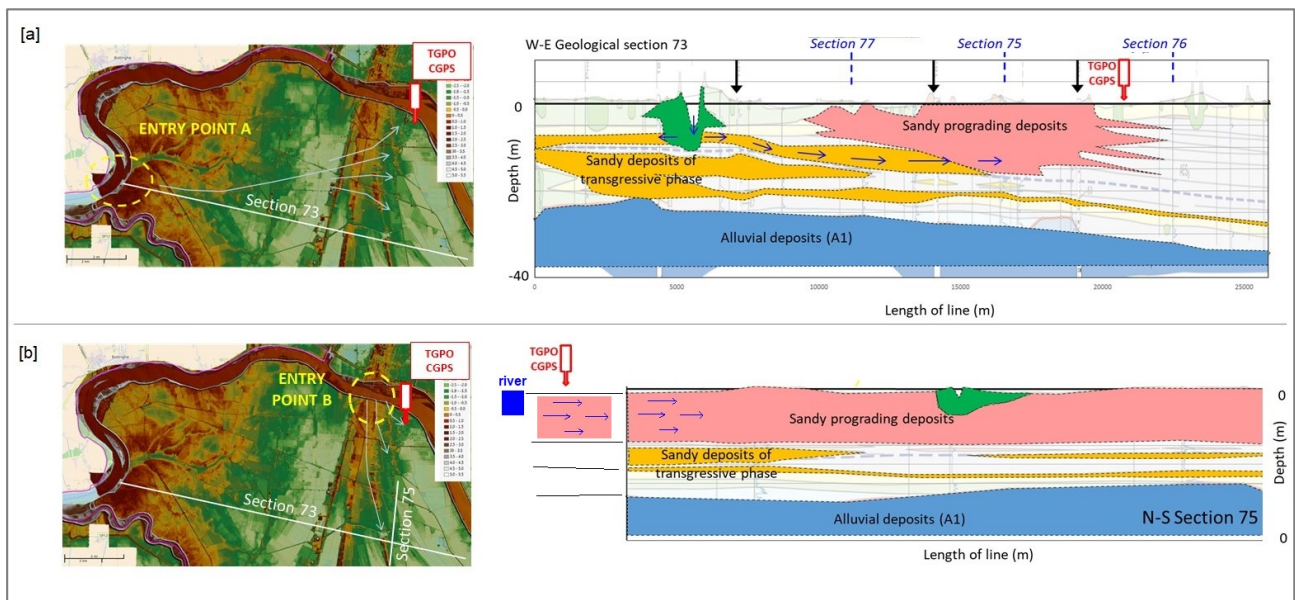
Figure 3.36 – Two examples of aquifer water-charging mechanisms: a) "long path", more than 15 km away from the water river entry point A to the main sandy prograding layers envelop; b) "short path", nearly 2 km away from the water river entry point B to the sands layers.

Both the models simulate the elastic compaction and expansion of the compressible fine-grained beds within the aquifer (inter-beds), caused by head or pore-pressure changes and thus by change in effective stress within the inter-beds. The propagation of head changes within the inter-beds is defined by a transient diffusion equation, which accounts for delayed release of water from storage

or vice-versa, for uptake of water into storage in the inter-beds. The main governing equations are implemented through two available equation solvers referenced hereafter.

Model 1 has been performed using FlexPDE (www.pdesolutions.com), a finite element model builder, developed by PDE Solutions Inc. The main equations on the groundwater flow and soil mechanics consolidation have been written according to the classical theory proposed by Darcy and Bjerrum, respectively (Domenico and Schwartz, 1998), and the modelling has been solved on 2D domain (length and depth of simulated line) (see Appendix for details). A sensitivity analysis on the geometry and permeability of the layers and on the hydraulic head oscillation amplitude has been done through 7 tests, varying the values within lithology-associated ranges in accordance with literature (Domenico and Schwartz, 1998). One of these tests is shown in Fig. 3.37, wherein the deeper sandy layer (A1) is assumed in contact with the shallower one (A0) creating an interconnected permeable region (Fig. 3.37a). The decay from river to floodplain of the hydraulic head in steady-state has been built according to the mean level of Po River stage at Cavanella SIAP station and the mean groundwater table of Piezometer 143, thus assuming that river and shallow aquifer are connected (see also Fig. 3.26 for location) (Fig. 3.37a). The obtained elastic subsidence (1 mm of amplitude) depicted in Fig. 3.37b underestimates the geodetic motion observed in the CGPS station (10 mm of amplitude). The other tests compute elastic subsidence value minor than 1 mm and confirm that the simulated process, although might be active in Taglio di Po area, gives a negligible contribution.
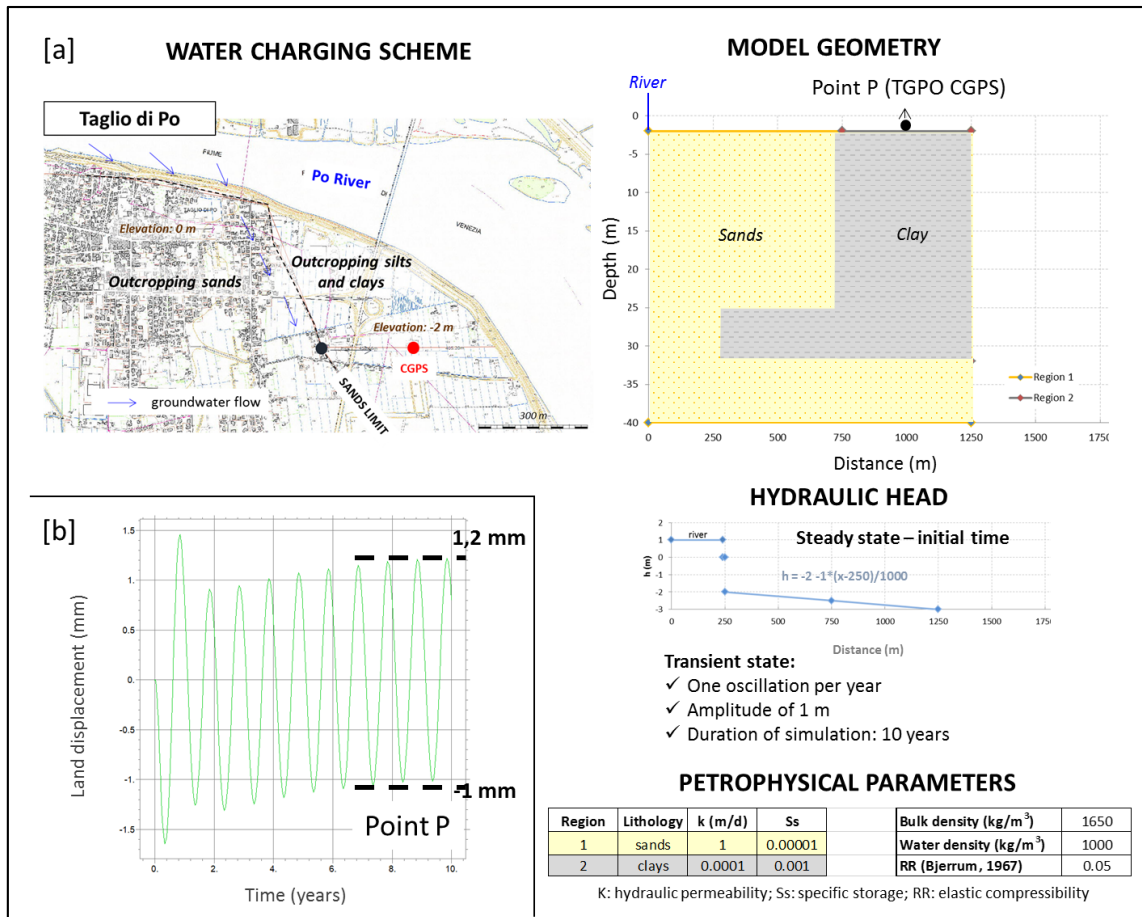
Figure 3.37 – Main inputs and results of Model 1: a) loading mechanism, geometry, hydraulic head and hydrogeological and petro-physical parameters; b) computed elastic subsidence. Base map is available on Geoportal of Veneto Region (http://idt.regione.veneto.it).

Model 2 has been performed using MODFLOW-2005 code (Harbaugh, 2005; available at https://water.usgs.gov/ogw/modflow/), the U.S. Geological Survey modular finite-difference ground-water flow model, and SUB Package (Hoffman et al., 2003), the module for simulating the land subsidence. Differently from the previous case, herein the model is characterised by a 3D mesh, which covers 12.5 km^2 and reach 25 m of depth. The model bottom reproduces the base of the prograding sands envelope and has been obtained interpolating 17 points, which correspond to lithological boreholes, piezocone tests and points selected from geological sections (http://ambiente.regione.emilia-romagna.it/geologia/cartografia). The model geometry is characterised by two layers: the deeper one is sandy-rich and extends over the entire grid reaching a maximum thickness of 15 m, while the shallower one has a constant thickness of 5 m and is made by silts in the eastern part of the grid and by sands in the western one. The hydraulic head has been calculated in accordance with the Po River hydrometric trend measured at Cavanella SIAP (Fig. 3.38a) and Pila SIAP stations, considering a short hydrometric gradient diminishing to the river

mouth. The range of the computed head in the point T, which corresponds to TGPO CGPS site, is comparable with the range calculated in the piezometers 143, 138 and 134, placed in similar geological condition with respect to the study area (Fig. 3.38). A sensitivity analysis on the hydrogeological and petro-physical parameters has been done through 11 tests, varying the values within lithology-associated ranges in accordance with literature (Piccinini et al., 2008a; 2008b) and also accounting for the inelastic compressibility coefficient. Although the computed amplitudes are comparable to those observed in TGPO CGPS residuals (linear trend removed by original data), the modelled trends mismatch the observed one, as it is shown in Fig. 3.38b, and demonstrate that water pressure-dependent processes are not the sources of the periodic oscillations found in the GPS data.
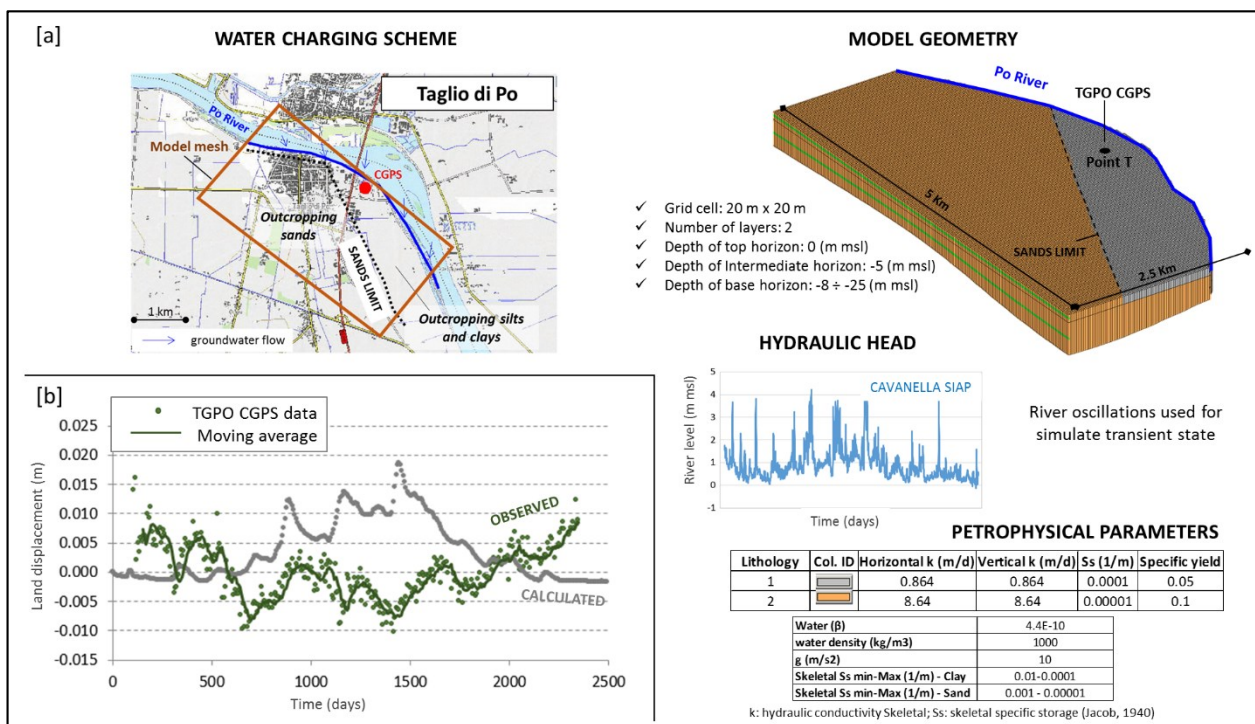
Figure 3.38 – Main input and results of Model 2: a) charging mechanism, geometry, hydraulic head and hydrogeological and petro-physical parameters; b) computed elastic subsidence during April 2011 – June 2017 period, according with European TGPO CGPS data. Proposed base map is available on Geoportal of Veneto Region (http://idt.regione.veneto.it).

In order to verify the water mass-dependent processes, the effect of the loading associated to the rainfalls-soil moisture on the ground level, has been carried out over the entire Po Delta using Modern-Era Retrospective analysis for Research and Applications (MERRA2) (Gelaro et al., 2017) and Global Land Data Assimilation System (GLDAS) (Rodell et al., 2004) models. Computation of ground displacement for all GPS stations used in this study has made available on http://loading.u-

strasbg.fr/. Indeed, these models do not account for surface water, including rivers and deep groundwater processes, but simulate the mass transfer at Earth's surface and other environmental parameters by integrating satellite- and ground-based observations into land surface models through data assimilation techniques. The results of MERRA2, GLDAS/Noah v1.0 and GLDAS/Noah v2.1 models slightly differ due to some modelling basic conditions. For instance, GLDAS model uses the Noah v1.0/v2.1 land surface models for calculating the surface loads due to soil moisture, vegetation water content and snow on a global mesh of one degree (Puskas et al., 2017). Conversely, the land surface model used in MERRA2 is the Catchment model (Koster et al. 2000), which downscales the soil moisture variability and its effect on the runoff and the evaporation amounts. Both the models calculate the elastic displacements at specified station coordinates using Green's functions and other algorithms. The computed elastic displacements have been calculated in the three CGPS stations: TGPO, PTO1 and CODI (Fig. 3.39).
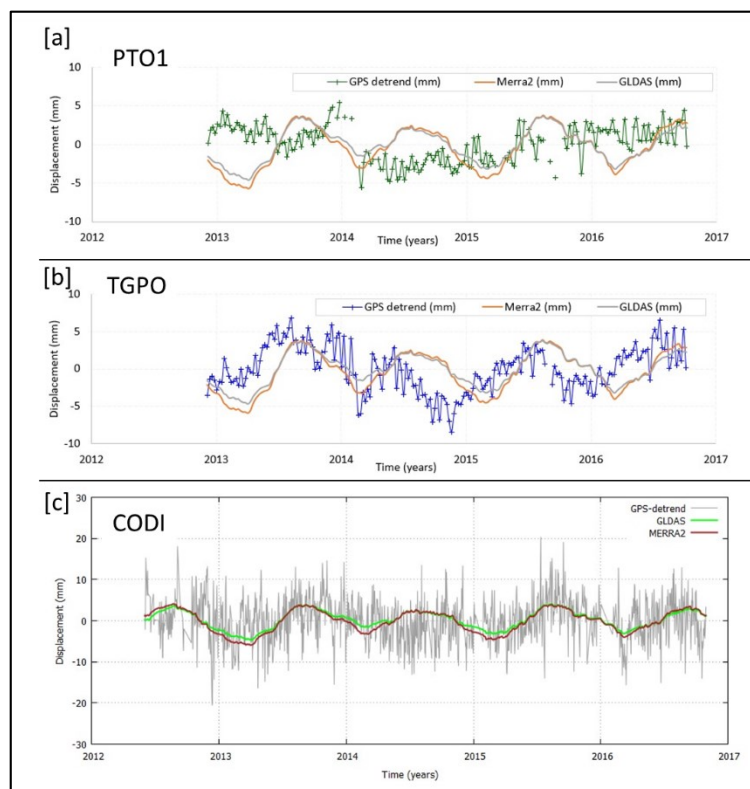
Figure 3.39 – Comparison between residual CGPS data and computed displacement on the basis of the hydrological loading models during 2012 – 2016 period: a) PTO1 (weekly time series); b) TGPO (weekly time series) and c) CODI (daily time series).

Only the GPS station located far from the main Po River course shows a good match between modelling and observations (Fig. 3.39a), thus indicating that in the floodplains far from the river

influence, a process of water loading can act in the topsoil. In addition, at CODI station it has been also verified that significant differences are obtained by using alternatively the hydrological or the statistical models for retrieving the subsidence velocity.

The last modelling has been performed in TGPO area in order to investigate the elastic rebound of the riverbank in relation with the volume change of the river water. As already mentioned in Par. 2.3.1., such mechanism may be possible if soil and shallow layers are impermeable to the water infiltration and more influenced by the surface loading due to water mass changes. This condition is verified by the occurrence of clay-rich layers deposed since the 17th Century eastwards of Taglio di Po village (see also Par. 3.2.) and cut by the main Po River course. For this modeling, the river bed has been approximatively assimilated to the building foundations affected by transient loading, which produces instantaneous settlements. In particular, a portion of the Po River has been schematized through a square plate of 25 m of side length and the instantaneous settlement has been evaluated in correspondence of the point C, located at the corner of the western plate side (Fig. 3.40a). According to this model, the terrain that underlies the GPS station is mainly formed by clay. Its elastic property has been attributed on the basis of the literature available in the near Porto Tolle area (Cortellazzo and Simonini, 2011). The river level oscillations measured at Cavanella SIAP station between January 2011 and December 2017, have been residuated respect to the mean value and then transformed in weight. On the basis of the equations associated to flexible plate foundations, which root on saturated clay and under undrained conditions (Janbu, 1956; Christian and Carrier, 1978), and with respect to the geometric and elastic properties and to the water river load, the good match between the TGPO CGPS residuals (linear trend removed from original data) is evident in Figs. 3.39b and 3.39c. Another test has been performed by applying the same procedure to the sea level measured at Venice mareographic station. In this case, the computed settlement best fits with the geodetic residuals, thus indicating that the water loading influence significantly the periodic oscillations observed in the GPS time series, and that the sea level has an important role even in the inner part of the Delta.
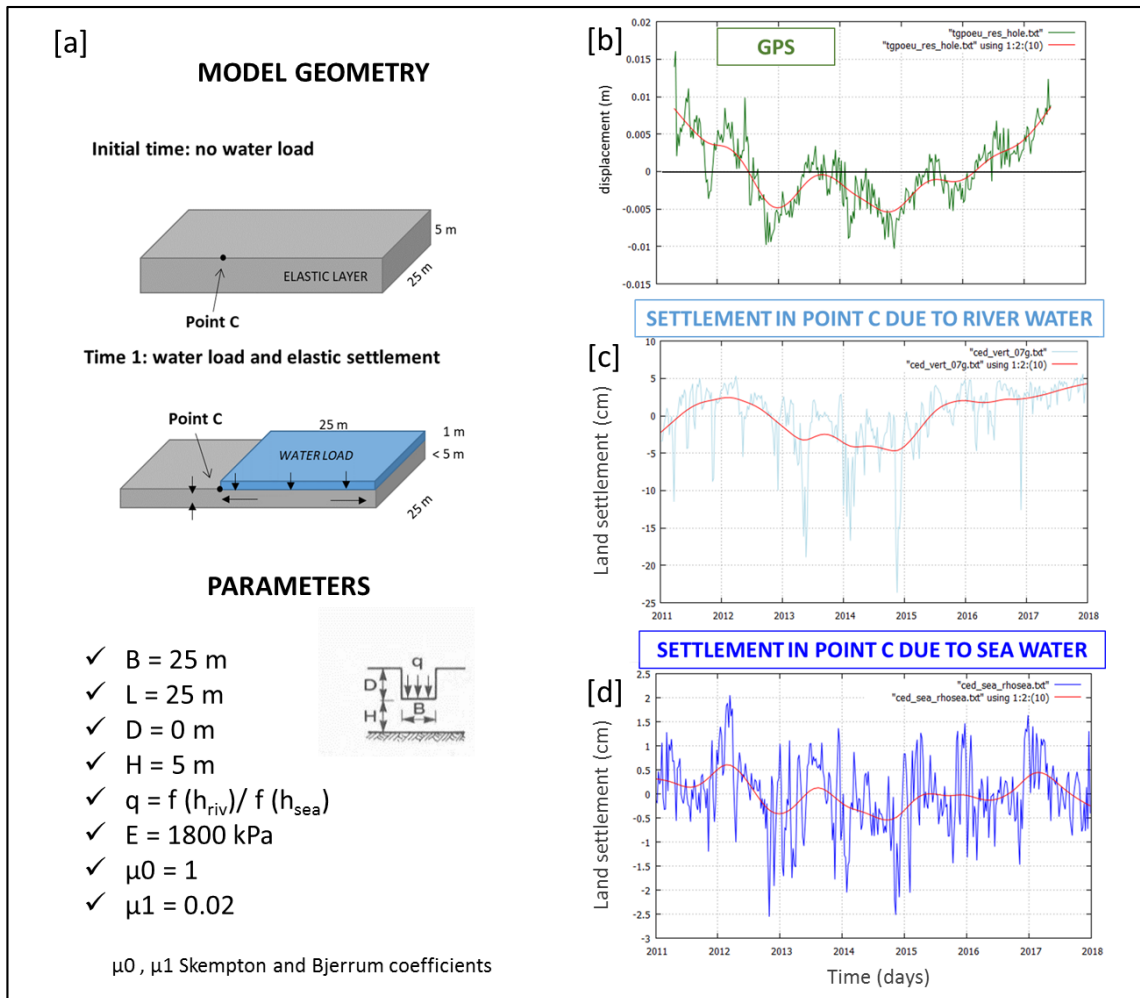
Figure 3.40 – Main inputs and computed displacement according to the instantaneous settlement: a) geometry and model parameters; b) TGPO CGPS residuals and smoothed 6-months CMA (red line); c) settlement computed on the basis of the river level trend; d) settlement computed on the basis of the sea level trend.

Although the proposed model is a rough simplification of the real site configuration (Fig. 3.41) and does not account for in-situ elastic properties, as well as only one solution, consisting of flexible plate foundations with square mesh, has been suggested for calculating shallow settlements based on elastic methods (see also Appendix), it provides interesting insights for understanding the mechanisms acting at ground level in proximity of the river course. Further evaluations of vertical stress and strain distributions within soil under loading will be performed in future studies.
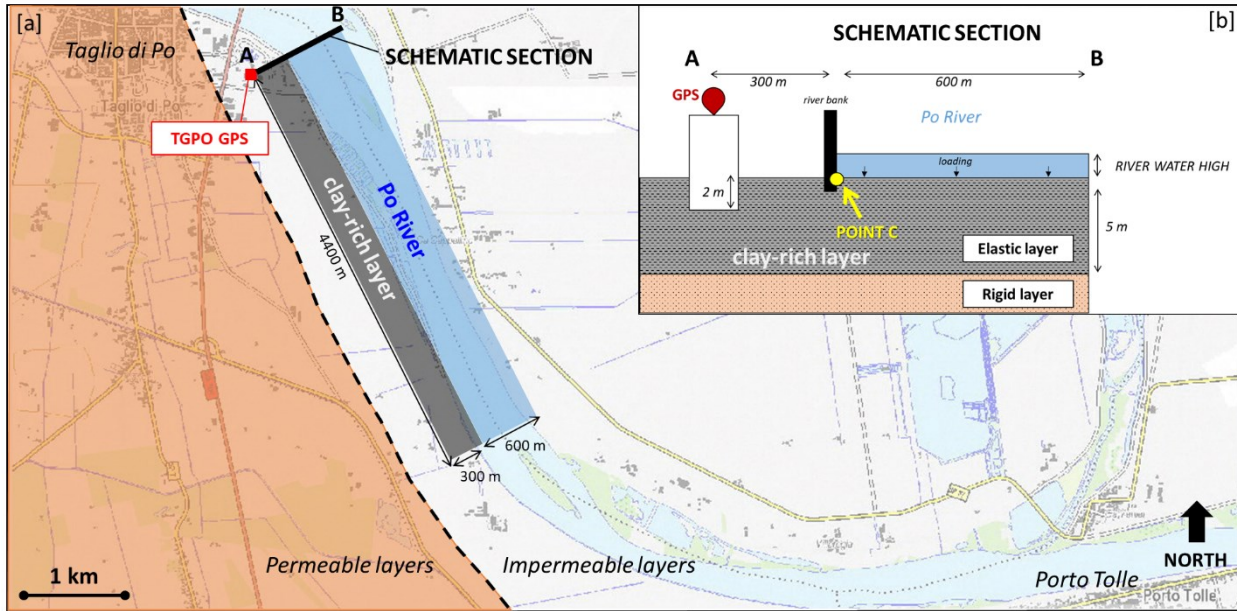
Figure 3.41 – TGPO site configuration: a) map view of facies boundary and river dimensions near TGPO CGPS station; proposed base map is available on Geoportal of Veneto Region (http://idt.regione.veneto.it); b) section passing through TGPO CGPS station that schematizes water loading on the top of the elastic layer.

Conclusions

This thesis focuses on the research of a study approach able to deal with the complexity of the land subsidence phenomenon in deltas. In the framework of the most up- to-date multi-methodological and multi-disciplinary studies concerning land subsidence and targeting to predict and prevent flooding risk, the thesis introduces a procedure based on two main innovations: the multi-component study and the multi-source analysis. It is a "multi-component" procedure, since it investigates in the available geodetic datasets the permanent component apart from the periodic one, and at the same time is a "multi-source" approach because it attempts to identify the relevant processes causing subsidence (sources) by a modelling based on multi-source data analysis. The latter task is accomplished first through multi-disciplinary and multi-methodological comparative analyses, then through modelling of the selected process.

With respect to the past and current study approaches, the defined procedure allows to:

i. overcome the one-component investigation, improving the accuracy in the estimate of the geodetic velocity;

ii. fix the "analyses to modelling" procedure, enhancing qualitative or semi-quantitative procedures that often characterize the "data to source" and the "residual to source" approaches;

iii. quicken the source validation phase accrediting the relevance of the source on the basis of the analyses results and before the modelling phase, differently from the "peering approach", which validates the source on the basis of the model findings.

The proposed procedure has been tested on the Po Delta (northern Italy), an area influenced by climate changes (Simeoni and Corbau, 2009), historically affected by land subsidence and recently interested by accurate continuous geodetic monitoring through GNSS stations. Daily-CGPS time series (three stations), weekly- CGPS time series (two stations) and seven sites of DInSAR-derived time series spanning over the time interval 2009 – 2017 constituted the used geodetic datasets. Several meteo/hydro parameters collected from fifty-seven stations and wide stratigraphic-geological information formed the base for the performed comparative analyses.

The main outcome of this study is that two water mass-dependent processes are active over the Po Delta and explain the seasonal annual component highlighted in the continuous GPS stations. Since

these mechanisms are mass-dependent, the ground level up-or-down lift occurs according to the elastic rebound due to the mass change, specifically to:

I. the soil moisture mass change, which appears to be controlled by shallow hydrological mechanisms and acts on the floodplains at regional scale (rain water infiltration in the topsoil, runoff and evapo-transpiration). Such outcome has been found at CODI station, located in the southern part of the Delta;

II. the river water mass change, which depends on the river-sea interplay and acts at local scale, on the riverbed and riverbanks. This result has been achieved for TGPO station, situated in the central part of the Delta and close to the main Po River course.

Moreover, the use of the most accurate physically-based global hydrological models, i.e. MERRA2 (Gelaro et al., 2017) and GLDAS (Rodell et al., 2004), allowed to better understand the origin of the seasonal modulation in the geodetic series, and further to unveil the role played by the water mass-dependent processes. Since these models allow to take into account the loading effects due to rainfalls and soil moisture, significant differences turned out by using or not the hydrological models for retrieving the subsidence velocity, indeed the mean subsidence rate calculated over the period June 2012 - October 2016 at CODI station, passes from -1.9 ± 0.1 mm/yr to -2.3 ± 0.12 mm/yr (Vitagliano et al., 2018).

Since DInSAR data offer a better covering over the Delta area with respect to the CGPS, SAR-derived LOS velocities have been used to validate the proposed study approach and to get insights into the geological processes controlling the subsidence. The LOS velocities vary over the Delta, being lower in the southern part (CODI site) and higher in the eastern one (Albarella, Boccasette, Pila and Scardovari sites), while assume low and intermediate values in the central part of Delta (TGPO and PTO1 sites). We have tentatively interpreted the lower rate found over 2012 - 2016 period in the TGPO site with respect to PTO1 site (located to the East) as due to the sediment compaction process of the Holocene prograding sequences and to the increase of rich-clay deposits to the eastern part of the Delta. However, the model geometry uncertainty (e.g. present-day topography) and the lack of specific data for better constrain the reconstruction of the paleo-water depths (e.g. micro-paleontological study), do not allow to compute reliable subsidence rates and to discriminate the shallow sedimentary contribution from the tectonics one.

As it regards the future outlines, the limitations hereafter described, constitute the main aspects on which the improvements of such promising multi-component and multi-source approach may be addressed. In particular:

1) as the defined approach has been applied only in the Po Delta, it would be a suitable reliability check accounting for other case studies;

2) since the presence of noise affects the accuracy of the subsidence rate estimates, it is also fundamental enhancing the new approach by introducing a noise analysis in the component recognition phase;

3) since the proposed approach considers only the mechanical compaction of sediments for modelling the soil strain, other processes, likely occurring in delta areas, should be taken into account (e.g. chemical alteration of clay due to the saltwater intrusion and the peat oxidation);

4) the results obtained for the permanent component raise the importance of better managing even the accuracy on the domain, boundary conditions and setting parameters for a more realistic geological modelling of the subsidence phenomena;

5) the results calculated at TGPO site for the periodic component enhanced the importance of developing a more accurate 3D model over the entire Delta for simulating the vertical stress and strain distributions caused by transient river water mass changes.

References

Aiello G., Barra D., De Pippo T. and Donadio C.; 2012: Pleistocene Foraminifera and Ostrocoda from the Island of Procida (Bay of Naples, Italy). Bollettino della Società Paleontologica Italiana, 51 (1), 49-62.

Allen A.S.; 1984: Type of Land Subsidence. In: Guidebook to studies of land subsidence due to ground-water withdrawal, edited by Poland J.F., UNESCO Studies and Reports in Hydrology 40, UNESCO, Paris.

Allen P.H. and Allen J.R.; 2005: Basin Analysis, Principles and Applications. Second ed., Blackwell Publ., 560 pp.

Altamimi Z., Collilieux X., Métivier L.; 2011: ITRF2008: an improved solution of the International Terrestrial Reference Frame. J. Geodesy 85, 457–473.

Amorosi A., Colalongo M.L., Fiorini F., Fusco F., Pasini G., Vaiani S.C. and Sarti G.; 2004: Palaeogeographic and palaeoclimatic evolution of the Po Plain from 150-ky core records. Glob. Planet. Chang. 40, 55–78.

Amorosi A., Dinelli E., Rossi V., Vaiani S.C. and Sacchetto M.; 2008: Late Quaternary paleoenvironmental evolution of the Adriatic coast plain and the onset of Po River Delta. Palaeogeogr. Palaeoclimatol. Palaeoecol., 268, 80–90.

Amorosi A., Maselli V. and Trincardi F.; 2016: Onshore to offshore anatomy of a late Quaternary source-to-sink system (Po Plain–Adriatic Sea, Italy). Earth-Science Reviews 153, 212–237.

Antonellini M., Mollema P., Giambastiani B., Bishop K., Caruso L., Minchio A., Pellegrini L., Sabia M., Ulazzi E. and Gabbianelli G.; 2008: Salt water intrusion in the coastal aquifer of the southern Po Plain, Italy. Hydrogeology Journal 16, 1541–1556.

Antonioli F., Ferranti L., Fontana A., Amorosi A., Bondesan A., Braitenberg C., Dutton A., Fontolan G., Furlani S., Lambeck K., Mastronuzzi G., Monaco C., Spada G. and Stocchi P.; 2009: Holocene relative sea-level changes and vertical movements along the Italian and Istrian coastlines. Quaternary International 206, 102–133.

Baldwin M.P., Gray L.J., Dunkerton T.J., Hamilton K., Haynes P.H., Randel W.J., Holton J.R., Alexander M.J., Hirota I., Horinouchi T., Jones D.B.A., Kinnersley J. S., Marquardt C., Sato K. and Takahashi M.; 2001: The quasi-biennial oscillation. Rev. Geophys. 39 (2), 179–229.

Balugani E. and Antonellini M.; 2011: Barometric pressure influence on water table fluctuations in coastal aquifers of partially enclosed seas: An example from the Adriatic coast, Italy. Journal of Hydrology 400, 176–186.

Barends F.B.J., Brouwer F.J.J. and Schröder F.H.; 1995: Land Subsidence (Proceedings of the FISOLS). IAHS Publ. 234.

Bates R.L. and Jackson J.A.; 1980: Glossary of Geology. American Geological Institute Ed., Falls Church, Virginia, 749 pp.

Benetazzo A., Bergamasco A., Bonaldo D., Falcieri F.M., Sclavo M., Langone L. and Carniel S.; 2014: Response of the Adriatic Sea to an intense cold air outbreak: Dense water dynamics and wave-induced transport. Progress in Oceanography 128, 115–138.

Bennema J., Geuze E.C.W.A., Skits H. and Wiggers A.J.; 1954: Soil compaction in relation to Quaternary movements of sea-level and subsidence of the land especially in the Netherlands. Geologie en Mijnbouw, new ser., vol. 16, 6, 173-178.

Berardino P., Fornaro G., Lanari R. and Sansosti E.; 2002: A new algorithm for surface deformation monitoring based on small baseline Differential SAR Interferograms. IEEE Transactions on Geoscience and Remote Sensing 40, 2375–2383.

Bergeot N., Bouin M.N., Diament M., Pelletier B., Re´gnier M., Calmant S. and Ballu V.; 2009: Horizontal and vertical interseismic velocity fields in the Vanuatu subduction zone from GPS measurements: evidence for a central Vanuatu locked zone. J. of Geophys. Res., vol. 114, B06405.

Beutler G., Bock H., Brockmann E., Dach R., Fridez P., Gurtner W., Hugentobler U., Ineichen D., Johnson J. and Meindl M.; 2001: Bernese GPS software version 4.2 Astron. Inst. Univ. Berne 515, 1–12.

Bigi G., Cosentino D., Parotto M., Sartori R. and Scandone P.; 1992: Structural model of Italy. Consiglio Nazionale delle Ricerche (CNR)—1:500 000—Florence, Italy.

Bitelli G., Bonsignore F., Pellegrino I. and Vittuari L.; 2015: Evolution of the techniques for subsidence monitoring at regional scale: the case of Emilia-Romagna region (Italy). Proc. IAHS, 372, 315–321.

Bjerrum L.; 1967: Engineering geology of Norwegian normally-consolidated marine clays as related to settlements of buildings. Seventh Rankine Lecture. Geotechnique, 17, 81-118.

Blanco-Sánchez P., Mallorquí J.J., Duque S. and Monells D.; 2008: The coherent pixels technique (CPT): an advanced DInSAR technique for nonlinear deformation monitoring. Pure and Applied. Geophys. 165, 6, 1167–1193.

Blewitt G. and Lavallée D.; 2002: Effect of annual signals on geodetic velocity J. Geophys. Res.

Blunden J., Arndt D.S. and Hartfield G.; 2018: State of the climate in 2017. Special Supplement to the Bulletin of the American Meteorological Society Vol. 99, 8.

Bock Y. and Melgar D.; 2016: Physical applications of GPS geodesy: a review. Rep. Prog. Phys. 79 106801, 119. IOP Publ. Ltd, UK.

Bondesan M.U. and Simeoni; 1983: Dinamica E Analisi Morfologica Statistica Dei Litorali Del Delta Del Po E Alle Foci dell'Adige E Del Brenta. Memorie Di Scienze Geologiche 36, 1–48.

Bondesan M., Castiglioni G.B., Elmi C., Gabbianelli G., Marocco R., Pirazzoli P.A. and Tomasin A.; 1995: Coastal areas at risk from storm surges and sea-level rise in north-eastern Italy. J. Coastal Res. 11, 1354–1379.

Bonzi L., Calabrese L., Severi P. and Vincenzi V.; 2010: Coastal unconfined aquifer of Emilia Romagna: geological model and salinization state. Il Geologo dell'Emilia-Romagna 1, 21–34. In Italian.

Bos M., Bastos L. and Fernandes R.M.S.; 2010: The influence of seasonal signals on the estimation of the tectonic motion in short continuous GPS time-series. J. Geodyn., 49, 205–209.

Brambilla F.; 2000: Compaction Monitoring Using Radioactive Markers. SPE Bulletin 2/00.

Burrato P., Ciucci F. and Valensise G.; 2003: An inventory of river anomalies in the Po Plain, Northern Italy: evidence for active blind thrust faulting. Ann. Geophys. 46, 5, 865-882.

Caputo M., Pieri L. and Unguendoli M.; 1970: Geometric Investigation of the Subsidence in the Po Delta. Bollettino Di Geofisica Teorica E Applicata 47, 187–207.

Carbognin L., Gambolati G. and Johnson A.I. Eds.; 2000: Land Subsidence Proceedings of the 6th International Symposium on Land Subsidence. IAHS Publ., 817 pp.

Carisi F., Domeneghetti A., Gaeta M. G. and Castellarin A.; 2017: Is anthropogenic land subsidence a possible driver of riverine flood-hazard dynamics? A case study in Ravenna, Italy. Hydrological Sciences Journal, 62, 15, 2440–2455.

Carminati E. and Di Donato G.; 1999: Separating natural and anthropogenic vertical movements in fast subsiding areas: the Po plain (N. Italy) case. Geophys. Res. letters, vol. 26, 15, 2291-2294.

Carminati E. and Martinelli G.; 2002: Subsidence rates in the Po plain, Northern Italy: the relative impact of Natural and Anthropogenic causation. In: Engineering Geology, vol. 66.

Carminati E., Doglioni C. and Scrocca D.; 2003a: Apennines subduction-related subsidence of Venice. Geophys. Res. Letters, 30, 1717.

Carminati E., Martinelli G. and Severi P.; 2003b: Influence of glacial cycles and tectonics on natural subsidence in the Po Plain (Northern Italy): insights from 14C. Geochemistry, Geophysics, Geosystems, 4, 10.

Carminati E., Doglioni C. and Scrocca D.; 2006: The fragile balance of the Po Valley. Le Scienze, 450 (2), 88–94. In Italian.

Carminati E., Cavazza D., Scrocca D., Fantoni R., Scotti P. and Doglioni C.; 2010: Thermal and tectonic evolution of the southern Alps (northern Italy) rifting: Coupled organic matter maturity analysis and thermos-kinematic modeling. AAPG Bulletin, 94, 3, 369–397.

Carreón-Freyre D., Cerca M., Galloway D.L. and Silva-Corona J.J. Eds.; 2010: Land subsidence, associated hazards and the role of natural resources development – Proceedings of 8th International Symposium on Land Subsidence. IAHS Publ. 339.

Castellarin A., Vai G.B. and Cantelli L.; 2006: The Alpine evolution of the Southern Alps around the Giudicarie faults: A Late Cretaceous to Early Eocene transfer zone. Tectonophysics, 414, 203–223.

Cattaneo A., Correggiari A., Langone L. and Trincardi F.; 2003: The late-Holocene Gargano subaqueous delta, Adriatic shelf: Sediment pathways and supply fluctuations. Marine Geology 193, 61-91.

Cazzini F., Dal Zotto O., Fantoni R., Ghielmi M., Ronchi P. and Scotti P.; 2015: Oil and gas in the Adriatic foreland, Italy. Journal of Petroleum Geology, 38, 3, 255-279.

Christian J.T. and Carrier W.D.; 1978: Janbu, Bjerrum and Kjaernsli's Chart Reinterpreted. Canadian Geothecnical Journal, 15, 123-128.

Cibin U. and Stefani M., with contributions from: Bondesan M., Cattani L., Ceriani A., Colalongo M.L., Di Giulio A., Marchesini L., Pugliese N., Serra F., Tsakiridis E., Vaiani S.C. and Vincenzi S.; 2006: Notes to the Geological Map of Italy, 1:50.000, 187 – Codigoro. ISPRA CARG Project, Geological Survey of Emilia Romagna Region, InfoCartoGrapica Ed., 161 pp. In Italian.

Correggiari A., Cattaneo A. and Trincardi F.; 2005: Depositional patterns in the Late-Holocene Po delta system. In: Giosan L. and Bhattacharya J.P. (Eds.), River Deltas—Concepts, Models, and Examples. SEPM Special Publication, Tulsa, 365–392.

Cortellazzo G. and Simonini P.; 2011: Permeability evaluation and its implications for consolidation analysis of an Italian soft clay deposit. Canadian Geotechnical Journal 38(6), 1166-1176.

Curlander J.C. and McDonough R.N.; 1991: Synthetic Aperture Radar — Systems and Signal Processing. John Wiley & Sons, New York.

D'Agostino N., Jackson J.A., Dramis F. and Funiciello R.; 2001: Interaction between mantle upwelling, drainage volution and active normal faulting: an example from the central Apennines (Italy) Geophys. J. Int., 147, 475-497.

Da Lio C., Tosi L., Zambon G., VianelloA., Baldin G., Lorenzetti G., Manfè G. and Teatini P.; 2013: Long-term groundwater dynamics in the coastal confined aquifers of Venice (Italy). Estuarine, Coastal and Shelf Science 135, 248-259.

Dacome M.C., Miandro R., Vettorel M. and Roncari G.; 2015: Subsidence monitoring network: an Italian example aimed at a sustainable hydrocarbon E&P activity. Proc. IAHS 372, 379–384.

Daito K. and Galloway D. Eds.; 2015: Prevention and mitigation of natural and anthropogenic hazards due to land subsidence - Proceedings of the 9th International Symposium on Land Subsidence. IAHS Publ. 372.

Dal Cin R.; 1983: Littorals of Po River delta and Adige and Brenta Rivers mouths: textural character and sediment disturbance, causes of receding and prevision of future developments. Boll. Soc. Geol. Ital. 102, 9–56. In Italian.

Dang V.K., Doubre C., Weber C., Gourmelen N. and Masson F.; 2014: Recent land subsidence caused by the rapid urban development in the Hanoi region (Vietnam) using ALOS InSAR data. Nat. Hazards Earth Syst. Sci., 14, 657–674.

Davis J.L., Wernicke B.P. and Tamisie M.E.; 2012: On seasonal signals in geodetic time series. J. Geophys. Res., 117.

Day J., Ibáñez C., Scarton F., Pont D., Hensel P., Day J. and Lane R.; 2011: Sustainability of Mediterranean Deltaic and Lagoon Wetlands with Sea-Level Rise: The Importance of River Input. Estuaries and Coasts, 34, 3, 483-493.

Denton G.H. and Karlen W.; 1973: Holocene climatic variations: their pattern and possible cause. Quaternary Research 3, 155 – 205.

Dickinson G.; 1953: Geological aspects of abnormal reservoir pressures in Gulf Coast, Louisiana. AAPG Bulletin, 37, 410–432.

Dickman S.R.; 1988: Theoretical investigation of the oceanic inverted barometer response. J. Geophys. Res., 93, 14 ,941– 946.

Doglioni C.; 1993: Some remarks on the origin of foredeeps. Tectonophysics, 228, 1-20.

Domenico P.A. and Schwartz F.W.; 1998: Physical and Chemical Hydrogeology. John Wiley & Sons, New York, 2nd Ed.

Donadio C., Stamatopoulos L., Stanislao C. and Pennetta M.; 2017: Coastal dune development and morphological changes along the littorals of Garigliano, Italy, and Elis, Greece, during the Holocene. J. Coast. Conserv.

Dong D., Fang P., Cheng M.K. and Miyazaki, S.; 2002: Anatomy of apparent seasonal variations from GPS-derived site position time series. J. Geophys. Res. 107, B4.

Fabris M., Achilli V. and Menin A.; 2014: Estimation of Subsidence in Po Delta Area (Northern Italy) by Integration of GPS Data, High-Precision Leveling and Archival Orthometric Elevations. International Journal of Geosciences, 5, 571-585.

Fantoni R. and Franciosi R.; 2010: Tectono-sedimentary setting of the Po Plain and Adriatic Foreland. Rend. Fis. Acc. Lincei, 21, 1.

Fergason K.C., Rucker M.L. and Panda B.B.; 2015: Methods for monitoring land subsidence and earth fissures in the Western USA. Proc. IAHS, 372, 361–366.

Ferretti A., Prati C. and Rocca F.; 2001: Permanent scatterers in SAR interferometry. IEEE Trans Geosci. Remote Sens., 39, 8–20.

Ferretti A., Fumagalli A., Novali F., Prati C., Rocca F. and Rucci A.; 2011: A new algorithm for processing interferometric data-stacks: SqueeSAR. IEEE Transactions on Geoscience and Remote Sensing 49, 9, 3460–3470.

Fiaschi S., Fabris M., Floris M. and Achilli V.; 2018: Estimation of land subsidence in deltaic areas through differential SAR interferometry: the Po River Delta case study (Northeast Italy). GIScience & Remote Sensing, 54, 3.

Fu L.-L. and Pihos G.; 1994: Determining the response of sea level to atmospheric pressure forcing using TOPEX/POSEIDON data. J. Geophys. Res., 99, 24, 633– 642.

Fuhrmann T., Heck B., Knöpfler A., Masson F., Mayer M., Ulrich P., Westerhaus M. and Zipplt. K.; 2013: Recent surface displacements in the Upper Rhine Graben – Preliminary results from geodetic networks. Tectonophysics, 602, 300-315.

Galloway D., Jones D.R. and Ingebritsen S.E. (eds); 1999: Land subsidence in the United States. US Geol Surv Circ 1182.

Galloway D.L. and Burbey T.J.; 2011: Review: Regional land subsidence accompanying groundwater extraction. Hydrogeology J., vol. 19, 8, 1459–1486.

Galloway D.L.; 2014: The current situations and developing trend of international land subsidence research. Shanghai Land & Resources, 35 (2).

Gambolati G., Putti M., Teatini P., Camporese M., Ferraris S., Gasparetto-Stori G., Nicoletti V., Rizzetto F., Silvestri S. and Tosi L., 2005. Peatland oxidation enhances subsidence in the Venice watershed. EOS Trans. AGU 86, 23, 217–224.

Gambolati G. and Teatini P.; 2015: Geomechanics of subsurface water withdrawal and injection. Water Resour. Res., 51, 3922–3955.

Gelaro R., McCarty W., Suárez M.J., Todling R. et al., 2017; The Modern-Era Retrospective Analysis for Research and Applications, Version 2 (MERRA-2). J. Clim., 30, 5419-5454.

Geological Survey of Italy; 2009: Geological Map of Italy, 1:50000, F. 187 Codigoro. ISPRA, Roma.

Ghielmi M., Minervini M., Nini C., Rogledi S. and Rossi M.; 2013: Late Miocene-Middle Pleistocene sequences in the Po Plain - Northern Adriatic Sea (Italy): The stratigraphic record of modification phases affecting a complex foreland basin. Marine and Petroleum Geology, 42, 50-81.

Glass C.E.; 2013: Interpreting Aerial Photographs to Identify Natural Hazards. Elsevier Ed., 184 pp.

Glopper R.J. and De Ritzema H.P.; 1984: Land Subsidence. ILRI Publication 16. The Netherlands.

Grinsted A., Moore J.C. and Jevrejeva S.; 2004: Application of the cross wavelet transform and wavelet coherence to geophysical time series. Nonlinear Proc. Geophys. 11, 561–566.

Gvirtzman Z., Faccenna C. and Becker T.W.; 2016: Isostasy, flexure, and dynamic topography. Tectonophysics 683, 255–271.

Hanssen R.F.; 2001: Radar interferometry: data interpretation and error analysis, vol. 2. Remote sensing and digital image processing, Springer, New York.

Hantschel T. and Kauerauf A.I.; 2009: Fundamentals of basin and petroleum systems modeling. Springer-Verlag Berlin Heidelberg.

Harbaugh A.W.; 2005: MODFLOW-2005, the U.S. Geological Survey modular groundwater model - the Groundwater Flow Process: U.S. Geological Survey Techniques and Methods 6-A16.

Hensley S., Zebker H., Jones C., Michel T., Muellerschoen R. and Chapman B.; 2009: First deformation results using the NASA/JPL UAVSAR instrument. 2nd Asian-Pacific Conference on Synthetic Aperture Radar, 1051–1055.

Herring T., King R. and McClusky S.; 2008: Introduction to Gamit/ Globk Technical Report Version 10.50. Massachusetts Institute of Technology, Cambridge, MA.

Higgins S.A., Overeem I., Steckler M.S., Syvitski M.J.P., Seeber L. and Akhter S.H.; 2014: InSAR measurements of compaction and subsidence in the Ganges-Brahmaputra Delta, Bangladesh. J. Geophys. Res. Earth Surf., 119, 1768–1781.

Hoffmann J., Leake S.A., Galloway D.L. and Wilson A.M.; 2003: MODFLOW-2000 Ground-Water Model - User Guide to the Subsidence and Aquifer-System Compaction (SUB) Package. U.S. Geological Survey, open-file report, 03-233.

Hofmann-Wellenhof B., Lichtenegger H. and Wasle E.; 2008: GNSS Global Navigation Satellite Systems – GPS, GLONASS, Galileo & more, Springer-Verlag Wien, 516 pp.

Hooper A., Zebker H., Segall P. and Kampes B.; 2004: A new method for measuring deformation on volcanoes and other natural terrains using InSAR Persistent Scatterers. Geophys. Res. Letters 31, 23, 5.

Hooper A., Bekaert D., Spaans K. and Arıkan M.; 2012: Recent advances in SAR interferometry time series analysis for measuring crustal deformation. Tectonophysics 514-517, 1–13.

IAHS; 1977: Proceedings of the 2nd International Symposium on Land Subsidence (Anaheim, California, December 1976). IAHS Publ. 121, 669 pp.

Ingebritsen S.E. and Jones D. R.; 1999: Santa Clara Valley, California, a case of arrested subsidence. In Land Subsidence in the United States, edited by Galloway D., Jones D.R. and Ingebritsen S.E., U.S. Geological Survey Circular 1182. Washington, DC: U.S. Geological Survey, 1999.

IPCC; 2001: Climate Change 2001: Impacts, Adaptation, and Vulnerability. McCarthy J.J et al., Cambridge Univ. Press, 2007.

IPCC; 2013: Summary for Policymakers. In: Climate Change 2013: The Physical Science Basis. Contribution of Working Group 1 to the 5th Assessment Report of the Intergovernmental Panel on Climate Change. Cambridge University Press, Cambridge, United Kingdom and New York, NY, USA.

Jacob C.E.; 1940: On the flow of water in an elastic artesian aquifer. Eos (Transactions American Geophysical Union), 2, 574-586.

Janbu N., Bjerrum L. and Kjaernsli B.; 1956: Unloading foundations. Geotechnical Institute, Oslo, 30-32. In Norwegian.

Johnson A.I., Carbognin L. and Ubertini L. Eds.; 1986: Land Subsidence Proceedings of the 3rd International Symposium on Land Subsidence. IAHS Publ. 151, 939 pp.

Johnson A.I. Ed.; 1991: Land Subsidence Proceedings of the 4th International Symposium on Land Subsidence. IAHS Publ. 200, 690 pp.

Kanamitsu M., Ebisuzaki W., Woolen J., Potter J. and Fiorino M.; 1999: Overview of NCEP/DOE Reanalysis-2, paper presented at the Second International Conference on Reanalyses. World Clim. Res. Prog., Reading, UK.

Karakhanian A., Vernant P., Doerflinger E., Avagyan A., Philip H., Aslanyan I.R., Champollion C., Collard P., Peyret M., Davtyan V., Calais E. and Masson F.; 2013: GPS constraints on continental deformation in the Armenian region and Lesser Caucasus. Tectonophysics, 592, 39-45.

Karegar M.A., Dixon T.H. and Engelhart S.E.; 2016: Subsidence along the Atlantic Coast of North America: Insights from GPS and late Holocene relative sea level data. Geophys. Res. Lett., 43, 3126–3133.

Ketelaar V.B.H.; 2009: Satellite Radar Interferometry: subsidence monitoring techniques. Springer Netherlands, 243 pp.

Kjennerud T.; 2001: Palaeo-bathymetry and rift basin evolution - With particular reference to the northern North Sea Basin. PhD Thesis, NTNU Trondheim, 320 pp.

Klaucke I.; 2018: Sidescan sonar. In: Micallef A. et al. (eds.), Submarine Geomorphology, Springer Geology, 556 pp.

Kontny B. and Bogusz J.; 2012: Models of vertical movements of the Earth crust surface in the area of Poland derived from Leveling and GNSS Data. Acta Geodyn. Geomater., 9, 331–337.

Koster R., Suarez M.J., Ducharne A., Stieglitz M. and Kumar P.; 2000: A catchment-based approach to modeling land surface processes in a general circulation model. Journal of Geophysical Research, 105, D20, 24809-24822.

Kourkouli P.; 2015: Dinsar/psi hybrid methodologies for groundmotion monitoring. A dissertation submitted to the department of geography of university of Leicester for the degree of doctor of philosophy.

Kundzewicz Z.W., Pin´ skwar I. and Brakenridge G.R.; 2013: Large Floods in Europe, 1985–2009. Hydrol. Sci. J. 58, 1–7.

Lambeck K. and Chappell J.; 2001: Sea level change through the last glacial cycle. Science, vol. 292.

Lambeck K., Antonioli F., Anzidei M., Ferranti L., Leoni G., Scicchitano G. and Silenzi S.; 2011: Sea level change along the Italian coast during the Holocene and projections for the future. Quaternary International 232, 250-257.

Lambeck K., Rouby H., Purcell A., Sun Y. and Sambridge M.; 2014: Sea level and global ice volumes from the Last Glacial Maximum to the Holocene. PNAS 111 (43), 15296–15303.

Lee E.Y., Novotny J. and Wagreich M.; 2016: BasinVis 1.0: A MATLAB®-based program for sedimentary basin subsidence analysis and visualization. Computers & Geosciences, 91, 119-127.

Luckman AJ.; 1998: Correction of SAR imagery for variation in pixel scattering area caused by topography. IEEE Trans Geosci. Remote Sens. 36, 344–350.

Lurton X.; 2002: An introduction to underwater acoustics, principles and applications. Springer, Praxis Publishing.

Marfai M.A. and King L.; 2008: Tidal inundation mapping under enhanced land subsidence in Semarang, Central Java Indonesia. Natural Hazards, 44 (1), 93–109.

Maselli V., Trincardi F., Cattaneo A., Ridente D. and Asioli A.; 2010: Subsidence pattern in the central Adriatic and its influence on sediment architecture during the last 400 kyr. Journal of Geophysical Research, 115, B12106.

Maxwell S.C., Rutledge J., Jones R. and Fehler M.; 2010: Petroleum reservoir characterization using downhole micro-seismic monitoring. Geophysics 75, 129-137.

Mayewski P.A., Rohling E.E., Stager J.C., Karle´n W., Maasch K.A., Meeker L.D., Meyerson E.A., Gasse F., van Kreveld S., Holmgren K., Lee-Thorp J., Rosqvist G., Rack F., Staubwasser M., Schneider R.R., Steig E.J.; 2004: Holocene climate variability. Quaternary Research, 62, 243 – 255.

McCarthy D.D. Ed.; 1996: IERS Tech. Note 21. Int. Earth Rotation Serv., Obs. de Paris, Paris.

McClusky S. and Tregoning P.; 2013: Background paper on subsidence monitoring and measurement with a focus on coal seam gas (CSG) activities. Res. School of Earth Sciences The Australian National University Canberra ACT 0200.

McKenzie D.P.; 1978: Some remarks on the development of sedimentary basins. Earth and Planetary Science Letters, vol. 40, 25–32.

Monserrat O., Crosetto M. and Luzi G.; 2014: A review of ground-based SAR interferometry for deformation measurement. ISPRS Journal of Photogrammetry and Remote Sensing 93, 40-48.

Montanari A.; 2012: Hydrology of the Po River: looking for changing patterns in river discharge. Hydrol. Earth Syst. Sci. 16, 3739-3747.

Niebauer T.M., Sasagawa G.S., Faller J.E., Hilt R. and Klopping F.; 1995: A new generation of absolute gravimeters. Metrologia 32, 159-180.

Nikolaidis R.; 2002: Observation of geodetic and seismic deformation with the Global Positioning System. La Jolla, CA: University of California.

NOAA; 2018: State of the Climate: Global Climate Report for Annual 2017.

Oude Essink G.H.P. and Kooi H.; 2011: Land subsidence and sea level rise threaten freshwater resources in the coastal groundwater system of the Rijnland Water Board, the Netherlands. In: Climate change effects on groundwater resources. A global synthesis of findings and recommendations, International Contributions to Hydrogeology, 27, 13.

Peyret M., Masson F., Yavasoglu H., Ergintav S. and Reilinger R.; 2013: Present-day strain distribution across a segment of the Central Bend of the North Anatolian fault zone from a Persistent Scatterers InSAR analysis of the ERS and Envisat archives. Geophys. J. Int., 192, 929-945.

Pfeifer N. and Lichti D.; 2004: Terrestrial laser scanning. GIM International, 18 (12), 50-53.

Piccinini L., Vincenzi V. and Gargini A.; 2008a: Monitoring and modelling variable density flow for the prediction of salt water intrusion effects in a shallow coastal aquifer. Ingegneria e Geologia degli Acquiferi, 23, 77-86.

Piccinini L., Vincenzi V. and Gargini A.; 2008b: Modelling variable density flow of phreatic aquifer affected by salt intrusion. (Italian) Journal of Applied Geology 9(2), 249–261. In Italian.

Piovan S., Mozzi P. and Stefani C.; 2010: Bronze Age Paleohydrography of the Southern Venetian Plain. Geoarchaeology: An International Journal, 25, 1, 6–35. DOI:10.1002/gea.20300

Pola M., Ricciato A., Fantoni R., Fabbri P. and Zampieri D.; 2014: Architecture of the western margin of the North Adriatic foreland: the Schio-Vicenza fault system. Ital. J. Geosci. (Boll. Soc. Geol. It.), 133, 2, 223-234.

Poland J.F., Johnson I., Vega G.F., Yamamoto S. and Carbognin L.; 1984: Mechanics of land subsidence due to fluid withdrawal. In: Guidebook to studies of land subsidence due to ground-water withdrawal, Poland J.F. Ed., UNESCO Studies and Reports in Hydrology 40, UNESCO, Paris.

Poland J.F.; 1984: Guidebook to studies of land subsidence due to ground-water withdrawal. UNESCO Studies and Reports in Hydrology 40, UNESCO, Paris.

Prokopovich N.P.; 1972: Land subsidence and population growth. Engineering Geology, 24th International Geological Congress, Section 13, Montreal, Canada, 44-54.

Prokopovich N.P.; 1979: Genetic classification on land subsidence. Paper presented at the international conference on evaluation and prediction of subsidence, Pensacola Beach.

Puppo A.; 1957: Po Delta subsidence: early outlines of a cinematic phenomenon. Metano Petrol. Nuove Energ. XI 10, 567–575. In Italian.

Puskas C.M, Meertens C.M. and Phillips D.; 2017: Hydrological Loading Model Displacement from the National and Global Data Assimilation Systems (NLDAS and GLDAS). UNAVCO Geodetic Data Service Group.

Raspini F., Cigna F. and Moretti S.; 2012: Multi-temporal mapping of land subsidence at basin scale exploiting Persistent Scatterer Interferometry: Case study of Gioia Tauro plain (Italy). J. Maps 2012, 8, 514–524.

Riley F.S.; 1986: Developments in borehole extensometry. In: Johnson A.I., Carbognin L., Ubertini L. eds., Land subsidence: proceedings of the Third International Symposium on Land Subsidence, Venice, Italy, 1984, IAHS Pub. 151, 169–186.

Roads J., Reichler T., Chen S., Kanamitsu M. and Ebisuzaki W.; 1999: Surface water characteristics and influences in NCEP/DOE Reanalysis-2, paper presented at the Second International Conference on Reanalyses. World Clim. Res. Prog., Reading, UK.

Rodell M., Houser P.R., Jambor U., Gottschalck J. et al.; 2004: The Global Land Data Assimilation System. Bull. Amer. Meteor. Soc., 85(3), 381–394.

Rossi M., Minervini M., Ghielmi M. and Rogledi S.; 2015: Messinian and Pliocene erosional surfaces in the Po Plain-Adriatic Basin: Insights from allo-stratigraphy and sequence stratigraphy in assessing play concepts related to accommodation and gateway turnarounds in tectonically active margins. Marine and Petroleum Geology 66, 192-216.

Rossi V. and Vaiani S.C.; 2008: Benthic foraminiferal evidence of sediment supply changes and fluvial drainage reorganization in Holocene deposits of the Po Delta, Italy. Marine Micropaleontology 69, 106–118.

Royden L. and Keen C.E.; 1980: Rifting processes and thermal evolution of the continental margin of eastern Canada determined from subsidence curves. Earth and Planetary Science Letters, 51, 343–361.

Royden L., Patacca E. and Scandone P.; 1987: Segmentation and configuration of subducted lithosphere in Italy: An important control on thrust-belt and foredeep-basin evolution. Geology, 15, 714 – 717.

Rosen P., Hensley S., Joughin I., Li F., Madsen S., Rodriguez E. and Goldstein R.; 2000: Synthetic aperture radar interferometry. Proceedings of the IEEE 88 (3), 333–382.

Rüeger J.M.; 1990: Electronic Distance Measurement. Springer-Verlag Ed., 288 pp.

Rytter J. and Schonhowd I.; 2015: Monitoring, Mitigation, Management, The Groundwater Project – Safeguarding the World Heritage Site of Bryggen in Bergen. Opplag: 625 Riksantikvaren Oslo.

Salvioni G.; 1957: Land motion in the Central and Northern Italy. Bollettino Di Geodesia E Scienze Affini 16, 325–366. In Italian.

Sanabria M.P., Guardiola-Albert C., Tomás R., Herrera G., Prieto A., Sánchez H. and Tessitore S.; 2013: Subsidence activity maps derived from DInSAR data: Orihuela case study. Nat. Hazards Earth Syst. Sci.2013, 14, 1341–1360.

Santamaría-Gómez A., Bouin M.N., Collilieux X. and Wöppelmann G.; 2011: Correlated errors in GPS position time series: implications for velocity estimates. J. Geophys. Res.

Scafetta N.; 2014: Multi-scale dynamical analysis (MSDA) of sea level records versus PDO, AMO, and NAO indexes. Clim. Dynam. 43, 175–192.

Schmidt C.W.; 2015: Delta subsidence – An imminent threat to coastal populations. Environmental Health Perspectives, 123, 204–209.

Schomaker M.C. and Berry R.M.; 1981: Geodetic leveling. NOAA Manual NOS NGS 3.

Sclater J.G. and Christie P.A.F.; 1980: Continental stretching: an explanation of the post-mid-Cretaceous subsidence of the central North Sea basin. J. Geophys. Res., 85, 3711-3739.

Severi P., Biavati G., Bonzi L., Guadagnini L. and Martelli L.; 2012: Continuous monitoring of Po aquifers. Ecoscienza, 6, 72-74. In Italian.

Simeoni U. and C. Corbau.; 2009: A Review of the Delta Po Evolution (Italy) Related to Climatic Changes and Human Impacts. Geomorphology 107, 64–71.

Smith R.G., Knight R., Chen J., Reeves J.A., Zebker H.A., Farr T. and Liu Z.; 2017: Estimating the permanent loss of groundwater storage in the southern San Joaquin Valley, California. Water Resour. Res., 53, 2133–2148.

Soja M.J., Sandberg G. and Ulander L.M.H.; 2010: Topographic correction for biomass retrieval from P-band SAR data in boreal forests. In: Proceedings of the Geoscience and Remote Sensing Symposium (IGARSS 2010), Honolulu.

Stefani M. and Vincenzi S.; 2005: The interplay of eustasy, climate and human activity in the Late-Quaternary depositional evolution and sedimentary architecture of the Po Delta system. Mar. Geol. 222–223, 19–48.

Stefani M.; 2017: The Po Delta Region: Depositional Evolution, Climate Change and Human Intervention Through the Last 5000 Years. In: M. Soldati and M. Marchetti (eds.), Landscapes and Landforms of Italy, World Geomorphological Landscapes, Springer International Publishing AG.

Stenvold T., Eiken O., Zumberge M.A., Sasagawa G.S. and Nooner S.L.; 2006: High-precision relative depth and subsidence mapping from seafloor water-pressure measurements. J. of the Society of Petroleum Engineers, Paper No.SPE 97752, 380–389.

Stocker T., Qin D., Plattner G.K., Tignor M., Allen S.K., Boschung J., Nauels A., Xia Y., Bex V. and Midgley P.M.; 2014: Climate change 2013: the physical science basis, Cambridge: Cambridge University Press.

Stramondo S., Bozzano F., Marra F., Wegmuller U., Cinti F.R., Moro M. and Saroli M.; 2008: Subsidence induced by urbanisation in the city of Rome detected by advanced InSAR technique and geotechnical investigations. Remote Sensing of Environment, 112 (6), 3160-3172.

Sun G., Ranson K.J. and Kharuk V.I.; 2002: Radiometric slope correction for forest biomass estimation from SAR data in the Western Sayani Mountains, Siberia. Remote Sens Environ. 79, 279 – 287.

Teatini P., Tosi L., Strozzi T., Carbognin L., Wegmüller U. and Rizzetto F.; 2005: Mapping regional land displacements in the Venice coastland by an integrated monitoring system. Remote Sens. Environ. 98, 403–413.

Teatini P., Ferronato M., Gambolati G. and Gonella M.; 2006: Groundwater pumping and land subsidence in the EmiliaRomagna coastland, Italy: Modeling the past occurrence and the future trend, Water Resour. Res., 42, W01406.

Teatini P., Tosi L. and Strozzi T.; 2011: Quantitative evidence that compaction of Holocene sediments drives the present land subsidence of the Po Delta, Italy. J. Geophys. Res. 116, B08407.

Teferle F.N., Williams S.D.P., Kierulf H.P., Bingley R.M., Plag HP.; 2008: A continuous GPS coordinate time series analysis strategy for high-accuracy vertical land movements. Physics and Chemistry of the Earth, 33, 205–216.

Terzaghi K. and Peck R.B.; 1967: Soil mechanics in engineering practice. John Wiley & Sons.

Tison L.J. Ed.; 1969: Land Subsidence Proceedings of the Tokyo Symposium. IAHS Publ. 88–89, 661 pp.

Tomás R., Romero R., Mulas J., Marturià J.J, Mallorquí J.J., Lopez-Sanchez J.M., Herrera G., Gutiérrez F., González P.J., Fernández J., Duque S., Concha-Dimas A., Cocksley G., Castañeda C., Carrasco D. and Blanco P.; 2014: Radar interferometry techniques for the study of ground subsidence phenomena: a review of practical issues through cases in Spain. Environmental Earth Sciences, 71, 1, 163-181 pp.

Torge W.; 1986: Gravimetry for monitoring vertical crustal movements: Potential and problems. Tectonophysics 130 (1–4), 385-393.

Tornaghi R. and Perelli Cippo A.; 1985: Soil improvement by jet grouting for the solution of tunneling problems. Proc. Tunneling '85, Brighton, 265-275.

Tosi L., Rizzetto F., Bonardi M., Donnici S., Serandrei Barbero R. and Toffoletto F.; 2007: Notes to the Geological Map of Italy, 1:50.000, 128 - Venice. APAT, Geological Survey of Italy, SystemCart Ed., 164 pp. In Italian.

Tosi L., Teatini P., Carbognin L. and Brancolini G.; 2009: Using high resolution data to reveal depth-dependent mechanisms that drive land subsidence: The Venice coast, Italy. Tectonophysics, 474, 271–284.

Tosi L., Teatini P., Strozzi T., Carbognin L., Brancolini G. and Rizzetto F.; 2010: Ground Surface Dynamics in the Northern Adriatic Coastland over the Last Two Decades. Rendiconti Lincei. Scienze Fisiche E Naturali 21 (S1), 115–129.

Tosi L., Teatini P. and Strozzi T.; 2013: Natural versus anthropogenic subsidence of Venice. Nat. Sci. Reports, 3, 2710.

Tosi L., Da Lio C., Strozzi T. and Teatini P.; 2016: Combining L- and X-Band SAR Interferometry to Assess Ground Displacements in Heterogeneous Coastal Environments: The Po River Delta and Venice Lagoon, Italy. Remote Sens. 8(4), 308.

Tosi L., Da Lio C., Teatini P. and Strozzi T.; 2018: Land subsidence in coastal environments: knowledge advance in the Venice coastland by TerraSAR-X PSI. Remote Sens. 10, 1191.

Turcotte D.L. and Schubert G.; 1982: Geodynamics. John Wiley Ed., New York, 450 pp.

Turrini C., Lacombe O. and Roure F.; 2014: Present-day 3D structural model of the Po Valley basin, Northern Italy. Marine and Petroleum Geology, 56, 266-289.

Ubertini L.; 2009: Hydraulic risk mitigation in Italy. In: Quaderni della Società Geologica Italiana, 4. In Italian.

Verdecchia F., Mosconi A., Miandro R., Nista A. and Schiavon R.; 2011: Deep Compaction Electromagnetic Monitoring System. Experimental Phase. Offshore Mediterranean Conference OMC-2011-065.

Vermeersen L.L.A., Fournier A. and Sabadini R.; 1997: Changes in rotation induced by Pleistocene ice masses with strati ed analytical Earth models. J. Geophys. Res., 102, 27, 689-27, 702.

Vezzoli R., Mercogliano P., Pecora S., Zollo A.L. and Cacciamani C.; 2015: Hydrological simulation of Po River (North Italy) discharge under climate change scenarios using the RCM COSMO-CLM. Science of the Total Environment 521–522, 346–358.

Vitagliano E., Di Maio R., Scafetta N., Calcaterra D. and Zanchettin M.; 2017: Wavelet analysis of remote sensing and discharge data for understanding vertical ground movements in sandy and clayey terrains of the Po Delta area (Northern Italy). Journal of Hydrology 550, 386–398.

Vitagliano E., Di Maio R., Piegari E., Riccardi U., Boy J.P., Fabris M. and Achilli V.; 2018: Hydrological model for retrieving subsidence velocity from GPS data: application to Po Delta area. National Congress GNGTS, Bologna 2018.

Webb F.H. and Zumberge J.F.; 1997: An introduction to GIPSY/OASIS II. JPL Publication D-11088.

Weitkamp C.; 2005: LIDAR Range-Resolved Optical Remote Sensing of the Atmosphere. Springer series in optical sciences, Weitkamp C. (Ed.), 2005.

Werner C., Wegmuller U., Strozzi T. and Wiesmann A.; 2003: Interferometric point target analysis for deformation mapping. In Proceedings of IEEE International Geoscience and Remote Sensing Symposium 7, 4362–4364.

Woodworth P.L.; Introduction to GPS and Absolute Gravity at Tide Gauges, teaching materials. Proudman Oceanographic Laboratory, UK.

Ye. X; 2010: Synthetic aperture Radar Interferometry, in: Chap. 11 Sciences of Geodesy – Advances and Future Directions, G. Xu Editor, Springer, 415-474.

Yin J., Yu D., Yin Z., Wang J. and Xu S.; 2013: Modelling the combined impacts of sea level rise and land subsidence on storm tides induced flooding of the Huangpu river in Shanghai, China. Climatic Change, 119, 919–932.

Yuill B., Lavoie D. and Reed D.J.; 2009: Understanding subsidence processes in coastal Louisiana. J. of Coastal Res., 54.

Zanchettin D., Traverso P. and Tomasino M.; 2008: Po River discharges: a preliminary analysis of a 200-year time series. Clim. Change 89, 411–433.

Zastrozhnov D., Gernigon L., Gogin I., Abdelmalak M.M., Planke S., Faleide J. I. and Myklebust R.; 2018: Cretaceous-Paleocene evolution and crustal structure of the northern Vøring Margin (offshore mid-Norway): results from integrated geological and geophysical study. Tectonics, 37, 497–528.

Zhang A., Gong S., Carbognin L. and Johnson A.I. Eds.; 2005: Land Subsidence Proceedings of the 7th International Symposium on Land Subsidence. IAHS Publ., 918 pp.

Zhang J., Bock Y., Johnson H., Fang P., Williams S., Genrich J., Wdowinski S. and Behr J.; 1997: Southern California permanent GPS geodetic array: error analysis of daily position estimates and site velocities. J. Geophys. Res., 102, 18035–18055.

List of figures

List of tables